

NRC-CNRC CONSTRUCTION

Rail Tank Cars Exposed to Fires: Experimental Analyses of Thermal Conditions Imposed to a Railcar Engulfed in Crude Oil Fires (Series 1-3 Tests)

Author(s): Yoon Ko, Ph.D., Cecilia Lam, Ph.D., Eric Gibbs,
Pier-simon Lafrance and Mark Weinfurter

Report No.: A1-010647-01

Report Date: October 07, 2020

Contract No.: A1-010647

Agreement Date: 3 September 2015 (Original agreement)
8 January 2016 (Amendment No. 1)
17 February 2017 (Amendment No. 2)
14 September 2017 (Amendment No. 3)
16 January 2018 (Amendment No. 4)
28 March 2018 (Amendment No. 5)
19 July 2018 (Amendment No. 6)
20 December 2018 (Amendment No. 7)
17 September 2019 (Amendment No. 8)
20 January 2020 (Amendment No. 9)



© 2020 Her Majesty the Queen in Right of Canada,
as represented by the National Research Council Canada.

TP Number: TP 15465

ISBN: 978-0-660-37228-0

Catalogue: T86-69/2021E-PDF




Rail Tank Cars Exposed to Fires:

Experimental Analyses of Thermal Conditions Imposed to a Railcar Engulfed in Crude Oil Fires (Series 1-3 Tests)

PM 

Yoon Ko, Ph.D.

Approved  Ahmed Kashef
2020-10-28 19:28:37

Ahmed Kashef, Ph.D.
Program Leader
Fire Laboratory Transition Program
NRC Construction

Report No: A1-010647-01
Report Date: 28 October 2020
Contract No: A1-010647
Agreement date: 3 September 2015 (Original agreement)
8 January 2016 (Amendment No. 1)
17 February 2017 (Amendment No. 2)
14 September 2017 (Amendment No. 3)
16 January 2018 (Amendment No. 4)
28 March 2018 (Amendment No. 5)
19 July 2018 (Amendment No. 6)
20 December 2018 (Amendment No. 7)
17 September 2019 (Amendment No. 8)
20 January 2020 (Amendment No. 9)
Program: Fire Laboratory Transition Program

This report may not be reproduced in whole or in part without the written consent of the National Research Council Canada and the Client.

Acknowledgement

This project was funded by Transport Canada, and the fire tests were conducted by Sandia National Laboratories. Additional support was provided for the Crude Oil Characterization Research Study by the U.S. Department of Energy, U.S. Department of Transportation.

Table of Contents

Executive Summary	1
1 Introduction	2
2 Objectives	2
3 Overview of the project and the report	2
4 Methods	3
4.1 Fuel handling and characterization	3
4.2 Fire testing	3
5 Work Plan	4
6 Calorimeter construction	6
7 Preliminary testing	7
8 Fuel characterization	7
9 Fire Testing: Series 1, Series 2 and Series 3	11
9.1 Test parameters	11
9.2 Fuel handling and fuel feed systems	12
9.2.1 Heptane (Series 1 tests)	12
9.2.2 Bakken crude oil (Series 2 tests)	12
9.2.3 Dilbit crude oil (Series 3)	13
9.3 Testing facility	13
9.4 Test set up	13
9.5 Measurements	15
9.5.1 Heat Release Rates (HRR)	15
9.5.2 Mass burning rates	16
9.5.3 Flame/plume temperatures	16
9.5.4 Flame height	17
9.5.5 Surface emissive power on the flame	17
9.5.6 Heat flux at a distance from fire	17
9.5.7 Total heat flux to an engulfed object (measurements by the calorimeter)	18
10 Fire Test Results and Discussion	19
10.1 Overall burning behavior	19
10.2 Mass burning rates	20
10.2.1 Burning behavior and fuel characteristics	20

10.2.2	Parameter impact on mass burn rate.....	21
10.3	Flame heights.....	21
10.4	Heat release rates.....	22
10.4.1	Heat release rate measurement verification.....	22
10.4.2	Convective and radiative heat release rate.....	23
10.5	Flame temperature and surface emissive power.....	25
10.5.1	Measurement verification.....	25
10.5.2	Vertical profiles of flame temperature and surface emissive power.....	25
10.5.3	The effects of the test parameters on flame temperature and surface emissive power	27
10.5.4	Mean SEP and total radiation emitted from the flame.....	27
10.6	Heat flux received by the calorimeter.....	28
10.6.1	Heat flux variation around the circumference of the calorimeter.....	28
10.6.2	The effects of the test parameters and fuel characteristics on the total heat flux to the calorimeter.....	30
10.7	Incident heat flux away from the fire.....	31
11	Conclusions.....	33
12	Recommendations for future study.....	35
13	References.....	37
Supplement A. Test Report		
Supplement B. Crude oil Characterization report		
Supplement C. Preliminary test report		

List of Figures

Figure 1 Calorimeter being instrumented with thermocouples on the outer shell and inner shell; and the hollow centre to be filled with insulation materials	6
Figure 2 Whole oil carbon number plots for Bakken and dilbit oil sampled at the burn site.	9
Figure 3 Temperature versus boiling point distribution for fuel samples	10
Figure 4 Test set-up	14
Figure 5 Calorimeter instrumentation	14
Figure 6 HRR (Q) and convective HRR (Qc) measured in the heptane, Bakken and dilbit tests	20
Figure 7 HRRs measured by oxygen consumption calorimetry and mass burning rates in comparison with convective HRRs	23
Figure 8 Radiative heat fractions	24
Figure 9 Radiative heat release rates compared with convective heat release rates	25
Figure 10 Fire plume temperatures from IR camera measurements	26
Figure 11 Vertical variations of SEP with elevation relative to the flame height for heptane (T1.1), Bakken (T2.3) and dilbit (T3.5) crude oils.	27
Figure 12 Total heat flux [kw/m^2] measured by the calorimeter	29
Figure 13 Average total heat flux to the calorimeter placed at 1 m above the pan against the maximum flame surface emissive power	31
Figure 14 Incident heat fluxes	32

List of Tables

Table 1 Physical properties 9
Table 2 Test matrix 11
Table 3 Test results summary 36

Nomenclature

C_p	the specific heat (KJ/kg/K)
DOE	United States Department of Energy
DOT	United States Department of Transport
E_{O_2}	heat release per unit mass of O ₂ consumed in the reaction (MJ/kg of O ₂)
E_{CO}	heat release per unit mass of O ₂ consumed for combustion of CO to CO ₂ (MJ/kg of O ₂)
f	incomplete combustion factor
FLAME	Fire Laboratory for Accreditation of Models and Experiments
H_c	Complete Heat of Combustion (MJ/kg)
HRR	Heat Release Rate (MW)
\dot{m}_b	Burning rate (kg/s)
\dot{m}_e	mass flow rate of gas measured in the duct (kg/s)
$\dot{m}_{O_2}^o$	the mass flow rate of oxygen in air
MWIR	mid-wave infrared
NRC	National Research Council Canada
Q	heat release rate (MW)
Q_C	Convective heat release rate (MW)
Q_r/Q_C	the ratio of the radiative HRR to the convective HRR
q_{total}	total heat flux (kW/m ²)
$q_{incident}$	incident heat flux (KW/m ²)
$q_{convection}$	convective heat flux (KW/m ²)
$q_{absorbed}$	absorbed heat flux (KW/m ²)
$q_{emitted}$	emitted heat flux (KW/m ²)
SAP	fuel Sampling and Analysis Plan
SNL	Sandia National Laboratories
ΔT	temperature rise (°C)
$T_{surface}$	Surface temperature (K)
x	incomplete combustion factor
X_r	a fraction of radiative heat
Z/l_f	Elevation relative to flame height

Greek symbols

α	Absorptivity
\emptyset	oxygen depletion factor
σ	Stefan-Boltzmann constant ($5.67 \times 10^{-8} \text{ W m}^{-2} \text{ K}^{-4}$)
ε	Emissivity

Rail Tank Cars Exposed to Fires: Experimental Analyses of Thermal Conditions Imposed to a Railcar Engulfed in Crude Oil Fires (Series 1-3 Tests)

Author(s): Yoon Ko, Ph.D., Cecilia Lam, Ph.D., Eric Gibbs, Pier-simon Lafrance and Mark Weinfurter

Executive Summary

A series of 2-m pool fire experiments were performed to better evaluate the comparative thermal hazard between different crude oils as a result of pool fires, which could occur as a consequence of an accident in the land transport of crude oils. In order to assess the thermal conditions to which a rail tank car could be exposed, a calorimeter designed to simulate a 1/10th scale tank car was placed above a 2-m diameter pool fire fueled by heptane in Series 1 tests, Bakken crude oil from North Dakota in Series 2 tests and diluted bitumen (dilbit) crude oil from Alberta in Series 3 tests. The calorimeter was instrumented to measure the total heat flux at various locations along its surface.

The crude oils used in the testing program were specially handled to ensure no change in its composition over the course of the testing program, from the time of fuel acquisition to the time of fire testing. In conjunction with the fire testing, a fuel characterization study was conducted to enable the study of fire effects in relation to fuel properties.

The burning behaviours of the fuels were observed by measuring the burning rate, flame height and heat release rate (HRR), the flame surface emissive powers (SEP) and the incident heat fluxes away from the fire. Overall, the Bakken crude oil and heptane fires displayed continuous steady burning throughout the test while the dilbit crude oil fires displayed unsteady burning behaviour, which was mainly caused by the fuel composition containing a larger fraction of heavy end hydrocarbons than the Bakken crude oil and heptane.

The total heat flux measured by the calorimeter indicated that the measurements were uneven around the circumference of the calorimeter. The average heat flux to the calorimeter from the Bakken and dilbit crude oil fires was higher than that from the heptane fires although the measured HRRs of the Bakken and dilbit crude oil pool fires were less than those of the heptane pool fires. The main reason for the increased heating of the object in particular by the Bakken and dilbit crude oil fires is that the total heat flux to the object is mostly affected by radiative heat exposure from the flame, and the Bakken and dilbit crude oil fires have higher radiative heat fraction.

The study also investigated the effects of test parameters on fire characteristics. These parameters include the effect of fuel types, the presence and placement of a calorimeter engulfed in the fire, fuel feed temperature, and allowing the fuel to burn down. The results indicate that there was no significant effect of “fuel supply temperature” and “fuel to burn down (i.e., non-continuous fuel feed)”. The higher fuel supply temperature increased the burn rate by about 10% for the heptane and Bakken crude oil tests. For the dilbit crude oil fires, due to the non-steady burning behaviour, the impact of the calorimeter was difficult to capture. Allowing the fuel to burn down, rather than maintaining a constant fuel level in the pool pan, resulted in minimal effect on average values of the mass burning rate and general fire characteristics of the Bakken crude oil pool fires. For the dilbit crude oil, the fuel compositional effect on the burning behaviour was observed in both continuous and non-continuous fuel feeding. The non-uniform burning behaviour became easier to discern when there was no continuous fuel feed into the fuel pan.

1 Introduction

Transport Canada and National Research Council Canada (NRC) have established an experimental research program to better evaluate the comparative thermal hazard between different crude oils as a result of pool fires, which could occur as a consequence of an accident in the land transport of crude oils. More specifically, the research program focuses on evaluating the thermal hazard presented by exposing rail tank cars to hydrocarbon pool fires. Gaps in understanding burning behaviour of crude oil fires and their thermal effects on tank cars were first identified in a literature review conducted by NRC [1]. Subsequently, reduced-scale fire testing was conducted to experimentally analyse the thermal conditions of tank cars engulfed in pool fires fueled by heptane in Series 1 tests, Bakken crude oil from North Dakota in Series 2 Tests and dilbit crude oil from Alberta in Series 3 tests (see Supplement A. Test Report). Fuel characterization was also conducted to enable the study of fire effects in relation to fuel properties (see Supplement B. Crude oil Characterization report).

2 Objectives

The focus of the present experimental study is to experimentally characterize, at reduced scale, the thermal conditions external to tank cars engulfed in different crude oil pool fires. Two crude oils having different fuel characteristics were selected for the fire testing to study the fire effects in relation to their fuel properties.

3 Overview of the project and the report

Experiments were designed to simulate a tank car at 1/10th scale engulfed in a crude oil pool fire. The focus of the experiments was to assess the thermal environment outside the tank car and the levels of heat flux to the tank car itself. As such, a cylindrical object (calorimeter) representing the tank car was built for the fire testing. The cylinder (calorimeter) was instrumented to measure the total heat flux at various locations along its surface. The study also investigated the effects of certain test parameters, which include the effects of fuel type, the presence and placement of a calorimeter engulfed in the fire, fuel feed temperature, and allowing the fuel to burn down in the pool pan.

A preliminary study (see Supplement C. Preliminary test report) was conducted to optimize the initial testing methods and to generate a set of baseline data for subsequent tests. The preliminary study was terminated due to closure and decommissioning of the NRC full-scale fire test facility. The subsequent experimental testing was contracted to Sandia National Laboratories (SNL). The experimental study involved a total of 15 fire tests conducted in three series; Series 1 (3 heptane tests), Series 2 (6 Bakken crude oil tests) and Series 3 (6 dilbit crude oil tests).

This report focuses on Series 1, 2 and 3 tests by:

- describing the methods implemented in the experimental study (Section 4);
- summarizing the work plan (Section 5);
- describing the calorimeter construction (Section 6);
- illustrating the preliminary testing (Section 7);
- describing findings from the fuel characterization study (Section 8), which was conducted in parallel with the testing of Series 1, 2 and 3;
- describing testing set-ups of Series 1, 2 and 3 (Section 9)
- highlighting findings from Series 1, 2 and 3 tests (Section 10); and,
- presenting conclusions and recommendations for future study (Section 11 and 12).

For detailed descriptions of tasks and results, please refer to Supplement A, B and C.

4 Methods

Experiments were conducted in an indoor facility by engulfing a cylindrical object representing a rail tank car at 1/10th scale in a crude oil pool fire to examine fire-related parameters affecting the heating of a tank car. The cylindrical calorimeter was instrumented such that the total heat flux to the calorimeter can be measured at various locations on its surface.

The crude oil was acquired in pressure vessels that are capable of preserving all light ends in the crude oil, and also of ensuring the crude oil remain in a single (liquid) phase throughout the duration of the project. During the fire tests, the crude oil was continuously transferred directly from the pressure vessel to a fuel pan placed in the indoor facility.

4.1 Fuel handling and characterization

Fire is a chemical reaction of fuel oxidation. As such, burning behaviour of a fuel depends, in general, on its hydrocarbon mixture composition [2, 3]. Crude oil is a complex mixture containing many different hydrocarbon components including light hydrocarbons with low densities. These light-end components that tend to volatilize at lower temperatures and at atmospheric pressure are of particular interest for this study since their presence has an impact on fuel characterisation and may have an impact on overall burning behaviour. Therefore, fuels were acquired and handled to preserve the fuel compositions and characteristics so that the fire tests can capture the burning behaviours (e.g. fuel mass burning rate, soot generation and heat release) of each oil as a whole without losing any component including the light ends. The following describes the procedure used in this study to ensure proper fuel handling and characterization;

- 1) The Bakken crude oil was acquired, in a custom-built pressure vessel transport tanker, at the loading site in North Dakota, US, by using a water displacement method that allows the oil to be transferred without being exposed to atmospheric air. The dilbit crude oil was acquired in 12 modified propane cylinders. The acquired crude oil was stored in these pressurised vessels to retain light-end components until testing.
- 2) A fuel feed system was designed for the Bakken and dilbit crude oils to provide continuous fuel flow into a testing pan. This is to simulate an accident scenario involving continuous leakage of fuel from a rail tank car to a pool fire. Thus, the fuel needs to be transferred into the pan without being exposed to atmospheric air until it reaches the pan.
- 3) The acquired crude oils were characterized, and the fuel characterization study was coupled with the fire testing program to explore potential links between the properties of the fuel and fire behaviour of the fuel.

4.2 Fire testing

The fire testing was planned as follows;

- 1) Set up a 1/10th scale tank car to be engulfed in pool fires to assess the total heat flux to a crude oil tank car exposed to a pool fire. A cylindrical object (calorimeter) representing the tank car at 1/10th scale was designed and built for the fire testing. The calorimeter did not contain any lading and instead was instrumented such that the total heat flux to the calorimeter could be measured at various locations on its surface.

- 2) Arrange 2-m diameter pool fire testing with a fuel feed system: The calorimeter was placed above a 2-m diameter pool fire. Tests were conducted to investigate the effect of various parameters on heating of the cylindrical object. The parameters tested in this study include fuel type, calorimeter placement within the fire, initial fuel temperature, and a continuous versus non-continuous fuel feed. Section 9.1 discusses these parameters in detail.
- 3) Instrument the test set-up for measurements of temperature in the fire, radiation from the fire, temperature in the fuel layer, temperature of the calorimeter, heat flux onto the calorimeter, heat release rate from the fire and fuel burning rate.

5 Work Plan

The following tasks have been conducted in this project:

Year 1 (fiscal year (FY) 2015/16):

- 1) Designed, built and instrumented the first cylindrical calorimeter, 0.3 m in diameter and 1.8 m long.
- 2) Conducted preliminary tests at the NRC fire lab: Three tests (two diesel and one heptane) were conducted to test a fuel feed system, instrumentation and performance of the calorimeter. Crude oil was also sourced from Alberta.

Year 2 (FY 2016/17):

- 1) Improved the design of the fuel-handling equipment from Year 1.
Note: implementation of these improvements was aborted due to the change of testing site.
- 2) Prepared the crude oil sourced from Alberta from Year 1 for potential shipping to a new testing site.
Note: shipping was aborted, and it was planned to acquire a new crude oil for the testing scheduled in Year 3.

Year 3 (FY 2017/18):

- 1) Refurbished the 1st calorimeter and built the 2nd calorimeter to be used for fire testing.
- 2) Confirmed and secured access to the new testing site (Sandia National Laboratories, SNL). Due to the closure of the NRC fire lab, the testing was moved to a new testing site.
- 3) Procured heptane and coordinated the handling of the heptane and the Bakken crude oil following proper methods required for safe storage and delivery to the testing site. The crude oil sourced from Alberta in Year 1 could not be used for the testing conducted in Year 3. Instead, the Bakken crude oil was used in the testing. The procurement and storage of the crude oil was provided by SNL through approval and funding from the US Department of Energy (DOE) and Department of Transportation (DOT).
- 4) Developed a test plan and test setup, calibrated instrumentation.
- 5) Conducted 3 heptane tests (Series 1).
- 6) Conducted 6 Bakken crude oil tests (Series 2).
- 7) Coordinated 3 fuel sampling and testing events.
 - a. Arranged acquisition of heptane samples at the burn site and had heptane samples tested for purity and quality.
 - b. Arranged acquisition of Bakken crude oil samples and post-test residue samples for the first and last crude oil tests; and coordinated sample analyses.
- 8) Characterized the acquired Bakken crude oil and verified the fuel handling for the testing which included coordination of the fuel transfer from the tanker to the fuel pan in the test facility.
 - a. Developed a detailed fuel Sampling and Analysis Plan (SAP) for fuel characterization (see Section 8 for details). Verified fuel subsample test data and reduced data for fuel characterization.

- b. Coordinated the fuel transfer to the test site and helped develop the fuel handling system in consultation with an oil and gas industry expert for fire testing; and verified the fuel handling performance including fuel storage.

Year 4 (FY 2018/19):

- 1) Analysed the test data from Series 1 and 2 tests.
- 2) Developed a detailed test plan and test setup; and calibrated instrumentation for Series 3.
- 3) Refurbished the 1st calorimeter to be used for Series 3 tests.
- 4) Conducted exploratory tests with three different types of dilbit samples. These small-scale tests were performed to assess the residue and potential for boil-over of the sample fuels and to select one fuel most suitable for the fire testing,
- 5) Developed a detailed fuel Sampling and Analysis Plan (SAP) for fuel characterization (see Section 8 for details).
 - a. Determined the most suitable means of containment for the selected dilbit crude oil.
 - b. Collected the dilbit crude oil subsamples at the burn site prior to the first and last tests and sent the oil samples to a lab for analysis.
 - c. Verified fuel subsample test data and reduced data for fuel characterization.
- 6) Conducted 6 dilbit crude oil tests (Series 3) at the testing site (SNL).
- 7) Verified the fuel handling for the testing which included coordination of the fuel transfer from the modified propane tanks to the fuel pan in the test facility.
- 8) Conducted a feasibility review on numerical modelling of the crude oil fire test.

Year 5 (FY 2019/20)

- 1) Carried out close-out activities including disposals and cleaning.
- 2) Analysed the test data from Series 3 tests in comparison with Series 1 and 2.

6 Calorimeter construction

To assess total heat flux to a crude oil tank car that is exposed to a pool fire, a cylindrical object (calorimeter) representing the tank car at 1/10th scale was built for fire testing. The calorimeter has a diameter of 0.3 m and a length of 1.8 m. The calorimeter did not contain any lading and was instrumented such that the total heat flux into various locations along its surface could be measured. Detailed descriptions and drawings of the calorimeter are provided in Section 4.6 in Supplement A and Section 2.5 in Supplement C.

Using the commonly used design concept for the double-plate type heat flux measurement devices, such as directional flame thermometers, the calorimeter was constructed with double shells made of stainless steel, and the annular space between the shells was filled with insulation materials. The hollow centre was also filled with insulation materials (Figure 1). Thermocouples were installed on the unexposed side of the outer shell and on the exposed side of the inner shell, and the differential temperatures of the two thermocouples along the same radius were used to calculate absorbed heat flux into the calorimeter. Details of the instrumentation and heat flux calculations are discussed in Section 9.5.7.

The performance of the calorimeter was tested in the preliminary testing. A second fully instrumented calorimeter was built to serve as a backup in case of failure of the first calorimeter. Both calorimeters were sent to the testing facility for Series 1-3 tests.



Figure 1 Calorimeter being instrumented with thermocouples on the outer shell and inner shell; and the hollow centre to be filled with insulation materials

7 Preliminary testing

Two preliminary tests using diesel and one test using heptane were conducted in FY2015/16. In the preliminary tests, the fuel was floated on top of water inside the pan. The preliminary tests were intended to verify operation of the fuel feed system and the calorimeter; and to optimize the test protocol. Details of the preliminary testing are provided in Supplement C. Preliminary test report.

The diesel (which was used during the preliminary tests as a substitute for crude oil) was contained in barrels with ball valves in the lid of the barrel. Ball valves were installed to minimize exposure of the fuel inside the barrel to the ambient surroundings. During the tests, the fuel was fed into the pan by the fuel feed system using a water displacement technique to retain light ends of the fuel until it reached the fuel pan. With lower rates of fuel flow, the fuel feed system successfully delivered the fuel. However, when relatively high fuel flow rates were experimented, the fuel barrel became over pressurized, which compromised the safety of the testing.

In the diesel fire tests, boilover was observed, likely due to the water substrate that was heated above its boiling point through the course of the combustion of the diesel fuel floating on top of the water layer.

From the preliminary tests, it was concluded that:

- 1) devising an automatic control of the fuel feed system was necessary for successful testing;
- 2) water substrate tended to cause boilover; and,
- 3) a suitable pressure vessel/tank should be used as a run tank to withstand higher pressures and to achieve adequate flow rates.

These conclusions from the preliminary testing formed recommendations that fed into the planning for the subsequent pool fire tests of Series 1-3.

8 Fuel characterization

In order to address fire effects of the properties of the fuel, fuel characterization was conducted in conjunction with the fire testing.

The fuel Sampling and Analysis Plan (SAP) was developed prior to the start of sample acquisition and testing. Supplement B. Crude oil Characterization report contains details of the SAP. The SAP provides fuel sampling techniques and laboratory analysis techniques required to characterize the fuels (heptane, Bakken and dilbit crude oil) that allow un-biased lab results by minimizing risks of losing light-end components and permitting acquisition of representative samples from the tanker. The methods are consistent with current best practices based on recent Transport Canada studies. The full report of crude oil characterization methods and results are included in Supplement B. Crude oil Characterization report.

In Series 1, heptane was chosen to be tested as a baseline for comparison with crude oils due to its compositional purity. Heptane samples were analysed mainly for a composition check. Density, heat of combustion, flashpoint and average molecular weight were also measured. The measured values compared well with reference database values.

In Series 2, Bakken crude oil was used for the testing. Bakken is unconventional light sweet crude oil which contains higher concentrations of dissolved gases and light-end, volatile hydrocarbons than average conventional crude oils. The tanker load of Bakken crude oil, acquired by SNL using a custom-built pressure tanker in summer 2017, was used by the United States Department of Energy (DOE) and United States Department of Transport (DOT) for crude oil pool fire and fire ball tests. Samples were taken at three points

during the project to ensure compositional consistency for the Bakken crude oil (i.e., to ensure no changes in the crude oil over time). The first fuel characterization sampling was conducted at the loading site under the DOE/DOT project, and two post-test samplings were conducted under this project. Under this project, Bakken crude oil samples were taken at the SNL burn site after homogenization and just prior to use in the first test (Bakken Event #4 prior to Test 2.3) and the last test (Bakken Event #6 prior to Test 2.6). For vapour pressure and compositional analyses, the above Bakken samples, were taken using closed cylinder sampling methods, compliant with GPA 2174 (Obtaining Liquid Hydrocarbons Samples for Analysis by Gas Chromatography).

For Series 3, it was decided to test a heavier crude oil to make a relative comparison with Bakken crude oil. Diluted bitumen (dilbit) was considered as it is known to be among the heaviest varieties of crude oil transported in Canada. To choose the most suitable type of dilbit crude oil for these fire tests, small-scale exploratory tests were performed with three different types of dilbit crude oil. Since dilbit is a heavy oil, there was concern that the residue remaining after burning could damage equipment within the testing facility. Also, dilbit crude oil can contain a small percentage of water which could result in a boil-over (fuel ejection from the pan). Thus, to assess the residue and potential for boil-over, exploratory tests were performed outdoors using a 0.5 m diameter pan. None of the dilbits displayed boilover, and the dilbit that resulted in the least amount of residue was selected for Series 3 tests.

Dilbit crude oil was acquired in pressure vessels (420-lb modified propane tanks) using a nitrogen displacement method to minimize loss of light ends in the crude oil. The first sampling for fuel characterization (dilbit #1) was conducted at the loading site by InnoTech Alberta, and two additional samplings were conducted under this project at the SNL burn site. The latter two dilbit crude oil samples were taken after homogenization and just prior to use in the first test (dilbit #2 prior to Test 3.1) and the last test (dilbit #3 prior to Test 3.6). The dilbit samples were taken using closed cylinder sampling methods, compliant with GPA 2174 (Obtaining Liquid Hydrocarbons Samples for Analysis by Gas Chromatography).

Post-test residue samples were taken from the pool fire pan after the first and last tests in both Series 2 and 3 for chemical analysis. The residue sample analyses are outside the scope of the current study.

Table 1 compares basic physical properties of the three fuels: heptane, Bakken and dilbit. Heats of combustion for the three fuels were similar across the three fuels, ranging from 43-48 MJ/kg. The diluted bitumen was the densest fuel tested, with a value of 923.9 kg/m³. The densities of heptane and Bakken crude oil were 687.6 and 810.9 kg/m³, respectively. Table 1 also shows the initial boiling point (IBP) analysed using gas chromatography (GC) (ASTM 8003 and ASTM 7169). The analyses of fuel compositions and boiling point distributions were conducted as per ASTM D8003 (Standard Test Method for Determination of Light Hydrocarbons and Cut Point Intervals in Live Crudes and Condensates by Gas Chromatography) and ASTM D7169 (Standard Test Method for Boiling Point Distribution of Samples with Residues Such as Crude Oils and Atmospheric and Vacuum Residues by High Temperature Gas Chromatography). The initial boiling point (IBP) determined by GC analysis is the temperature at which 0.5 wt% of the sample has eluted when determining the boiling range as defined in ASTM D7169 and API Recommended Practice 3000. Crude oil is included in the scope of this GC method used to determine IBP.

Detailed description and results are provided in Supplement B. Crude oil Characterization report.

Figure 2 shows chemical compositions of the Bakken and dilbit oil samples, which show wide distribution of carbon numbers for both types. Most notably, the dilbit crude oil contains a relatively large fraction of C₂₅₊, at approximately 29 mole% (Figure 2) and 60 mass% (Figure 3), whereas the Bakken crude oil contains C₂₅₊ of approximately 7 mole% (Figure 2) and 20 mass% (Figure 3). The results also show light-end components (e.g. ethane, methane and up to pentane) and low number hydrocarbons as well as benzene in the Bakken and dilbit crude oils. The whole oil compositions including light ends in Figure 2 showed little variation across all samples from Event #4 and Event #6 for the Bakken stored in the custom-built tanker. Also for the dilbit stored in the modified propane tanks, the results showed little variation across all samples from Event #1 to #3.

A range of the boiling points was identified for the different components of the fuels. As shown in Figure 3, each component of the Bakken and dilbit crude oil boils at a different temperature while pure heptane boils homogeneously at a single boiling point of 100°C. The higher the carbon number, the higher the boiling point. At a temperature of 300°C, the Bakken crude oil boils and burns off 60% mass, but to burn the same 60% mass, the dilbit crude oil needs to be heated to 510-530°C.

Table 1 Physical properties

Test Method			Heptane	Bakken	Dilbit
ASTM D8003 & ASTM D7169 merge	Initial Boiling Point	°F; °C		-44.0; -42.2	30.9; -0.6
ASTM D3828	Flash Point, Closed Cup	°F; °C		< -22; < -30	< -22; < -30
ASTM D5002M	Density @ 15°C	kg/m ³	687.5	805.9	923.9
ASTM D240	Heat of Combustion	MJ/kg	47.8	46.8	43.0

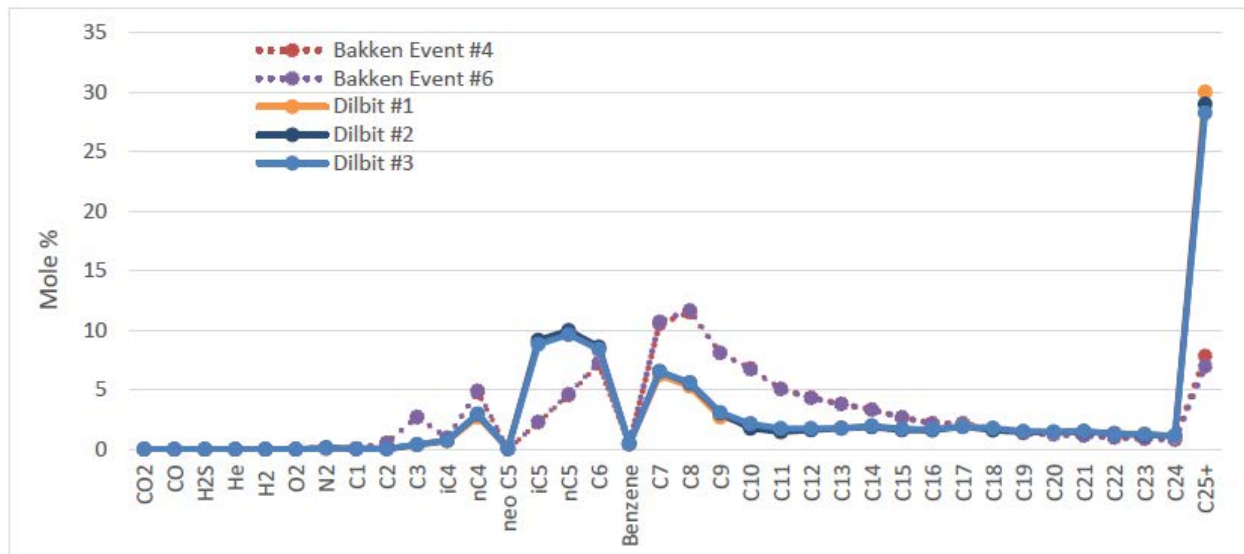


Figure 2 Whole oil carbon number plots for Bakken and dilbit oil sampled at the burn site.

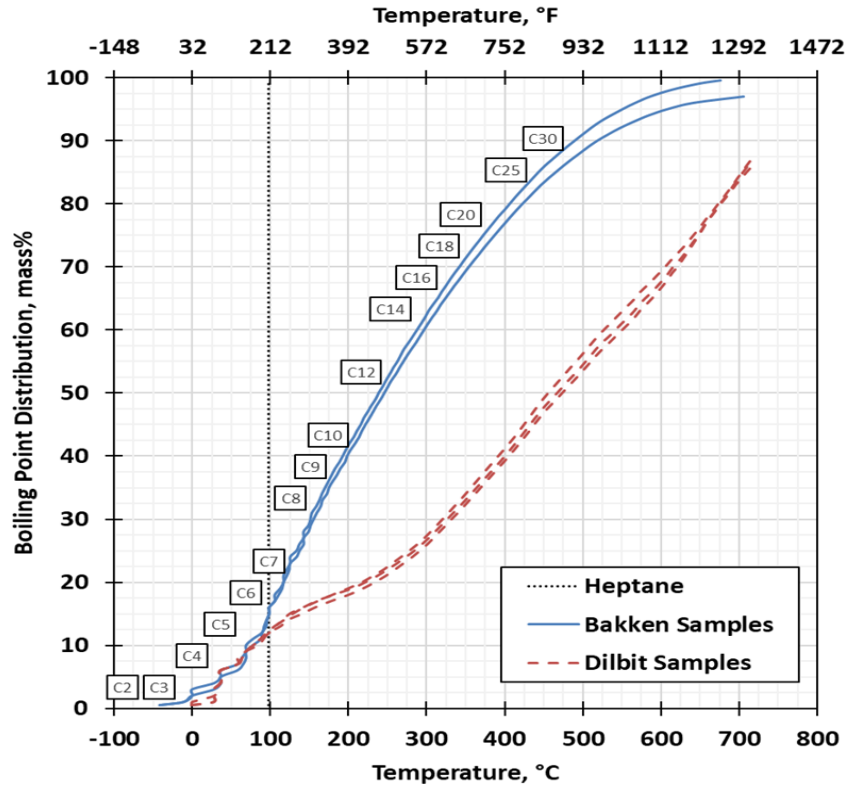


Figure 3 Temperature versus boiling point distribution for fuel samples

9 Fire Testing: Series 1, Series 2 and Series 3

The cylindrical calorimeter, representing a tank car at approximately 1/10th scale, was exposed to 2-m diameter pool fires. Fire experiments were conducted at SNL on behalf of the National Research Council of Canada (NRCC). This section provides a brief test description. Detailed test description and results are provided in Supplement A.

9.1 Test parameters

Heptane pool fire (Series 1) and crude oil fire (Series 2 and Series 3) experiments were conducted to examine the effects of the following parameters;

- Fuel type: Bakken crude oil and dilbit crude oil were primarily investigated. Heptane was also tested to provide baseline data against which Bakken and dilbit test results could be compared.
- Fuel feeding method: In most tests, fuel was supplied continuously through a fuel feed system maintaining a constant fuel level in the pan. In one test in each of Series 2 and Series 3, crude oil was allowed to burn down rather than maintain a constant fuel level.
- Supply fuel temperature: Both crude oils and heptane were prepared at two different initial temperatures of 20°C and 60°C to investigate the effect of the supply fuel temperature on the burning mechanisms.
- Presence of the cylindrical object: The focus of the testing was on examining the heat exposure experienced by a cylindrical object engulfed in the pool fire. However, pool fires without an object were also tested to examine the effect of the presence of the object on fire characteristics.
- Placement of the cylindrical object: The testing was conducted with the calorimeter at two different elevations above the fuel surface.

Table 2 shows the test matrix. Although tests were initially planned to be conducted in numerical order, technical considerations resulted in the tests being re-ordered. They were conducted in the order they are listed in Table 2.

Table 2 Test matrix

Test #	Fuel	Calorimeter Elevation (m)	Sampling	Fuel Supply Temperature (°C)	Fuel Feed Method
Test series 1					
1.1	Heptane	1-m, centered	fuel sampling	20 ± 5	Constant Level
1.2	Heptane	no calorimeter	N/A	20 ± 5	Constant Level
1.3	Heptane	1-m, centered	N/A	60 ± 5	Constant Level
Test series 2					
2.3	Bakken	1-m, centered	Pre-test fuel and post-test residue sampling	20 ± 5	Constant Level
2.4	Bakken	1-m, centered	N/A	60 ± 5	Constant Level
2.5	Bakken	1-m, centered	N/A	20 ± 5	Constant Level
2.1	Bakken	no calorimeter	N/A	20 ± 5	Constant Level
2.2	Bakken	0.5-m, centered	N/A	20 ± 5	Constant Level
2.6	Bakken	no calorimeter	Pre-test fuel and post-test residue sampling	20 ± 5	Non-continuous fuel feed, allow to burn down

Test series 3					
3.1	Dilbit	1-m, centered	Pre-test fuel and post-test residue sampling	20 ± 5	Constant Level
3.2	Dilbit	0.5-m, centered	N/A	20 ± 5	Constant Level
3.3	Dilbit	no calorimeter	N/A	20 ± 5	Constant Level
3.4	Dilbit	no calorimeter	N/A	20 ± 5	Non-continuous fuel feed, allow to burn down
3.5	Dilbit	1-m, centered	N/A	20 ± 5	Constant Level
3.6	Dilbit	1-m, centered	Pre-test fuel and post-test residue sampling	60 ± 5	Constant Level

9.2 Fuel handling and fuel feed systems

9.2.1 Heptane (Series 1 tests)

Nine drums of heptane, each with a 189.3 liters (50 gallon) capacity, were sourced for Series 1 fire tests. Series 1 fire tests served as a baseline for comparison with crude oil tests. Heptane was chosen for this series of tests because it is a widely-studied, readily-available fuel. Three heptane pool fire tests were conducted with and without the calorimeter in place and at two different fuel temperatures. The results of the heptane tests were compared to Bakken and dilbit crude oil tests conducted under the same conditions to determine the effect of fuel type.

Heptane was pumped from the drums through a heat exchanger into the fuel pan. An automated fuel feed system was used to continuously supply the fuel and maintain a constant fuel level in the pan. The mass loss rate from the pool was measured by a load cell placed under the heptane drums.

9.2.2 Bakken crude oil (Series 2 tests)

Bakken crude oil from North Dakota was used in Series 2 fire tests. Bakken crude oil is an unconventional light sweet crude oil from tight-oil formations, which is known to contain higher concentrations of dissolved gases and light-end, volatile hydrocarbons.

Bakken crude oil was sourced from North Dakota by SNL in summer 2017 for the DOE/DOT crude oil project. Bakken crude oil (a total load of 7,949 liters (2,100 gallons)) was collected in a pressurized tanker, which was custom-designed by SNL to preserve the light ends of the oil. At the North Dakota loading site, a water displacement method was used in the collection of the Bakken oil into the tanker in order to ensure there is no contact between the fuel and air during the loading. By making up the balance of volume within tanker with water rather than air, the water displacement method also enabled the preservation of the light ends concentration of the fuel and kept the light ends in the liquid state.

The collected Bakken crude oil in the tanker was transported to the fire testing site. A total of 2,040 liters (539 gallons) of Bakken crude oil was used in Series 2 tests. Prior to the testing, the Bakken crude oil was mixed to minimize density stratification.

In parallel with conducting the pool fire testing, a fuel Sampling and Analysis Plan (SAP) was established. The SAP detailed the required sampling and analysis methods for characterization of the fuels. It included collection of pre-test fuel samples of the crude oil and post-test samples of the residue for analysis and characterization. Based on the SAP, fuel samples were collected at the loading site and prior to the first and last tests to monitor for potential changes over time in the composition of the crude oil stored in the pressurized tanker.

By injecting water into the tanker, Bakken crude oil was pushed out from the tanker and fed through the heat exchanger to the fuel pan. The fuel flow rate was controlled to maintain a constant fuel level in the pan. The mass loss rate of the fuel in the pan was calculated from the water supply rate to the tanker.

9.2.3 Dilbit crude oil (Series 3)

Tests were conducted in Series 3 using dilbit, which was delivered in a total of 10 tanks (420-lb (190-kg) modified propane cylinders), each containing approximately 360 liters (95 gallons) of the dilbit crude oil. In each test, one tank was used. Two dilbit samples for fuel characterization were taken after homogenization and prior to use in the first test (Test 3.1) and the last test (Test 3.6).

Dilbit crude oil was pushed out of a tank by injecting compressed nitrogen to the tank, and the fuel was fed through a heat exchanger to the fuel pan. In each test, the fuel feed system supplied dilbit for about 30 minutes. After 30 minutes, Jet A was supplied to the pan for approximately 5-10 minutes to flush oil out of the transfer lines. The cleaning of the fuel lines with Jet A was only conducted in Series 3 tests to help with anticipated cleanup efforts since dilbit left significant post-test residue compared to Bakken and heptane.

9.3 Testing facility

The 2-m pool fire tests were conducted in the Fire Laboratory for Accreditation of Models and Experiments (FLAME) test cell at SNL, which is cylindrical in shape, 18.3 m diameter with a height of 12.2 m (see Supplement A-Figure 2-1). This facility is designed to provide well-controlled conditions with minimal meteorological impacts. Air for fire experiments is supplied from a large underground ventilation channel system through the floor, which is made of steel grating.

The FLAME facility has a large hood system that can collect all the combustion products from a fire in the test cell and measure Heat Release Rate (HRR) using the method of oxygen consumption calorimetry.

9.4 Test set up

Figure 4 shows the test set-up in the testing facility. A 2-m diameter pan was placed at the centre of the floor in the testing facility. The fuel pan used for all three test series was 0.3 m (12") deep, which allowed for a distance between the top of the fuel surface and the top of the pan edge to be a height of approximately 0.27 m (10.5"). In each test, fuel burning was contained in the pan, and boilover was not observed during any test. Use of any substrate in the pan was avoided in an effort to prevent boilover.

The 0.3 m diameter by 1.8 m length calorimeter was centred in the pan, above the fuel surface. The calorimeter was held above the pan by placing two supports in the pan. The height of the supports was adjustable and the supports were designed to have minimal impact on the flow of the fuel entering the pan during the tests.

Figure 5 shows the calorimeter instrumentation. Thermocouples were installed on three cross-sectional planes (Figure 5-a), and at each measurement plane, thermocouples were installed along eight different radial directions (Figure 5-b).

The fuel pan was continuously supplied with fuel to make sure that the fire characteristics included the effects of light-end components in the fuel.

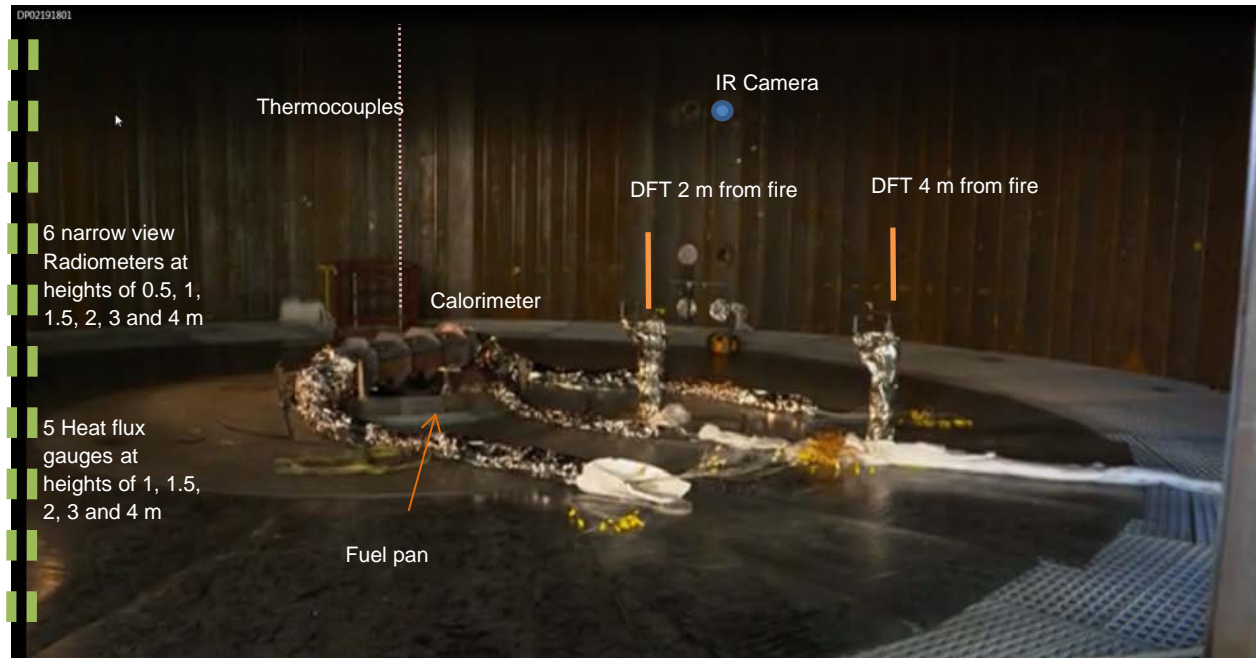
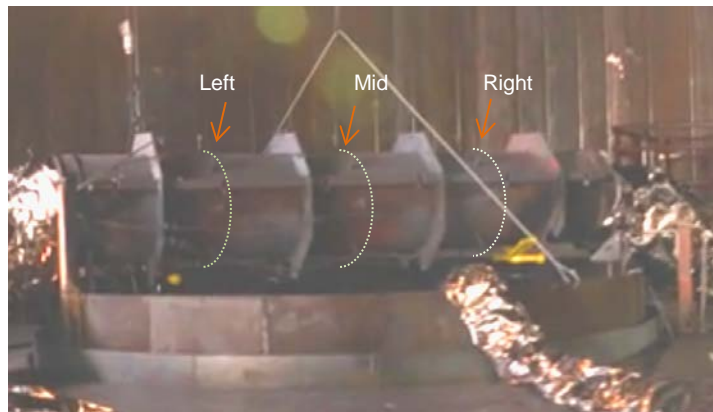
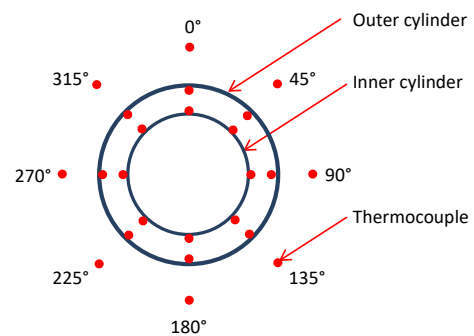


Figure 4 Test set-up



(a) Three measurement planes



(b) Thermocouple locations at each plane

Figure 5 Calorimeter instrumentation

9.5 Measurements

Data on heat release rate (HRR), fuel mass burn rate, flame/plume temperature and flame height were collected for fire characterization. Flame surface emissive power (SEP) and heat flux at a distance from fire were also measured. Using the calorimeter, total heat flux on the calorimeter was estimated. Supplement A, Section 4 contains details of the instrumentation.

9.5.1 Heat Release Rates (HRR)

The heat release rate (HRR) is an essential fire characteristic to describe the size of a fire in terms of rates of heat release from combustion reactions of a material [4]. In the case of a pool fire, the HRR is proportional to the heat of combustion of the fuel and fuel mass burning rate, which is proportional to the area of the pool. The HRR governs the flame height, and HRR also correlates with other fire characteristics, such as heat fluxes [2, 3].

In this study, two methods were used to determine HRR; 1) based on the mass burning rates measured during the tests and 2) by oxygen consumption calorimetry.

The HRRs (Q) can be measured based on the mass burning rates (\dot{m}_b) by Eq 1, using the complete heat of combustion (H_c). The complete heat of combustion (H_c) is the heat release from combustion of a unit quantity of a fuel, often measured in an idealised condition using oxygen bomb calorimetry (ASTM D240). The complete heat of combustion was identified for heptane, Bakken and dilbit crude oil in the fuel characterization study (see Supplement B. Crude oil Characterization report). It should be noted that combustion in air (even in abundant air) involves a certain portion of incomplete combustion. This incomplete combustion results in slightly less heat being released than in complete combustion; this is due to the generation of some partially oxidized species, such as carbon monoxide, along with other unburned volatiles and non-condensable hydrocarbons. Thus, to take into account incomplete combustion in the pool fire, an incomplete combustion factor (x) is used in the HRR calculation based on the mass burning rate. A value suggested by Tewarson [5] for heptane is approximately 0.9 and gasoline is also 0.9. This study found a value of 0.9 to be appropriate for heptane and Bakken crude oil based on the HRR calculated using oxygen consumption calorimetry (see Section 10.4). A value of 0.9 was also used for the dilbit pool fires (although there was insufficient data to verify the accuracy of this value for dilbit).

$$Q = x H_c \dot{m}_b \quad \text{Eq 1}$$

Additional measurements of HRRs (Q) were made based on oxygen consumption calorimetry, which calculates HRRs of fire by measuring the amount of oxygen consumed in the combustion process because a similar level of heat (E_{O_2}) is released per unit mass of oxygen consumed in the combustion of most organic materials [6]. A simplified equation for oxygen consumption calorimetry is given in Eq 2. The oxygen consumption calorimetry method estimates more accurate and reliable HRRs than the burning rate method because the calculation incorporates corrections for potential incomplete combustion. In Eq 2, ϕ is the oxygen depletion factor, and $\dot{m}_{O_2}^0$ is the mass flow rate of oxygen in air. To account for the difference (E_{CO}) in heat released due to carbon monoxide formation during the combustion process, the fraction (f) of oxygen used for carbon monoxide formation is incorporated in the method. The method requires a hood and duct system, which collects all combustion products (smoke) and measures flow rates of smoke and gas concentrations of oxygen, carbon monoxide and carbon dioxide. The FLAME facility was equipped with a large hood system that was instrumented to measure the flow rates of smoke, smoke temperatures and gas concentrations of oxygen, carbon monoxide and carbon dioxide. The collected data in the hood system were used to calculate HRRs. HRRs (Q) were evaluated for all Series 1 and 2 tests but not for all Series 3 tests due to problems in the gas analyser used to measure gas concentrations in the hood system. The complete calculation equations are given in Supplement A. Test Report – Section A.2.

$$Q = E_{O_2}(1 + f)(\phi \dot{m}_{O_2}^0) - E_{CO}f(\phi \dot{m}_{O_2}^0) \quad \text{Eq 2}$$

The total HRR of a pool fire is released mainly in the form of convection (i.e. thermal convective plume of combustion products) and radiation [2, 4], since the conduction loss is negligible when a steady-state is achieved for a pool fire condition.

Analysing the portions of the convective and radiative heat release is useful to understand mechanisms of heat transfer from a fire. The fraction of total combustion energy resulting in thermal radiation is particularly important in assessing the potential radiative hazards posed by hydrocarbon fuel pool fires (e.g. incident heat fluxes to external objects (see Section 9.5.6) and to engulfed objects (see Section 9.5.7)). The heat transfer to the tank car from a large-scale hydrocarbon pool fire is mainly by thermal radiation, and for large scale rail tank cars engulfed in fire, the heat transfer is about 90% by thermal radiation and 10% by convection [7]. Thus, quantifying the radiative heat release rate is important in understanding the heat transfer, and thus hazard, to the tank car [8]. Characterizing the convective component of the total HRR also becomes important in predicting the plume development and smoke temperature.

The portion of the heat released in the form of convection (convective HRR, or Q_c) can be estimated based on the temperature rise of the gas in the duct since the gas temperature rise is attributed to the convective heat [9]. For hydrocarbon pool fires up to roughly four meters in diameter, the fraction of radiative heat (X_r) is between 0.30 and 0.50, and this value decreases with increasing fire diameter due to smoke obscuration [2]. As suggested by Janssens [9], the convective portion of the heat can be calculated using the duct data of mass flow rate of the gas (\dot{m}_e) and temperature rise (ΔT) of the gas, as shown in Eq 3, and then the fraction of radiative heat (X_r) can be obtained using the measured total HRR (Q), as shown in Eq 4. In all Series 1-3 tests, the duct data of mass flow rate of the gas (\dot{m}_e) and temperature rise (ΔT) of the gas were collected so that convective HRR (Q_c) was obtained for each test.

$$Q_c = (1 - X_r)Q = C_p \dot{m}_e \Delta T \quad \text{Eq 3}$$

$$X_r = 1 - Q_c/Q \quad \text{Eq 4}$$

9.5.2 Mass burning rates

The mass burning rate was measured and used to provide a secondary estimate of the HRR of the fire. The mass burning rate of the fuel was determined based on the fuel flow rate. The rate of fuel flow was adjusted during the test to maintain a constant height of the fuel in the pan. The height of the fuel in the pan was monitored using a differential pressure gauge, and a liquid float was also used to ensure constant fuel level in the pan. Bakken crude oil was supplied into the pan by feeding water into the bottom of the pressurized tanker, and the flow rate of water was measured by load cells. The mass burning rate of the Bakken crude oil was determined based on the measured water flow rates supplied to the tanker. For heptane and dilbit crude oil, the mass burning rates were measured by the load cell placed under the heptane drums and the dilbit tank.

9.5.3 Flame/plume temperatures

A mid-wave infrared (MWIR) camera was used to measure flame temperature. The infrared (IR) camera was installed at the second level on the wall of the testing facility as shown in Figure 4. At this location, the camera provided a 7 m by 4 m view of the fire.

Flame/plume temperatures were also measured along the centre line of the pool as shown in Figure 4. Nine thermocouples were installed above the calorimeter at 0.5 m spacing.

9.5.4 Flame height

Flame heights were measured using the MWIR camera or the real-time camera by getting a time-averaged image of the flame.

9.5.5 Surface emissive power on the flame

The total HRR of a pool fire is released mainly in the form of convection (i.e. thermal convective plume of combustion products) and radiation [2, 4]. The radiation heat in large hydrocarbon fires is emitted mainly through the soot, water vapor and carbon dioxide [10]. As discussed in Section 9.5.1, in order to analyse the radiative hazards surrounding a fire, it is essential to characterize radiative properties of the flame, including the Surface Emissive Power (SEP). The SEP is the intensity of radiation energy emitted from the flame at the flame surface, which depends on fuel type/composition, fire size, soot production and flame temperature. The SEP of the flame was measured using various devices in the tests; narrow-view radiometers and a spectral imaging radiometer (IR camera) were installed in the test facility.

Six narrow-view radiometers were mounted on the wall of the testing facility at a distance of 9 m (30') and at heights of 0.5, 1, 1.5, 2, 3 and 4 m to measure the surface emissive power of the flame. The radiometers are designed to be sensitive only to the radiative heat flux, and due to the narrow view angle of 5.5 degrees (translating to a spot diameter of approximately 0.8 m on the fire), the radiometer has the potential to measure directional radiances within the view angle on the flame.

A MWIR camera was used as a spectral imaging radiometer to collect infrared radiation with wavelengths between 3 and 5 μm . The radiation from typical flames with high temperatures is emitted mainly in this range of wavelengths [11]. Using the data obtained from the IR camera, the SEP was calculated over the entire flame surface. Supplement A, Section 4.2 and Appendix A.3 contain details of the IR camera and data processing for the calculation of the SEP.

9.5.6 Heat flux at a distance from fire

Measurements of heat flux are important for assessing the overall hazards of a fire including analysing the radiative hazards surrounding a fire. To assess the level of heat flux imposed on objects near a fire, directional flame thermometers (DFT) and wide-view total heat flux gauges were used. The measurement is useful, for example, in assessing whether the flame provides sufficient radiant heat to ignite nearby combustible items. Incident radiant heats to a target depend mainly on the emissive power of the flame and decrease with distance from the flame.

Five total heat flux gauges were mounted on the wall of the testing facility at a distance of 9 m from the center of the pan, at heights of 1, 1.5, 2, 3 and 4 m. The view angle of the total heat flux gauges was 180 degrees, so the measurements were evaluated in terms of the total heat flux that could be received by an object at the same location and with the same orientation.

Two DFTs were placed at a height of 1 m and at distances of 2 and 4 m from the pan centre, as shown in Figure 4. A DFT consists of two Inconel plates sandwiching an insulation blanket in between, and it measures temperatures at the unexposed side of each plate. The differential temperatures measured between the two plates enable the calculation of the heat absorbed. A commercially available code, IHCP1D, developed by Beck [12], was used for one-dimensional inverse heat conduction analysis. Using the absorbed heat calculated by IHCP1D, the total incident heat flux to the surface of each device was estimated. Supplement A, Appendix A.1 contains details of the estimation of the total incident heat flux to the DFTs.

9.5.7 Total heat flux to an engulfed object (measurements by the calorimeter)

NRC designed and manufactured two calorimeters for use in the fire testing. Both calorimeters were instrumented with thermocouples such that the heat flux to various locations along its surface could be measured. Figure 4 shows the calorimeter placed in the test set-up, and Figure 5 shows the calorimeter instrumentation. The temperature data collected from the calorimeter was used for calculations of total heat flux (q_{total}) on the outer surface of the calorimeter. The total heat flux (q_{total}) is transferred from the flame to the calorimeter surface by radiation ($\alpha q_{incident}$) and convection ($q_{convection}$). Then, the transferred heat is either absorbed ($q_{absorbed}$) into the calorimeter or emitted ($q_{emitted}$) from the heated surface of the calorimeter. Eq 5 shows the calculation method of the total heat flux (q_{total}).

$$q_{total} = \alpha q_{incident} + q_{convection} = q_{absorbed} + q_{emitted} \quad \text{Eq 5}$$

Where $q_{emitted} = \epsilon \sigma T_{surface}^4$

α = absorptivity

ϵ = emissivity

$T_{surface}$ = Surface temperature of the outer shell

σ = Stefan-Boltzmann constant ($5.67 \times 10^{-8} \text{ W m}^{-2} \text{ K}^{-4}$)

The calorimeter measured temperatures on the unexposed side of the outer shell and on the exposed side of the inner shell. The differential temperatures measured between the outer and inner shells along the same radius were used to calculate the heat absorbed ($q_{absorbed}$) by the calorimeter at the measurement position. The absorbed heat ($q_{absorbed}$) was calculated at each measurement position by one-dimensional inverse heat conduction analysis using a commercially available code, IHCP1D, developed by Beck [12]. The surface temperature ($T_{surface}$) of the exposed side of the outer shell was also calculated using IHCP1D.

Using the surface temperatures and an emissivity of 0.795, which was measured on the surface of the calorimeter, the radiative heat emitted ($q_{emitted}$) from the surface of the heated calorimeter was estimated. The radiant emissive power is largely proportional to the fourth power of the temperature but also affected by the surface characteristics of the emitter. The emissivity describes the effectiveness of the surface of a material in emitting energy in terms of radiation. Thermal radiation transport can be described as energy exchanges through electromagnetic waves between emitters and absorbers. Thus, the surface characteristics of a material, such as roughness/smoothness/reflectiveness, affects the effectiveness in reflecting and absorbing electromagnetic waves. A perfect emitter (e.g. a black body) has an emissivity of 1, and gas-soot mixtures have emissivities close to 1.

Then, the total heat flux (q_{total}) to the calorimeter was estimated by summing the absorbed heat ($q_{absorbed}$) and the emitted heat ($q_{emitted}$) from the calorimeter surface. Supplement A, Appendix A.1 shows the detailed equation used for the calculation of the total heat flux to the calorimeter and the thermal properties of the materials used in the calculations. Based on the calculated values of the total heat flux to the calorimeter, incident heat fluxes on the outer surface of the calorimeter could be approximated by assuming the convective flux from the flame to the calorimeter ($q_{convective}$) is trivial compared to the incident heat flux ($q_{incident}$) since the calorimeter is immersed in the flame.

10 Fire Test Results and Discussion

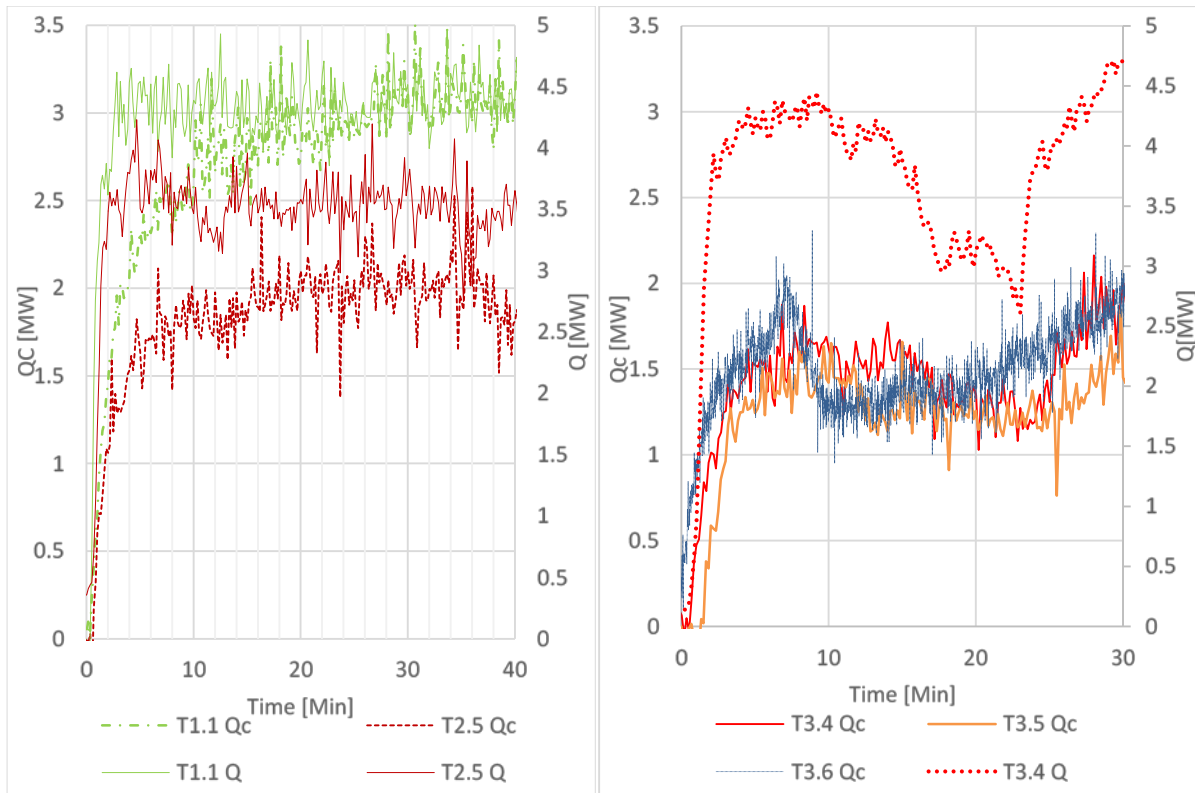
Fire characteristics including HRR, mass burning rates, flame heights and surface emissive power on the flame were measured for the 2-m diameter heptane, Bakken and dilbit crude oil fires in Series 1, Series 2 and Series 3, respectively. The total heat flux received by the calorimeter and the incident heat flux outside the fire were also measured. This section discusses highlights of test results and comparisons between equivalent tests for the measured fire characteristics. Detailed test results for all tests in Series 1-3 are provided in Supplement A. Test Report. Conclusions from the findings and recommendations for future analysis are provided in Section 11 and 12, respectively.

10.1 Overall burning behavior

Overall, Bakken crude oil and heptane fires reached steady-state burning within about 5-10 minutes after ignition and thereafter displayed continuous steady burning throughout the test. In contrast to the Bakken and heptane pool fires, the dilbit crude oil fires displayed unsteady burning behaviour in which the burning rates changed over the burn time. For example, as illustrated in Figure 6 (a), the HRR by Eq 2 (Q) and convective HRR (Q_c) by Eq 3 from T 1.1 and T2.5 (equivalent tests where each type of fuel had a calorimeter at 1 m above the fuel surface) displayed continuous steady burning. Similar steady burning behaviours were found in other heptane and Bakken tests (see Supplement A Section 6.1 and 6.2).

Due to the variation in the burning rate, the HRRs measured in the dilbit tests displayed high values initially, then decreased followed by a subsequent increase. In Test 3.4, starting at approximately 10 minutes, HRRs measured by the hood system (by Eq 2) decreased by 30% and then increased. The convective HRR in Test 3.4 also displayed similar profiles with a decrease of approximately 30%. Since HRRs by the hood system (by Eq 2) were not measured in other dilbit fire tests, the calculated convective HRRs (by Eq 3) were investigated, and a similar level of decrease in the convective HRRs was found for all the dilbit crude oil fire tests. Figure 6 (b) illustrates the non-steady burning behaviour in some of the dilbit tests. The measured flame height and flame SEP by the narrow-view radiometers also displayed similar time-varying profiles for the dilbit crude oil fires.

The total mass of residual materials remaining in the pan after each fire test was measured in the Bakken and dilbit crude oil tests. Dry and brittle solid residue with a total amount of about 0.7-0.8 kg, which is 0.2-0.4% of the total fuel mass supplied for the tests, was found after the Bakken pool fire tests. Much greater amounts of post-burn residue remained after the dilbit pool fire tests. Porous solid residue with amounts of 28-40 kg, which is 11-18% of the total fuel mass supplied for each test, remained in the pan after the dilbit tests.



(a) Heptane and Bakken

(b) Dilbit

Figure 6 HRR (Q) and convective HRR (Qc) measured in the heptane, Bakken and dilbit tests

As discussed, the overall burning behaviour was affected mostly by the fuel type among the parameters tested.

The averaged test data are summarized in Table 3. The test data obtained from Series 1 and 2 tests were averaged based on the steady-state time period in each test. Due to the variable burning behaviour in Series 3 tests; however, the test data from Series 3 were averaged by integrating the data over time and then dividing by the same time. Supplement A. Test Report provides details on how and over what time periods these average test data were obtained for each test. The following sub-sections discuss these average measurements of the fire characteristics (e.g. mass burn rates, flame height, HRR, Flame temperature, SEP, Calorimeter measurements and DFT measurements).

10.2 Mass burning rates

10.2.1 Burning behavior and fuel characteristics

The non-steady burning behaviour of the dilbit pool fires was mainly caused by the fuel composition, which involves a blend of heavy bitumen and lighter condensate, and contains a larger fraction of heavy end hydrocarbons than the Bakken crude oil and heptane. The Bakken crude oil consists of approximately 20 mass% C25+, whereas the dilbit crude oil consists of 60 mass% C25+ (as shown in Figure 3). As discussed in Section 8, each component of the Bakken and dilbit crude oils boils at a different temperature unlike pure heptane (see Figure 3). As a consequence of having various boiling temperatures, multi-component fuels are

expected to undergo multi-vaporization processes, which would result in distillation of light ends and gradual pyrolysis of heavy ends in pool fires. Containing 60 mass% C25+, whose boiling points are greater than 400°C, the dilbit crude oil fire is expected to undergo more gradual burning than the Bakken crude oil fire, in which 80% of its mass boils and burns off within the temperature range less than 400°C.

The variation in the mass burning rate over time affected the flame height and heat release rate, which displayed time-varying profiles for dilbit. Also, the time-varying behaviour was reflected in the measurements of flame SEP by the narrow view radiometers (see Supplement A, Section 6.3 and Section 7.2.3). Although more analysis is needed to allow firm conclusions to be drawn, it is presumed that the decrease in burning rate for dilbit was caused by the fact that vaporizing the heavy ends requires large amounts of energy to be transferred to the fuel in the pan through the heat feedback from the flame. In addition to the energy required for vaporization of heavy ends, the heavy ends also require the absorption of large amounts of energy for their pyrolysis. These two requirements for energy potentially contributed to the lag in heavy-ends boiling and the drop in the burning rate in the middle of the testing.

10.2.2 Parameter impact on mass burn rate

The measured average mass burning rates were 0.03 kg/m²s for Bakken crude oil fires and 0.04 kg/m²s for heptane fires without the presence of the calorimeter. Significant variation in the burn rates was observed in all dilbit crude oil tests. The burn rate averaged among all the dilbit tests is 0.02 kg/m²s, but the value varied from 0.005-0.060 kg/m²s (over the course of all fire tests). The average burn rate measured in each test is provided in Table 3, and for the dilbit tests, two values are provided for different periods in which a burn rate could be identified.

When the calorimeter was placed over the pool, the mass burning rate was reduced by 10-15% in the heptane and Bakken crude oil tests. The burning rate of a liquid pool fire is known to be affected by the radiation heat feedback from the flame to the fuel surface. The reduction in the mass burning rate observed in the tests with the calorimeter was in part caused by the cylindrical object which partially obstructed the radiation feedback from the flame to the fuel surface, although this would be counteracted by radiation from the heated calorimeter to the fuel surface.

The higher fuel temperature also increased the burn rate by approximately 10% in the heptane and Bakken crude oil tests. Allowing the fuel to burn down did not affect the mass burn rate.

Nonetheless, the impact of the presence of the calorimeter, initial fuel supply temperature and fuel feed methods on burning rates is not discernible outside the measurement uncertainty because of the inherently variable burning behaviour of pool fires. It was particularly difficult to detect the impact of the test parameters in the dilbit crude oil tests, due to the highly variable burn rate.

10.3 Flame heights

The 2-m diameter Bakken crude oil pool fire established a large flame over the pool with an average height of 4.3-4.5 m, observed in all Series 2 tests. Flame heights measured in Series 2 (Bakken crude oil tests) were somewhat shorter than the average flame heights of 5.6 - 6.8 m measured in Series 1 (heptane tests). The dilbit crude oil pool fires resulted in the shortest flame among the fuels tested, with an average height of 3.4-3.6 m.

The flame size of crude oil pool fires provides useful information in assessing the hazards around the fire, for example whether or not there would be fire spread to combustible items nearby the flame. While incident radiant heat to a target depends mainly on the distance from the flame and the emissive power of the flame, it

can be better estimated by taking into account the flame size and shape. The flame is often represented as a rectangular sheet, cylinder or cone, so that approximate view factors/configuration factors can be evaluated to better estimate the incident radiation heat to a target.

Among the parameters tested, the fuel type had the largest effect on the flame height. This is because the flame height is governed by the HRR, which is influenced by the mass burning rate and the heat of combustion of the fuel, both of which are also influenced by the fuel type. This will be further discussed below.

10.4 Heat release rates

10.4.1 Heat release rate measurement verification

The HRRs were calculated by two methods; (1) by measuring the mass burning rate of the fuel and (2) by analysing the combustion products using oxygen consumption calorimetry. The theoretical maximum heats that can be generated from the pool fires were calculated based on the mass burning rates and the complete heat of combustion (H_c), as per Eq 1 with $x=1$. The HRR values calculated based on mass burning rate in the heptane and Bakken fire tests were an average of approximately 10% greater than the HRRs calculated based on oxygen consumption calorimetry (see Table 3 for the value calculated for each test and Section 7.7 in Supplement A). This indicates that the incomplete combustion factor x (combustion efficiency) found in the tests was approximately 0.9.

Figure 7 compares the HRR measured by the two methods for all tests. Using the flow rates of smoke, smoke temperatures and gas concentrations of oxygen, carbon monoxide and carbon dioxide measured in the hood system of the FLAME facility, HRRs were calculated by oxygen consumption calorimetry (Eq 2). The calculated HRRs by oxygen consumption calorimetry showed similar overall trends between tests to the HRRs calculated using mass burning rates by Eq 1 with $x=0.9$. It should be noted that the HRR data obtained from the hood system need checks for biases in oxygen concentration measurements and the resulting calculations of HRR. Overall, both methods of HRR calculation resulted in comparable HRRs in the heptane and Bakken crude oil tests. However, the gas analyser used to measure gas concentrations in the hood system failed in all dilbit fire tests except Test 3.4. Using the mass burning rates the HRRs were calculated for all dilbit tests; however, due to the highly variable mass burning rates, these values indicated large uncertainty (see Supplement A, Figure 8-1).

The average HRR measured in the exhaust hood using oxygen consumption calorimetry was 3.2-3.8 MW for Bakken crude oil tests and 4.4-5.4 MW for heptane tests with the calorimeter above. With no calorimeter, the measured HRR was 5.2 MW, 3.5-4.8 MW and 3.7 MW for heptane, Bakken and dilbit fire, respectively. It should be noted that the HRR of the dilbit crude oil fire cannot be fairly compared with that of the Bakken and heptane fires due to its different burning behaviour.

As discussed in Section 10.2.2, among the parameters tested, the effect of the fuel type was most apparent on the fuel mass burning rate, and consequently the effect of fuel type was also reflected on the HRR. The heptane fire tests resulted in relatively higher HRR than the Bakken and dilbit crude oil fires. With the calorimeter placed over the pool, the HRR was reduced in the heptane and Bakken crude oil tests because of the reduction in the mass burning rate.

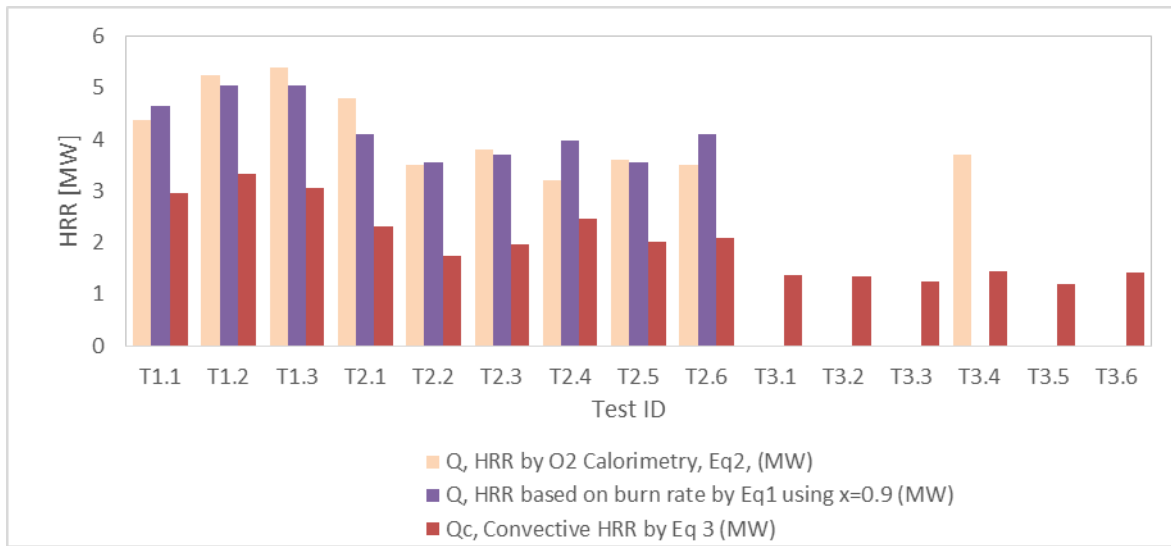


Figure 7 HRRs measured by oxygen consumption calorimetry and mass burning rates in comparison with convective HRRs

(Note that the HRR data obtained from the oxygen consumption calorimeter need checks for biases in oxygen concentration measurements and the resulting calculations of HRR. For Series 3, due to the variation in the mass burning rate, HRRs based on burning rate are not plotted.)

10.4.2 Convective and radiative heat release rate

As discussed in Section 9.5.1, the total HRR of a pool fire is released mainly in the form of convection and radiation. Differentiating the radiative and convective components of heat release from a fire helps to better understand the heat transfer from the flame.

The convective heat release rates (Q_c) were calculated for all tests by Eq 3, which uses smoke temperature and mass flow rate measured in the duct. A relatively consistent portion of heat is released by convection in the heptane (~60-65%) and Bakken crude oil (~50-60%) fire tests. In the dilbit crude oil tests, the measured convective HRRs were also consistent among the tests (1.2–1.5 MW), and the portion of heat released by convection was 0.39, which was evaluated for T3.4 with the HRR measured by the hood system. As shown in Figure 7, while the convective HRRs were similar among the six dilbit tests, the mass burning rates displayed large variability in Series 3 (see Table 3). The large variability in the burning behaviour makes it hard to compare Series 3 to Series 1 and Series 2.

Based on the convective HRRs, the radiative heat fraction (X_r) of the total HRR was calculated in each test as per Eq 3 and Eq 4 as discussed in Section 9.5.1. Figure 8 compares the radiative heat fractions calculated for the heptane, Bakken and dilbit crude oils. The radiative heat fraction (X_r) of the total heat released from the Bakken crude oil fires was slightly higher than that from the heptane fires. The average X_r values measured were approximately 0.46 and 0.36 for Bakken crude oil and heptane tests, respectively (see Figure 8). While these values of X_r were calculated using the HRR by mass burning rates (Eq1) in Series 1 and 2, the HRR by Eq 1 was not used for Series 3 due to the time-varying burning behaviour of the dilbit crude oil. The X_r value was calculated for the dilbit test based on the HRR measured by the hood calorimeter, and a value of 0.61 was obtained for Test 3.4. Further data analyses and confirmation of these X_r values are necessary, particularly for

the dilbit tests, given the time-varying behaviour (this is discussed further in Section 12 for suggested future studies).

The radiative heat fraction was only obtained from T3.4 in the dilbit tests, as shown in Figure 8, because the total HRR data was measured by the hood system (Eq 2) only in this test. Therefore, radiative HRRs were estimated alternatively based on average SEP, which was measured in all dilbit tests, rather than reducing from the total HRR by the hood system. The radiative HRR was estimated by multiplying the average SEP by the flame surface area. The flame surface area was approximated using the rectangular flame shape assumption [13]. In Figure 9, the calculated radiative HRRs based on the mean SEP are plotted against the measured convective HRR. It should be noted that the calculated radiative HRR is an approximated value. Then, the ratio (Q_r/Q_c) of the radiative HRR to the convective HRR was explored since characterizing radiative and convective heat release is important for hazard analyses, as discussed in Section 9.5.1, and this data could also be used for potential numerical modelling of the pool fires. The ratios (Q_r/Q_c) obtained are 0.49, 0.65 and 0.76, for the heptane, Bakken and dilbit crude oil fires, respectively. Thus, it can be inferred that the dilbit and Bakken crude oil fires released larger portions of heat in radiation than the heptane fires, and this is because they are expected to produce more soot than the heptane for the fuel compositions, as presented in Section 8. The chemical composition and structure of fuel affect the soot production during fire [2]. As found from the fuel composition analysis, the Bakken and dilbit crude oils contain a small amount of benzene and larger proportions of hydrocarbons with carbon numbers greater than the heptane (see Figure 2). This explains sootier flame produced from the crude oils since the main soot precursors, such as Polyaromatic hydrocarbons are generally formed due to the presence of long chain hydrocarbons, aromatics (e.g. benzene) and unsaturated compounds in the fuel composition.

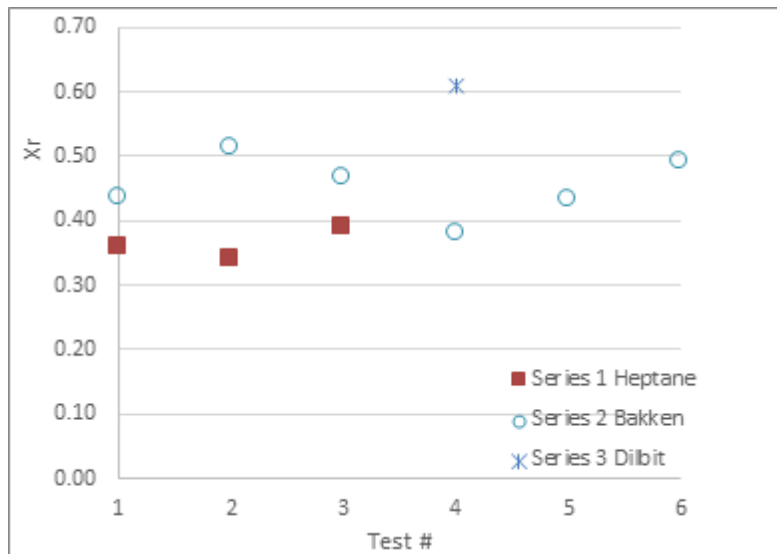


Figure 8 Radiative heat fractions

(For Series 1 and 2, the fractions were obtained by Eq 3 using HRR (Q) obtained based on mass burning rates (Eq 1). For Series 3, HRR (Q) measured by the calorimeter hood system (Eq 2) was used instead due to the variation in the mass burning rates in Series 3 tests)

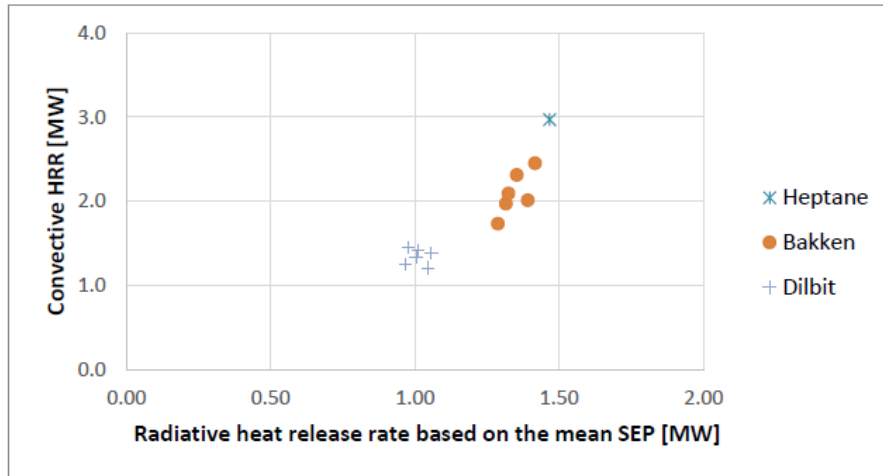


Figure 9 Radiative heat release rates compared with convective heat release rates

10.5 Flame temperature and surface emissive power

10.5.1 Measurement verification

The flame temperatures and surface emissive power (SEP) were measured by using the IR spectral imaging radiometer (based on the scanned infrared radiation from the flame). The narrow-view radiometers were also used to measure the SEP of the flame. The SEPs reduced from the IR camera measurements are in relative agreement with the values of SEP measured by the narrow-view radiometers [8], yet the IR camera was more effective in monitoring complete thermal profiles of the flame. When compared with the vertical profiles of the SEP along the pool centre line from the IR camera measurements, the spot measurements by the narrow-view radiometers were slightly lower due to its relatively large measurement area (0.8 m spot diameter) [8].

10.5.2 Vertical profiles of flame temperature and surface emissive power

Figure 10 shows fire plume temperature measured by the IR camera for heptane, Bakken and dilbit crude oil fires in Test 1.1, Test 2.3 and Test 3.5 (equivalent tests where each type of fuel had a calorimeter at 1 m above the fuel surface), respectively. As discussed in Section 9.5.1, since the flame height is strongly governed by the HRR [14], the flame height of the heptane fires was largest among the fuels tested due to the highest HRR of the heptane fires. The flame temperature above the pan is high for all fuels, and the flame temperature decreases with increasing height in the flame. The calorimeter was placed in the high temperature areas of the flame. In Supplement A. Test Report, Appendix A.3 shows the flame temperature and SEP along the centreline of the flame measured by the IR camera, and the maximum temperature and maximum SEP were observed in the lower part of the flame.

Like flame temperature, SEP gradually decreases along the height of the flame. Figure 11 shows the vertical SEP profiles along the centreline of the flame (as viewed in the image) measured in the fire tests of heptane

(T1.1), Bakken (T2.3) and dilbit (T3.5) crude oils. The vertical SEP profiles were plotted over relative elevation to the flame height (Z/l_f) of each (i.e. the elevation, Z , is from the floor, and l_f is the flame height), which enabled normalized comparisons among tests with different flame heights. In the lower part of the flame, the SEP displayed a steep increase with increasing elevation, showing low levels of SEP along the wall of the fuel pan and immediately above the top of the fuel pan, then rapidly reaching the maximum value. The maximum SEP along the centreline of the flame were observed in the lower part of the flame, specifically at 0.16 ± 0.01 m/m of Z/l_f in all Bakken and dilbit crude oil tests except the tests with the calorimeter at 0.5 m height. This suggests that the presence of the calorimeter in the fire at a height of 1 m did not affect the elevation where the maximum SEP was measured. With the calorimeter at a height of 0.5 m, the maximum SEP were measured at 0.18 m/m and 0.12 m/m of Z/l_f , for Bakken (Test 2.2) and dilbit (Test 3.2) tests, respectively. The average value found for all Bakken fire and dilbit fire was 0.16 ± 0.01 m/m of Z/l_f . For the heptane test (Test 1.1), the maximum centreline SEP were measured at 0.23 m/m of Z/l_f .

The IR camera measurements are based on line of sight from the fire to the camera and are affected by the optical thickness of the flame as well as radiation from the heated calorimeter, making it difficult to draw conclusions about heat transfer from the fire to the calorimeter. The vertical variance in the lower part of the flame could potentially affect the total heat flux from the fire to an external target, depending on the size, location and orientation of the target.

For all Bakken and dilbit tests, the vertical placement of the calorimeter was identified relative to the flame SEP profile, and the two calorimeter elevations of 0.5 m and 1.0 m used in the tests were relatively close to the height at which the maximum SEP along the centreline of the flame was measured. For the crude oil tests, the height of the calorimeter was 0.26 m/m and 0.13 m/m of Z/l_f , for the height 1 m and 0.5 m, respectively. In the heptane test (T1.1), the calorimeter was placed at 1.0 m, which was 0.18 m/m of Z/l_f .

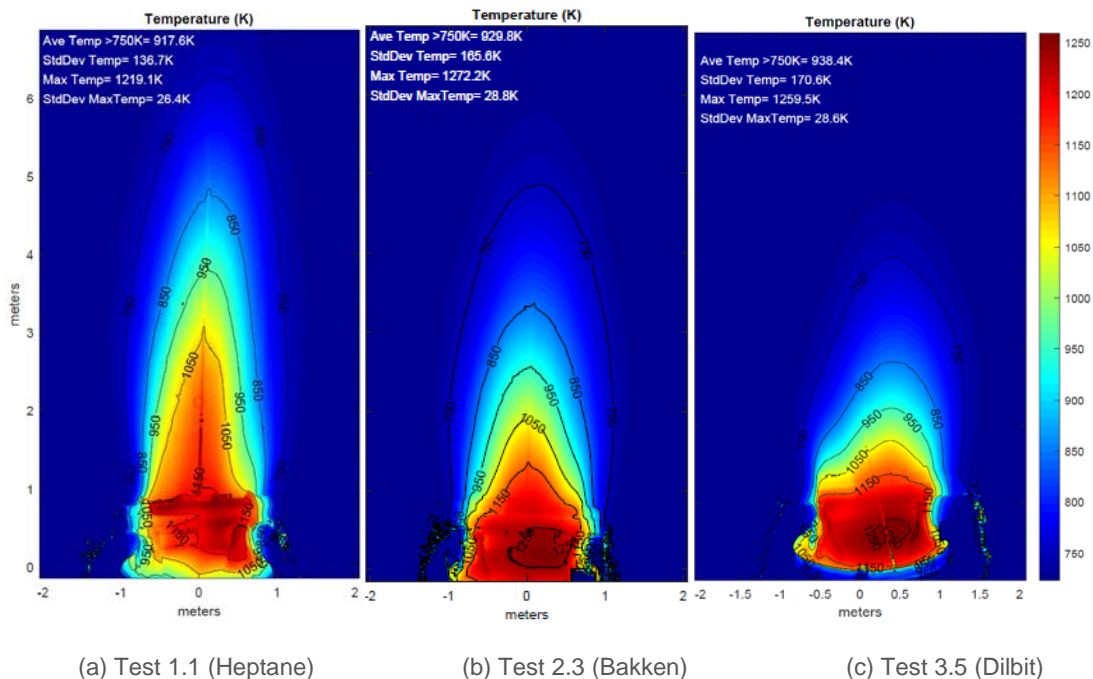


Figure 10 Fire plume temperatures from IR camera measurements.

(Height is from the floor in Series 3 and from the top of the fuel pan in Series 1 and Series 2 tests. It should also be noted that the IR camera was placed on the second floor, so the view of the fire was from a height of approximately 3.7 m above the floor of the test facility and the images are not representative of a vertical plane along the fire plume.)

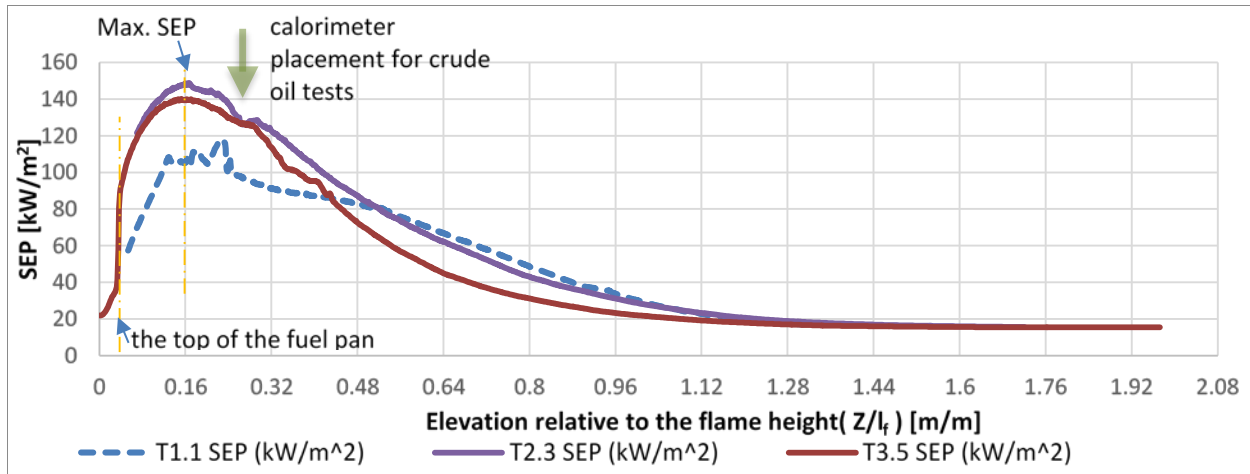


Figure 11 Vertical variations of SEP with elevation relative to the flame height for heptane (T1.1), Bakken (T2.3) and dilbit (T3.5) crude oils.

(Note that the floor is where $Z/l_f = 0$, and Z and l_f are assessed from camera views, which is not precisely representative of a vertical plane in the test facility.)

10.5.3 The effects of the test parameters on flame temperature and surface emissive power

There was no significant effect of the presence of the calorimeter, fuel supply temperatures, or maintaining a constant fuel level on the average and maximum flame temperature and SEP. The maximum flame temperature and SEP do vary slightly with fuel type. The Bakken and dilbit crude oil fires resulted in similar levels of maximum flame temperature and maximum SEP, which were 1260-1280 K (987-1007°C) and 196-207 kW/m², respectively, for the Bakken fires and 1230-1270 K (957-997°C) and 173-194 kW/m², respectively, for the dilbit fires (Note that these maximum values did not occur along the centreline of the fire). In comparison to heptane Test 1.1 results with the calorimeter at 1 m height (1220±26 K (947±26°C) and 181±15 kW/m²), the corresponding Bakken and dilbit crude oil tests (2.3, 2.5, 3.1 and 3.5) resulted in approximately 13% and 7% higher maximum SEP, respectively, which is not considered a significant effect. It should be noted that radiant emissive power, as discussed in Section 9.5.7) is strongly dependent on the temperature of the emitter (i.e. directly proportional to the fourth power of the temperature), and therefore minute differences in flame temperatures can cause notable changes in radiant emittance.

10.5.4 Mean SEP and total radiation emitted from the flame

The mean SEPs, averaged over the entire flame surface, were 66±6 kW/m², 73-79 kW/m² (±11 kW/m² on average), and 70-78 kW/m² (±8 kW/m² on average) for the heptane, Bakken and dilbit crude oil tests, respectively. The slightly higher average SEP measurements in the Bakken and dilbit crude oil tests agree with the fact that the radiative portion (X_r) of the total HRR of the Bakken and dilbit crude oil fires was greater than the radiative portion of the heptane fire. This can be attributed to the sootier plume generated from the Bakken and dilbit crude oil fires than the heptane fires. A similar result was found in experiments conducted by Blanchat and Suo-Anttila [15]. They measured soot generation and radiative fractions from pool fires of

alcohol, hydrocarbon and alcohol-hydrocarbon mixtures. In their hydrocarbon tests of JP8 and heptane, higher radiative fractions (X_r) and higher soot yields were measured for JP8 pool fires than heptane pool fires. In most petroleum-based fuels, soot radiation generally contributes more than gaseous radiation, but it depends on soot's optical properties including chemical composition and absorption capacity [10].

Overall for the Bakken and dilbit crude oils, the average temperature and SEP are similar because in sooty diffusion flames radiation energy is emitted dominantly by the soot particles rather than individual combustion species. While the average values of SEP and flame temperature were similar, the height and volume of the flame differed significantly between the heptane, Bakken and dilbit crude oil fires. Thus, it can be inferred that the total amount of radiative heat emission is approximately proportional to the flame volume or flame surface area of the fire. However, this does not take into account differences in smoke obscuration of the flame.

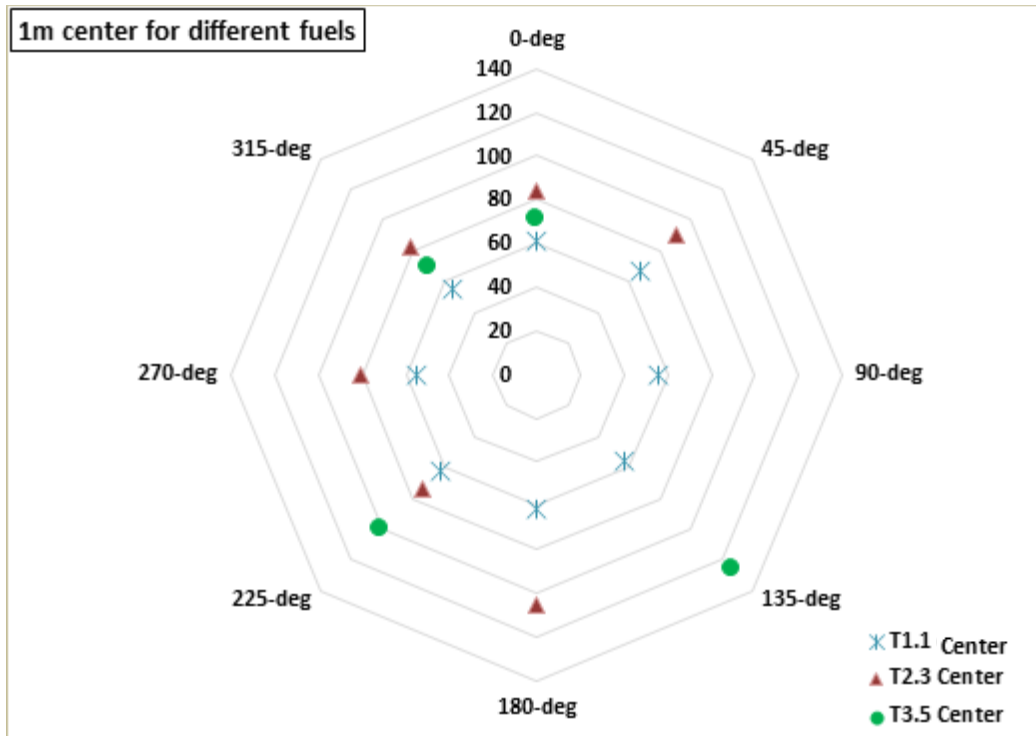
10.6 Heat flux received by the calorimeter

10.6.1 Heat flux variation around the circumference of the calorimeter

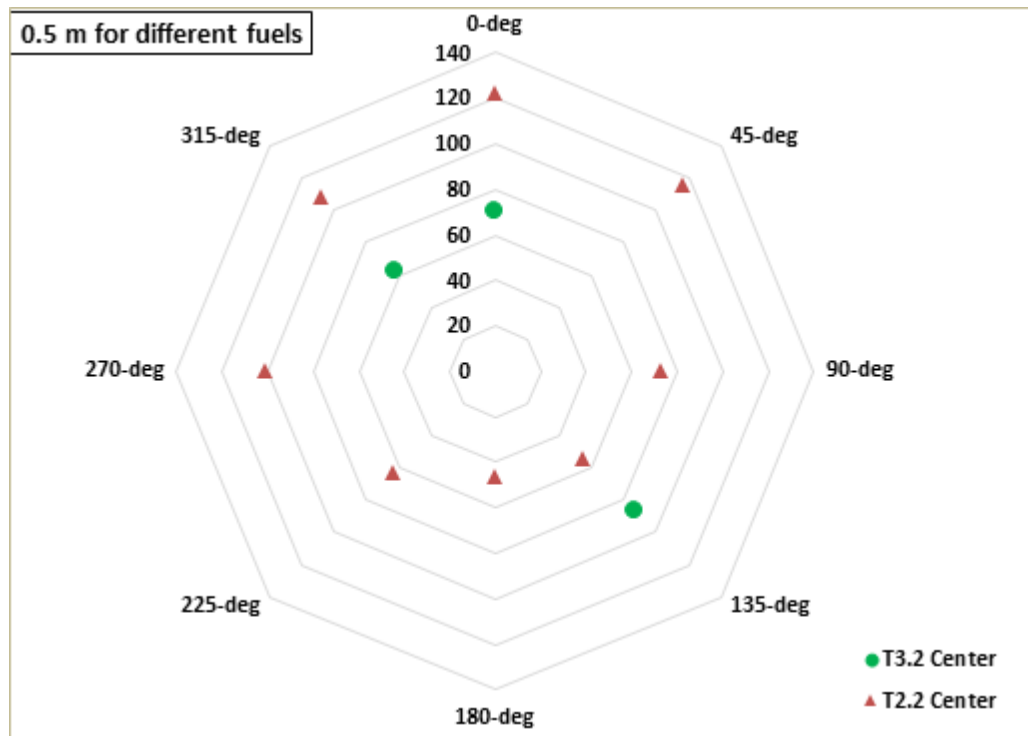
The average temperature of the calorimeter outer shell was approximately 917°C, 800°C and 670°C for Bakken crude oil, heptane and dilbit crude oil tests, respectively. It should be noted that the average values of the dilbit tests were obtained, differently from those of heptane and Bakken tests, by integrating the data over 0-25 minutes (as opposed to a test-specific steady burning period) and then dividing by 25 minutes. The total heat flux at each measurement point was calculated by Eq 5. Figure 12 compares the total heat flux measured in various radial directions across the centre plane of the calorimeter, which was placed 1 m above the fuel surface of heptane (Test 1.1), Bakken (Test 2.3) and dilbit (Test 3.5) and 0.5 m above the fuel surface of Bakken (Test 2.2) and dilbit (Test 3.2). In general, uneven circumferential profiles of the total heat flux were found for most tests. The variation in heat flux around the circumference of the calorimeter was more distinct in Bakken and dilbit crude oil tests than in heptane tests. This difference in the circumferential profiles between the fuels is mainly because the total heat flux is mostly governed by the flame characteristics surrounding the calorimeter.

The sensitivity of the total heat flux to the calorimeter height was well captured in the Bakken tests. When elevated at 1 m, the calorimeter experienced higher total heat flux on the bottom surface (180°) than the top surface (0°). When elevated at 0.5 m, the calorimeter measured much higher total heat flux on the top surface (123 kW/m²) than the bottom (47 kW/m²). The significantly low value measured at the bottom in Test 2.2 can be attributed to the fuel vapour zone immediately above the fuel surface, which is relatively cooler than the flame zone.

Similarly, in the dilbit tests, distinctly higher heat flux was measured at the bottom (127 kW/m²) than the top (71 kW/m²) of the calorimeter when the calorimeter was placed 1 m above the fuel surface in Test 3.5. In Test 3.5, the maximum flame temperature and SEP were measured at a height of 0.5 m, below the bottom of the calorimeter. When the calorimeter was placed 0.5 m above the dilbit pool, slightly higher values were measured at the bottom of the calorimeter than the top.



(a) Cross-sectional profiles of the calorimeter at 1 m above the fuel surface



(b) Cross-sectional profiles of the calorimeter at 0.5 m above the fuel surface

Figure 12 Total heat flux [kW/m²] measured by the calorimeter

10.6.2 The effects of the test parameters and fuel characteristics on the total heat flux to the calorimeter

The average total heat flux over the whole calorimeter surface was obtained in each test. Since the total heat transferred to an object engulfed in a large hydrocarbon pool fire is mainly by radiation [7], it is explored in this section how the calorimeter measurements relate to the emissive power of the flame. Due to a lack of measurements of the local emissive power inside the flame, the SEP measured on the flame surface was used for the comparison with the total heat transfer to the calorimeter. However, it should be noted that although correlations may be observed between the SEP at the flame surface and the total heat transfer to the calorimeter, consideration of the local radiative properties inside the flame (e.g. absorptivity, path length) must be considered in order to properly understand the heat transfer from the fire to the calorimeter. In Figure 13, the average total heat fluxes over the calorimeter surface are plotted against the maximum flame SEP for the 1 m calorimeter height tests because the calorimeter was placed in close proximity to the height where the maximum flame SEP was measured.

Overall, the average total heat fluxes to the calorimeter in the locations of 1 m height (as shown in Figure 13) as well as of 0.5 m were somewhat proportional to the measured maximum SEP, for the fuels tested. It should be clarified that the heat flux to the calorimeter is averaged both over time and over a large surface area, while the maximum SEP is averaged over time but is representative of only a small region of the flame (it is assumed that the location of the maximum SEP doesn't change much with time and thus can be estimated from the time-averaged IR images). It should also be noted that the SEP is measured at the flame surface, while the total heat flux measured by the calorimeter applies to inside the fire [8]. The average total heat flux measured by the calorimeter in the heptane test was lower than in the Bakken and dilbit tests, and this generally corresponds to the heptane fire emitting lower SEP than the Bakken and dilbit fires.

There was no significant impact of the heated fuel supply temperature and the non-continuous fuel feed on the average total heat flux to the calorimeter. The vertical placement of the calorimeter, however, appeared to affect the total heat flux. When the calorimeter was placed 1 m above the Bakken pool, the average total heat fluxes measured by the calorimeter were approximately 94.1-109.5 kW/m². When the calorimeter was placed 0.5 m above the fuel surface (Test 2.2), the average total heat flux to the calorimeter decreased to 77 kW/m² reflecting the exposure of the bottom of the calorimeter to the cooler fuel-rich vapour zone immediately above the fuel surface. For the dilbit tests, the average total heat fluxes were approximately 64-83 kW/m² and 67 kW/m² with the calorimeter placed at 1 m and 0.5 m heights, respectively. Although the dilbit results are not as conclusive as the Bakken results and would need further confirmation, the total heat flux measurements may have also been sensitive to the vertical location of the calorimeter in the flame. The bottom of the calorimeter could have been affected by the fuel vapour zone immediately above the fuel surface, the characteristics of which vary greatly depending on the fuel type [16, 17].

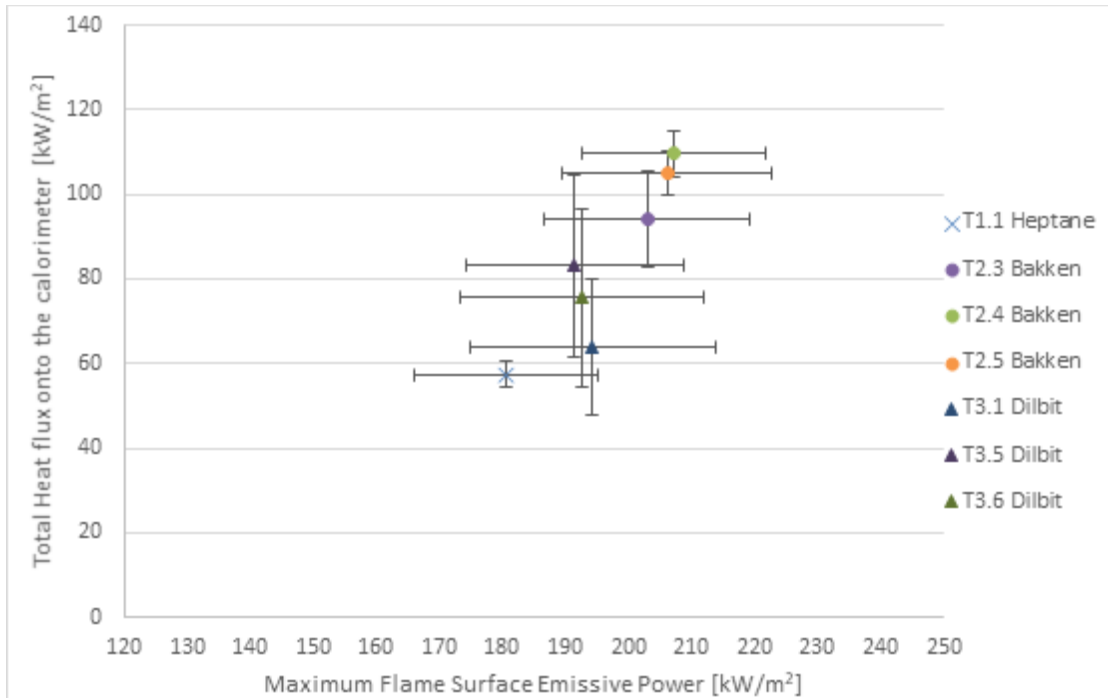


Figure 13 Average total heat flux to the calorimeter placed at 1 m above the pan against the maximum flame surface emissive power

(Averaged over the 24 measurement positions around the circumference of the calorimeter)

10.7 Incident heat flux away from the fire

Heat fluxes from the fire were measured at various distances from the fuel pool, to assess the thermal conditions around the fire. Two directional flame thermometers (DFT) were placed at 2 m and 4 m from the pool centre, at a height of 1 m, to assess the incident heat flux to the surface of the DFT facing the flame. At 9 m from the pool centre, a total heat flux gauge was also mounted on the wall of the testing facility at the same height of 1 m.

The incident heat flux data measured by the two DFTs and the heat flux gauge at the height of 1 m are plotted in Figure 14 against the measurement distance. The magnitude of the heat flux decreases as the distance from the pool to the target increases. The incident heat flux measured near the Bakken crude oil fire (2 m from the fire) was higher than that measured near the heptane fire mainly due to the higher radiative heat generated from the Bakken crude oil fire. The incident heat flux measured at 4 m (distance equal to 2 diameters of the pool) from the Bakken crude oil fire was approximately 19 kW/m², which could ignite any wood or plastic materials at the same location (Critical Heat flux values measured by the standard test method of ASTM E2058 to cause ignition of wood and polymers are 10 and 10-15 kW/m², respectively [18]). At the distance of 9 m (distance equal to 4.5 diameters of the pool), the measured incident heat fluxes from heptane, Bakken and dilbit crude oil fires were lower than 2.5 kW/m². At this location, the Bakken crude oil fire tests resulted in an incident heat flux of approximately 2 kW/m², which is the tenable limit for regular clothed people [19] but greater than the critical heat flux of 1.7 kW/m² for initiation of pain for exposed skin [20]. Applying the critical value of 5 kW/m² suggested for safe firefighting with protected gear [19], the closest distance that fire fighters can approach a Bakken or similar type of crude oil fire is approximately 8 m for the 2-m diameter pool. Overall, the dilbit tests displayed lower values than the Bakken and heptane tests, and at the locations of 2 m and 4 m, the lowest incident heat flux was measured with the dilbit fires. It should be noted that the presented dilbit values were obtained by a 25-minute time-integration from the start of the test (0 minutes) while the heptane and

Bakken values were averaged over the time period of steady-state burning (typically starting at least 10 minutes into the test).

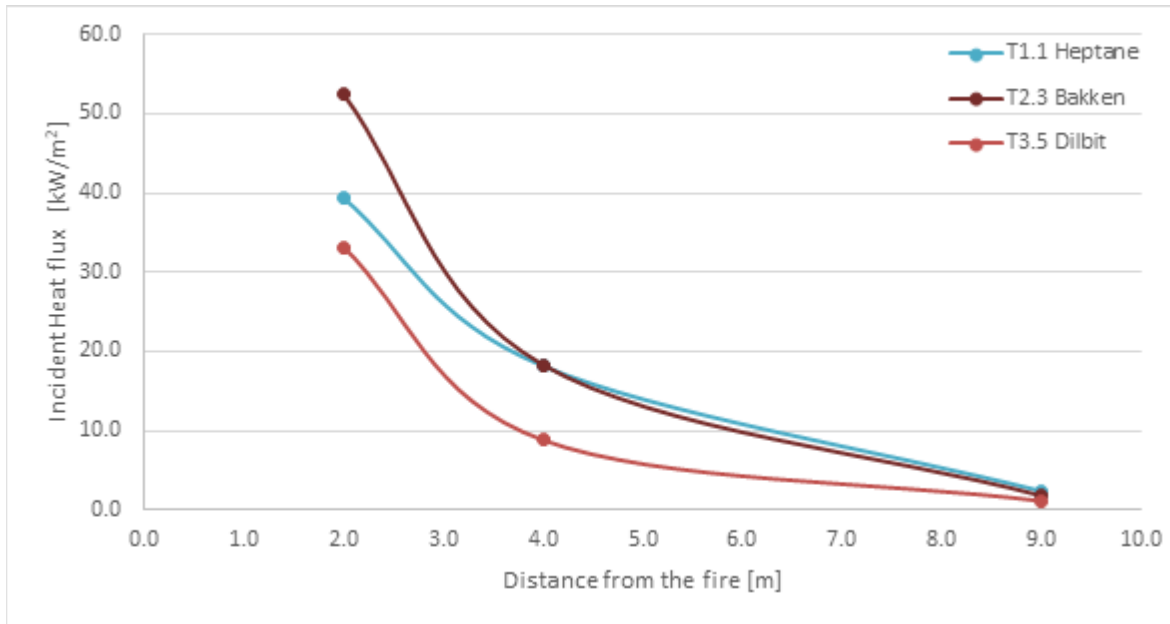


Figure 14 Incident heat fluxes

11 Conclusions

Experiments at approximately 1/10th scale were conducted to examine the effects of burning characteristics on the heating of a cylindrical object (calorimeter), representing a tank car in a pool fire. Series of 2-m diameter pool fire tests were conducted using heptane (Series 1), Bakken (Series 2) and dilbit (Series 3) crude oils to investigate the effects of fuel composition on fire characteristics. The study also investigated the effects of test parameters that include the presence and placement of a calorimeter engulfed in the fire, fuel feed temperature, and allowing the fuel to burn down. Fire characteristics including mass burning rates, HRR, flame heights, flame temperature and surface emissive power were measured for the 2-m diameter pool fires.

The crude oils used in the testing program were specially handled to ensure no change in its composition over the course of the testing program, from the time of fuel acquisition to the time of fire testing. In conjunction with the fire testing, a fuel characterization study was conducted to analyse the fuel samples and collect post-burn residue samples.

Burning behaviour and fuel characteristics

Overall, the Bakken crude oil and heptane fires displayed continuous steady burning throughout the test while the dilbit crude oil fires displayed unsteady burning behaviour in which the burning rates changed over the burn time.

The non-steady burning behaviour of the dilbit pool fires was mainly caused by the fuel composition, which contains a larger fraction of heavy end hydrocarbons than the Bakken crude oil and heptane.

Combustion of multi-component fuels is complex. The combustion process may generally involve initial fuel vaporization of light end components with low boiling points, then become dominated by the heavy ends toward the end of the burning period [1]. This variation in the burning rate would be expected to be more apparent for the fuels containing significantly large amounts of heavy ends, as demonstrated in the dilbit tests. Containing 60 mass% C25+, whose boiling points are greater than 400°C, the dilbit crude oil fire is expected to undergo larger changes in burning rate than the Bakken crude oil fire, in which 80% of its mass boils and burns off within the temperature range less than 400°C.

The time-variant burning behaviour observed in the dilbit crude oil tests was reflected in the measurements of the flame height and heat release rate, as well as the measurements of flame SEP by the narrow-view radiometers, which displayed similar time-varying profiles. Also, a larger amount of residue was remaining in each fire test in the dilbit series than in the Bakken series.

Total HRR, flame height and radiative fractions

The average HRR measured in the exhaust hood using oxygen consumption calorimetry was 3.2-3.8 MW for Bakken crude oil tests and 4.4-5.4 MW for heptane tests with the calorimeter placed above the pool. The measured average HRR of the dilbit fire was 3.7 MW (Test 3.4); however due to the highly variable burning behaviour of the dilbit crude oil fires, the average mass burning rate and HRR indicate large uncertainty. The flame height over the 2-m diameter pool fire, which is driven by the HRR, was 5.6-6.8 m, 4.3-4.5 m, and 3.4–3.6 m for the heptane, Bakken and dilbit crude oil fires, respectively.

Radiative fractions become important in assessing the potential radiative hazards posed by hydrocarbon fuel pool fires, which include potential fire spread to external objects by radiation heat transfer.

Radiative fractions were obtained by estimating the convective component of heat release rate from the fires, dividing by the measured total heat release rate and subtracting the result from unity. The average X_r values estimated by this method were approximately 0.46 and 0.36 for Bakken crude oil and heptane tests, respectively. For the dilbit crude oil, due to the large variation in HRRs, X_r values could not be evaluated for all Series 3 tests, yet a value of 0.61 was obtained for the dilbit pool fire with non-continuous fuel feeding (Test

3.4), which is higher than the value of 0.49 obtained from the Bakken pool fire with the same non-continuous fuel feeding (Test 2.6). The higher radiative heat fraction for Bakken and dilbit than heptane can be linked to the sootier plume generated from the Bakken and dilbit crude oil fires. The Bakken and dilbit crude oils contain a small amount of benzene and many heavy ends (see Figure 2). In general, soot precursors (e.g. Polyaromatic hydrocarbons) are formed due to the presence of long chain hydrocarbons, aromatics (e.g. benzene) and unsaturated compounds in the fuel composition. For n-alkanes, the sooting tendency increases with increasing carbon number [21]; however, further study is necessary to understand an analogy between the flame thermal radiation and fuel characteristics (e.g. chemical composition and sooting tendency).

Profiles of flame temperature/SEP

The measured flame temperature and SEP show high values in the lower part of the fire, and the values gradually decrease along the height of the flame. The maximum temperature and maximum SEP measured on the centre line of the flame using the IR camera were observed in the lower part of the flame, specifically for the maximum SEP at 0.16 ± 0.01 m/m of Z/l_f in all Bakken and dilbit crude oil tests. For all heptane, Bakken and dilbit tests, the calorimeter was placed in close proximity to the height where the maximum flame temperature and SEP (on the centreline of the plume) occurred. Given the vertical variation of the flame temperature and SEP, the measured heat fluxes at various locations along the calorimeter surface were uneven around the circumference of the calorimeter.

The heptane fires displayed the highest HRR but the lowest radiative fraction (X_r) and the lowest maximum SEP. At the same time, the average total heat transfer to the calorimeter measured in the heptane tests was lower than in the dilbit and Bakken crude oil tests. The thermal radiation is emitted predominantly by the soot particles rather than combustion species, in sooty diffusion flames for most hydrocarbons. The heat transfer from a fire to an engulfed object is mainly by thermal radiation [7] since presence of soot plays a dominant role in radiation energy transport. Therefore, due to their sootier plumes, Bakken and dilbit crude oil fires resulted in higher maximum SEP, higher radiative fraction (X_r) and consequently higher average total heat transfer to the calorimeter than heptane fires.

Heating of calorimeter

The heat fluxes were measured by the calorimeter at various locations along its surface. The heating of the calorimeter was uneven around the circumference of the calorimeter, which was more distinct in Bakken and dilbit crude oil tests than in heptane tests. The total heat flux measurements were also sensitive to the vertical location of the calorimeter in the flame because the total heat flux to the calorimeter was affected by the local emissive power of the surrounding flame at the elevation where the calorimeter was placed. For instance, the bottom of the calorimeter could be affected by the presence of a fuel vapour zone immediately above the fuel surface, the characteristics of which vary greatly depending on the fuel type. For this reason, when placed at 0.5 m above the Bakken fire, the heat flux measured at the bottom of the calorimeter was much lower than the top, indicating the impact of the cool fuel vapour zone on the bottom of the calorimeter.

The average heat flux to the calorimeter from the Bakken and dilbit crude oil fires was higher than that from the heptane fires although the measured HRRs of the Bakken and dilbit crude oil pool fires were less than those of the heptane pool fires. The average total heat flux to the calorimeter showed the highest value in the Bakken crude oil fires by about a factor of 1.3 and 1.6 higher than the dilbit crude oil and heptane fires, respectively (~ 96 kW/m² vs ~ 72 kW/m² and ~ 58 kW/m², respectively). The main reason for the increased heating of the calorimeter in particular by the Bakken and dilbit crude oil fires is that the total heat flux to the object is mostly affected by radiative heat exposure from the flame, and the Bakken and dilbit crude oil fires have higher radiative heat fraction. Overall, the average total heat fluxes to the calorimeter were somewhat proportional to the maximum measured surface emissive power of the flame for the fuels tested.

Parameter impacts

In considering the parameter effects, there was no significant effect of “fuel supply temperature” and “fuel to burn down (i.e., non-continuous fuel feed)” on any measured fire parameters. The higher fuel supply temperature increased the burn rate by about 10% for the heptane and Bakken crude oil tests, which is not considered to be significant considering the natural variability of fires. Allowing the fuel to burn down, rather than maintaining a constant fuel level, resulted in minimal effect on average values of the mass burning rate and general fire characteristics of the Bakken crude oil pool fires. For the dilbit crude oil, the fuel compositional effect on the burning behaviour was observed in both continuous and non-continuous fuel feeding. The distillation process and non-uniform burning behaviour became easier to discern when there was no continuous fuel feed into the fuel pan. The presence and placement of the calorimeter had effects on the burning rate and total heat flux from the flame to the calorimeter. When the calorimeter was placed over the pool, the mass burning rate was reduced by 10-15% in the Bakken tests. For the dilbit crude oil fires, due to the non-steady burning behaviour, the impact of the calorimeter was difficult to be captured.

12 Recommendations for future study

Based on the findings from Series 1, 2 and 3 tests, the following is recommended for future study involving crude oils.

Detailed analysis of the fire and calorimeter data

To increase insight into the thermal exposure of the calorimeter engulfed in fire, it is recommended to conduct detailed analysis of the data obtained from the three test series. The analysis should include the impact of the time-varying burning behavior observed in the dilbit tests and the tests with the fuel allowed to burn down. Also, the test data should be compared with other test data already published in order to identify potential differences in fire behavior between light and heavy crude oils and other hydrocarbon fuels (e.g. heptane, diesel and jet fuels).

The dilbit tests displayed time-variant burning behavior potentially caused by a distillation-type or other temporally non-uniform vapourization processes. Detailed investigation of the burning behavior observed in the three test series would provide insight into the crude oil fire characteristics and also help to develop a combustion model to be used in numerical modelling (see below). Residue analysis should be included to support the investigation of the combustion mechanism. The investigation would potentially provide insight into whether the fuel physical and chemical properties, such as fuel vapour pressure, fuel density, compositions of light and heavy ends, correlate with the fire characteristics and hazard parameters.

Numerical modelling

The reduced-scale data obtained from the testing program would need to be scaled up to an actual fire scenario to further understand the risks associated with tank cars exposed to fire. Using modelling tools currently available, crude oil fires tested in Series 2 and Series 3 can be modelled, utilizing some of fuel properties obtained from the fuel characterization study.

If validated for plume temperatures, HRR, burning rate, flame height, flame surface emissive power and heat flux field around the fire, the simulation could include the cylinder/calorimeter for simulating the heat transfer into the calorimeter. If validated against the experimental data from Series 1, 2 and 3 tests, the modelling could be used to examine other parameters of interest, such as fire and tank car at full scale, the presence of wind, changes in fire size, changes in the relative orientation or location of the tank car, partial engulfment of the tank car by the fire. Extrapolation of the model beyond the conditions tested in Series 1, 2 and 3 would not be fully validated without additional experimental testing (particularly if there are large changes in boundary conditions or scale); however, such simulations would provide reasonable indications of the likely fire behaviour at much lower cost and risk.

Table 3 Test results summary

Test #	Calorimeter Elevation (m)	Fuel Supply Temperature (°C)	Fuel Feed Method	Flame Height (m)	Burn rate (kg/m ² s)	Theoretical Max. Heat release (MW)	Q _o , HRR based on burn rate by Eq 1 using x=0.9 (MW)				Q _c , Convective HRR by Eq 3 (MW)	X _r , radiative heat fraction using HRR by Eq 1	X _c , convective heat fraction, Eq 3	IR Camera				Z/l _r , relative elevation for Max. SEP at the plume centre (m/m)	Calorimeter				Flame/Plume temperature (°C)										Narrow view radiometer Heat Flux (kW/m ²), 9 m from fire						DFT		Heat flux gauge (kW/m ²) 9 m from fire				
							Q _o , HRR by O ₂ Calorimetry, Eq 2, (MW)	x, Incomplete combustion factor	Mean Flame Temp (K)	Max. Flame Temp (K)				Mean Surface Emissive Power (kW/m ²)	Max. Surface Emissive Power (kW/m ²)	Outer shell avg. Temperature(°C)	Exterior cylinder avg. Temperature(°C)		Absorbed heat flux (kW/m ²)	Total heat flux (kW/m ²)	0.18 m high	0.5 m high	1.5 m high	2.0 m high	2.5 m high	3.0 m high	3.5 m high	4.0 m high	4.5 m high	5.0 m high	5.5 m high	0.5 m high	1 m high	1.5 m high	2 m high	3 m high	4 m high	DFT Heat Flux (kW/m ²) 2 m from fire	DFT Heat Flux (kW/m ²) 4 m from fire	1 m high	1.5 m high	2 m high	3 m high	4 m high	
T1.1	1	20	Continuous	5.6	0.037	5.15	4.64	4.4	0.85	3.0	0.36	0.64	918	1219	66	181	0.23	797	864	-2	58	719	878	799	739	652	591	558	493	428	404	89.1	93.1	91.3	77.4	47.6	33.8	39.4	18.2	2.3	2.9	2.5	2.5	2.3	
T1.2	No	20	Continuous	6.8	0.040	5.60	5.04	5.2	0.94	3.3	0.34	0.66	na	na	na	na		na	na	na	na	na	848	886	897	881	855	825	757	679	620	94.7	84.8	84.4	80.9	70.4	61.6	35.5	15.1	2.5	3.1	2.7	2.7	2.6	
T1.3	1	60	Continuous	5.8	0.040	5.60	5.04	5.4	0.96	3.1	0.39	0.61	na	na	na	na		771	816	-2	59	660	877	835	772	698	626	591	531	460	429	88.9	92.1	96.4	85.1	53.9	38.8	44.2	17.8	2.4	3.0	2.6	2.6	2.4	
T2.1	No	20	Continuous	4.5	0.030	4.56	4.10	4.8	1.05	2.3	0.44	0.56	904	1266	75	201	0.15					na	na	938	890	800	688	574	485	392	318	269	120.2	102.5	88.7	73.9	39.6	22.0	49.8	17.0	2.3	2.8	2.5	2.5	2.2
T2.2	0.5	20	Continuous	4.3	0.026	3.95	3.55	3.5	0.89	1.7	0.51	0.49	923	1262	75	200	0.18	846	881	-4	77	673	na	936	904	815	714	611	529	439	356	301	99.6	105.6	86.5	66.7	31.0	16.9	33.6	15.1	2.0	2.4	2.1	2.1	1.8
T2.3	1	20	Continuous	4.3	0.027	4.10	3.69	3.8	0.93	2.0	0.47	0.53	930	1272	77	203	0.17	909	975	-4	94	na	968	848	758	621	522	420	361	303	250	220	58.4	74.2	77.0	57.6	24.6	13.3	52.5	18.3	1.8	2.2	1.9	1.9	1.7
T2.4	1	60	Continuous	4.5	0.029	4.41	3.96	3.2	0.73	2.5	0.38	0.62	944	1280	79	207	0.16	952	993	-5	110	na	972	926	854	727	616	505	431	349	282	244	65.1	84.1	89.1	68.2	31.3	16.4	53.8	18.8	1.9	2.4	2.1	2.1	1.9
T2.5	1	20	Continuous	4.5	0.026	3.95	3.55	3.6	0.91	2.0	0.43	0.57	943	1280	77	206	0.15	946	991	-5	105	na	974	933	858	726	616	507	424	343	276	238	65.4	85.1	89.9	68.1	29.5	14.8	32.1	7.8	1.9	2.4	2.1	2.1	1.9
T2.6	No	20	Burn down	4.5	0.030	4.56	4.10	3.5	0.77	2.1	0.49	0.51	901	1258	74	196	0.16					na	na	950	883	770	660	537	448	367	303	254	116.3	93.6	75.0	60.7	30.1	15.5	32.4	8.3	2.1	2.5	2.2	2.2	2.0
T3.1	1	20	Continuous	3.4	0.049, 0.034	-	-	-	-	1.4	-	-	1075	1266	78	194	0.16	641	775	-13	64	na	902	397	308	238	191	164	145	128	115	107	70.7	56.1	51.6	36.9	12.0	5.5	35.2	9.5	1.1	1.4	1.2	1.0	1.0
T3.2	0.5	20	Continuous	3.6	0.060, 0.023	-	-	-	-	1.3	-	-	930	1234	70	173	0.12	615	825	-14	67	875	na	422	335	263	201	173	153	135	120	111	74.2	72.5	50.4	36.0	11.4	4.9	34.2	8.5	1.1	1.4	1.2	1.1	1.1
T3.3	No	20	Continuous	3.4	0.017, 0.014	-	-	-	-	1.3	-	-	913	1252	71	189	0.16	na	na	na	na	na	na	431	333	248	184	148	127	109	95	87	105.2	73.4	48.8	35.1	11.7	4.6	36.0	9.8	1.4	1.8	1.6	1.4	1.4
T3.4	No	20	Burn down	3.5	0.018	-	-	3.7	-	1.5	0.61	0.39	914	1246	70	188	0.18	na	na	na	na	na	na	419	329	250	186	153	135	116	103	96	102.6	74.3	51.3	37.2	12.0	4.9	35.2	9.3	1.4	1.7	1.5	1.3	1.4
T3.5	1	20	Continuous	3.6	0.015-0.019	-	-	-	-	1.2	-	-	938	1260	73	192	0.15	708	870	-16	83	na	964	454	362	290	226	193	170	148	132	123	64.0	59.6	48.9	33.0	10.6	4.6	33.2	8.8	1.1	1.5	1.3	1.1	1.1
T3.6	1	60	Continuous	3.5	0.018, 0.005-0.01	-	-	-	-	1.4	-	-	935	1251	72	193	0.15	696	773	-16	76	na	904	425	338	269	205	173	153	132	117	109	53.7	53.0	47.2	33.2	10.8	4.8	36.3	9.5	1.1	1.4	1.2	1.1	1.1

Note: The values presented for Series 1 and 2 tests were averaged over the steady-state burning period in each test. The test data from Series 3 were averaged by integrating the data over 0-25 minutes and then dividing by the same time. Supplement A. Test Report provides details on how and over what time periods these average test data were obtained for each test.

- Two burn rates were provided for Test T3.1, T3.2, T3.3 and T3.6 for different periods in which a burn rate could be identified. For Test 3.5, a range was provided for the burn rate since it could not be identified over a continuous period.
- It should be noted that the HRR data obtained by oxygen calorimeter need checks for biases in oxygen concentration measurements, and the resulting calculations of HRR should be checked to match the total energy content of the fuel (the product of chemical heat of combustion and total amount of fuel used in each test) by comparing with the total energy measured by the hood systems (time-integrated HRR curves).
- X_r, radiative heat fractions were calculated using HRR by Eq 1 for Series 1 and 2 tests, and for Series 3, X_r was calculated for T3.4 using HRR by O₂ calorimetry.
- Z/l_r presented in the table is the height where the maximum SEP occurred over the vertical SEP profiles along the centre line of the flame.

13 References

- [1] C. Lam, D. Edwards and G. Lougheed, "Rail tank cars exposed to fire: literature review of crude oil, condensate and ethanol behaviour," NRC Report # A1-005795-01.1, 2015.
- [2] D. Drysdale, "An introduction to fire dynamics, 3rd edition," Wiley, 2011.
- [3] G. Heskestad, "Fire plumes, flame height, and air entrainment," in *SFPE Handbook of Fire Protection Engineering*, National Fire Protection Association, 2002, pp. Section 2, Chapter 1; p. 2-1 - 2-17.
- [4] V. Babrauskas, "Heat release rates," in *SFPE handbook of Fire Protection Engineering*, National Fire Protection Association, 2002, pp. Section 3, Chapter 1; p. 3-1-3-37.
- [5] A. Tewarson, "Generation of heat and chemical compounds in fires," in *SFPE handbook of fire protection engineering. 3rd Ed.*, 2002, pp. Chapter 4, Section 3.
- [6] C. Huggett, "Estimation of rate of heat release by means of oxygen consumption measurements," *Fire and materials*, pp. Vol 4, NO. 2 61-65, 1980.
- [7] A. Birk, "Fire testing and computer modeling of rail tank-cars engulfed in fires," Transport Canada reprot TB14561E, 2006.
- [8] Y. Ko, C. Lam, A. Luketa, D. Lord, A. Butko, C. Kirney and M. Spiess, "Tank cars engulfed in fires: heat flux measurments," in *Interflam 2019*, UK, 2019.
- [9] M. Janssens, "Methods and equations of fire calorimetry," in *Fire Calorimetry*, DOT/FAA/CT-95/46, 1995, pp. 11-22.
- [10] C. L. Tien, K. Y. Lee and A. J. Stretton, "Radiation heat transfer," in *SFPE handbook of fire protection engineering*, NFPA and SFPE, 2002, pp. 1-73 - 1-89.
- [11] R. M. Schirmer and E. C. Miller, "Radiation from jet combustor flames," 1958.
- [12] J. V. Beck, "Users Manual for IHCP1D, a Program for Calculating Surface Heat Fluxes," Beck Engineering Consultants Co., Okemos, Michigan, 1999.
- [13] C. Beyler, "Fire hazard calculations for large, open hydrocarbon fires," in *SFPE Handbook of Fire Protection Engineering*, 2002.
- [14] G. Heskestad, "Luminous heightsof turbulent diffusion flames," *Fire SAfety Journal*, vol. 5, pp. 103-108, 1983.
- [15] T. K. Blanchat and J. Suo-Anttila, "Hydrocarbon characterization experiments in fully turbulent fires - Results and data analysis," Sadia national laboratories (SAND2010-6377), 2011.

- [16] D. Rasbash, "Properties of fires of liquids," *Fuel*, vol. 31, pp. 94-107, 1956.
- [17] H. Hayasaka, "Radiative characteristics and flame structure of small-pool flames," *Fire Technology*, vol. 32, no. 4, pp. 308-322, 1996.
- [18] SFPE, *SFPE Handbook of Fire Protection Engineering*, Springer, 2016.
- [19] UPTUN, "Development and Mitigation Measures: Target Criteria, Workpackage 2 D221Fire," 2008.
- [20] C. J. Wieczorek and N. A. Dembsey, "Effects of Thermal Radiation on People: Predicting 1st and 2nd Degree Skin Burns," in *SFPE Handbook of Fire Protection Engineering*, 2016, pp. 2705-2737.
- [21] C. S. McEnally and L. D. Pfefferle, "Sooting tendencies of oxygenated hydrocarbons in laboratory-scale flames," *Environmental science and technologies*, pp. 45, 2498-2503, 2011.
- [22] C. L. Beyler, "Fire Hazard Calculations for Large Open Hydrocarbon Fires," in *SFPE Handbook of Fire Protection Engineering*, 2016, pp. 2591-2663.

Supplement A. Test Report

SANDIA REPORT

SAND2021-3206
Printed March 2021



Experimental Results of 2-m Heptane, Bakken Crude Oil, and Dilbit Crude Oil Pool Fire Tests Performed for the National Research Council of Canada

Anay Luketa, Alvaro Cruz-Cabrera, Walt Gill, Shane Adee, Joe Hogge

Prepared by
Sandia National Laboratories
Albuquerque, New Mexico
87185 and Livermore,
California 94550

Issued by Sandia National Laboratories, operated for the United States Department of Energy by National Technology & Engineering Solutions of Sandia, LLC.

NOTICE: This report was prepared as an account of work sponsored by an agency of the United States Government. Neither the United States Government, nor any agency thereof, nor any of their employees, nor any of their contractors, subcontractors, or their employees, make any warranty, express or implied, or assume any legal liability or responsibility for the accuracy, completeness, or usefulness of any information, apparatus, product, or process disclosed, or represent that its use would not infringe privately owned rights. Reference herein to any specific commercial product, process, or service by trade name, trademark, manufacturer, or otherwise, does not necessarily constitute or imply its endorsement, recommendation, or favoring by the United States Government, any agency thereof, or any of their contractors or subcontractors. The views and opinions expressed herein do not necessarily state or reflect those of the United States Government, any agency thereof, or any of their contractors.

Printed in the United States of America. This report has been reproduced directly from the best available copy.

Available to DOE and DOE contractors from

U.S. Department of Energy
Office of Scientific and Technical Information
P.O. Box 62
Oak Ridge, TN 37831

Telephone: (865) 576-8401
Facsimile: (865) 576-5728
E-Mail: reports@osti.gov
Online ordering: <http://www.osti.gov/scitech>

Available to the public from

U.S. Department of Commerce
National Technical Information Service
5301 Shawnee Rd
Alexandria, VA 22312

Telephone: (800) 553-6847
Facsimile: (703) 605-6900
E-Mail: orders@ntis.gov
Online order: <https://classic.ntis.gov/help/order-methods/>



ABSTRACT

This report provides results from a series of 2-m pool fire experiments performed in the Thermal Test Complex at Sandia National Laboratories testing heptane, Bakken crude oil, and dilbit crude oil. The effect of the presence and placement of a calorimeter, fuel supply temperature, and maintaining a constant fuel level were assessed. Measurements include burn rate, surface emissive power, flame height, heat flux to an engulfed calorimeter, heat flux to external instruments, thermocouple temperatures within the fuel and fire plume, and heat release rate. The results indicate that the presence and placement of the calorimeter has the most effect on the measured quantities for the Bakken crude oil and indicated no effect for the Dilbit crude oil. The fuel feed temperature had a slight effect for the heptane fuel, but not for the crude oils. Allowing the fuel to burn down did not have a significant effect on any of the fuels. The Bakken crude oil resulted in the highest average total heat flux to the calorimeter by a factor of about 1.5 and 1.3 higher compared to heptane and the dilbit crude oil, respectively.

ACKNOWLEDGEMENTS

This work was funded by the National Research Council of Canada and Transport Canada.

We would like to thank Ray Allen of Allen Energy Services, Inc. for recommendations and review of the experimental set-up involving the pumping and heating system for the fuel.

CONTENTS

Abstract	3
Acknowledgements.....	4
Contents	5
List of Figures.....	7
List of Tables	16
Executive Summary.....	19
Acronyms and Definitions	20
1. Introduction.....	21
2. Testing facility.....	23
3. Fuel supply system for tests.....	27
4. Instrumentation.....	33
4.1. Heat Flux.....	33
4.2. Temperature and surface emissive power measurements.....	34
4.3. Heat Release Rate	35
4.4. Pool Fire Fuel Liquid Level Control and Regression Rate.....	36
4.5. Temperature Within Fuel	37
4.6. Pipe Calorimeter	37
4.7. Fire plume temperature measurements	40
4.8. Data Acquisition System and Data Quality.....	41
4.9. Measurement Device Range and Resolution.....	42
5. Test Matrix.....	43
6. Results.....	45
6.1. Heptane Pool Fire Tests	45
6.1.1. Test 1.1.....	45
6.1.2. Test 1.2.....	55
6.1.3. Test 1.3.....	62
6.2. Bakken Crude Oil Pool Fire Tests	72
6.2.1. Test 2.1.....	72
6.2.2. Test 2.2.....	81
6.2.3. Test 2.3.....	91
6.2.4. Test 2.4.....	100
6.2.5. Test 2.5.....	110
6.2.6. Test 2.6.....	120
6.3. Dilbit Crude Oil Pool Fire Tests	128
6.3.1. Test 3.1.....	128
6.3.2. Test 3.2.....	139
6.3.3. Test 3.3.....	150
6.3.4. Test 3.4.....	158
6.3.5. Test 3.5.....	165
6.3.6. Test 3.6.....	175
7. Comparison of Tests within a Series.....	187
7.1. Burn rate.....	187

7.1.1.	Heptane Pool Fire Tests.....	187
7.1.2.	Bakken Crude Pool Fire Tests.....	188
7.1.3.	Dilbit Crude Pool Fire Tests	190
7.2.	Radiometers	192
7.2.1.	Heptane Pool Fire Tests.....	192
7.2.2.	Bakken Crude Oil Pool Fires.....	194
7.2.3.	Dilbit Crude Oil Pool Fires	197
7.3.	Thermocouple Rake in Fire Plume	199
7.3.1.	Heptane Pool Fire Tests.....	199
7.3.2.	Bakken Crude Oil Pool Fire Tests.....	201
7.3.3.	Dilbit Crude Oil Pool Fire Tests.....	202
7.4.	Plume Temperatures and Surface Emissive Power	204
7.4.1.	Heptane Pool Fire Tests.....	204
7.4.2.	Bakken Crude Oil Pool Fire Tests.....	204
7.4.3.	Dilbit Crude Oil Pool Fire Tests.....	207
7.5.	DFT TC Temperatures and Derived Heat Flux	210
7.5.1.	Heptane Pool Fire Tests.....	210
7.5.2.	Bakken Crude Oil Pool Fire Tests.....	212
7.5.3.	Dilbit Crude Oil Pool Fire Tests.....	215
7.6.	Calorimeter TC Temperature and Derived Heat Flux	217
7.6.1.	Heptane Pool Fire Tests.....	217
7.6.2.	Bakken Crude Oil Pool Fire Tests.....	219
7.6.3.	Dilbit Crude Oil Pool Fire Tests.....	221
7.7.	Heat Release Rate	224
7.7.1.	Heptane pool fire tests	224
7.7.2.	Bakken Crude Oil Pool Fire Tests.....	225
7.7.3.	Dilbit Crude Oil Pool Fire Tests.....	226
7.8.	Flame Height	227
7.8.1.	Heptane Pool Fire Tests.....	228
7.8.2.	Bakken Crude Oil Pool Fire Tests.....	228
7.8.3.	Dilbit Crude Oil Pool Fire Tests.....	229
8.	Comparison of Test Series.....	231
8.1.	Burn rate.....	231
8.2.	Radiometers	236
8.3.	Thermocouple rake in fire plume	237
8.4.	Plume temperatures and surface emissive power.....	238
8.5.	DFT heat flux.....	239
8.6.	Calorimeter TC temperatures and heat flux	241
8.7.	Heat release rate	252
8.8.	Flame height	253
9.	Conclusions.....	255
	References.....	256
	Appendix A: Equations and Assumptions for Calculations.....	257
A.1.	Heat flux calculations	257
A.2.	Heat Release Rate	258
A.3.	IR Camera.....	259

LIST OF FIGURES

Figure 2-1: A cutaway view and interior of the FLAME facility. The view shows a liquid pool fire at the ground level, pipes supplying air flow through the basement, exhaust ductwork, and instrumentation rooms.23

Figure 2-2: Diffuser for fuel introduction into the 2-m diameter pan.24

Figure 2-3: Top view of experimental layout in the FLAME facility. Dimensions in meters.25

Figure 3-1: Pressurized tanker mounted on trailer.28

Figure 3-2: Nozzle locations on pressurized tanker.28

Figure 3-3: Oil tanker and water and fuel supply.29

Figure 3-4: Water manifold to drive oil out of tanker.29

Figure 3-5: Fuel feed of oil into pan within FLAME facility.30

Figure 3-6: Schematic of fuel supply system.31

Figure 4-1: Sc8313 MWIR camera picture (source: FLIR.com).34

Figure 4-2: FLAME facility bird’s eye view, top image. Cameras placement in the FLAME facility by level. The MWIR camera is located on the second floor at the NW location.35

Figure 4-3: Fuel feed and level control system for heptane.36

Figure 4-4: Thermocouple locations in each measurement plane in the calorimeter (not to scale).38

Figure 4-5. Calorimeter setup.39

Figure 4-6: Calorimeter thermocouple locations.40

Figure 4-7: Suspended cable above calorimeter which held the plume thermocouples.41

Figure 6-1: Temperature of fuel supply into pan (Test 1.1).45

Figure 6-2: Fuel Rake thermocouple temperatures (Test 1.1).46

Figure 6-3: Fuel weight over time based on scale measurement (Test 1.1).47

Figure 6-4: Heat flux measurement from narrow view radiometers at different heights (Test 1.1).47

Figure 6-5: Heat flux measurement from wide view radiometers at different heights (Test 1.1).48

Figure 6-6: Temperature measurements from vertical thermocouple rake in centerline of fire plume (Test 1.1).48

Figure 6-7: Fire plume temperatures and surface emissive power values from IR camera measurements (Test 1.1).49

Figure 6-8: Thermocouple temperatures from DFT instruments. Distances are from center of pan (Test 1.1).50

Figure 6-9: Derived heat flux values from DFT measurements. Distances are from center of pan (Test 1.1).50

Figure 6-10: Thermocouple temperatures at inner cylinder stations (Test 1.1).51

Figure 6-11: Thermocouple temperatures at outer cylinder stations (Test 1.1).52

Figure 6-12: Thermocouple temperatures at exterior cylinder stations (Test 1.1).52

Figure 6-13: Absorbed heat flux to calorimeter (Test 1.1).53

Figure 6-14: Total heat flux to calorimeter (Test 1.1).53

Figure 6-15: Heat release rate (Test 1.1).54

Figure 6-16: Flame height from IR camera measurements (Test 1.1).54

Figure 6-17: Time-averaged image (left). Stadia board (right) (Test 1.1).55

Figure 6-18: Temperature of fuel supply into pan (Test 1.2).56

Figure 6-19: Fuel rake thermocouple temperatures (Test 1.2).56

Figure 6-20: Fuel weight over time based on scale measurement (Test 1.2).....	57
Figure 6-21: Heat flux measurement from narrow view radiometers at different heights (Test 1.2)..	58
Figure 6-22: Heat flux measurement from wide view radiometers at different heights (Test 1.2).....	58
Figure 6-23: Temperature measurements from vertical thermocouple rake in centerline of fire plume (Test 1.2).....	59
Figure 6-24: Thermocouple temperatures from DFT instruments. Distances are from center of pan (Test 1.2).....	60
Figure 6-25: Derived heat flux values from DFT measurements. Distances are from center of pan (Test 1.2).....	60
Figure 6-26: Heat release rate (Test 1.2).....	61
Figure 6-27: Time-averaged image (left). Flame height determined by stadia board marked with 1- m increments (right) (Test 1.2).....	61
Figure 6-28: Temperature of fuel supply into pan (Test 1.3).....	62
Figure 6-29: Fuel rake thermocouple temperatures (Test 1.3).....	63
Figure 6-30: Fuel weight over time based on scale measurement (Test 1.3).....	64
Figure 6-31: Heat flux measurement from narrow view radiometers at different heights (Test 1.3)..	64
Figure 6-32: Heat flux measurement from wide view radiometers at different heights (Test 1.3).....	65
Figure 6-33: Temperature measurements from vertical thermocouple rake in centerline of fire plume (Test 1.3).....	66
Figure 6-34: Thermocouple temperatures from DFT instruments. Distances are from center of pan (Test 1.3).....	67
Figure 6-35: Derived heat flux values from DFT measurements. Distances are from center of pan (Test 1.3).....	67
Figure 6-36: Thermocouple temperatures at inner cylinder (Test 1.3).....	68
Figure 6-37: Thermocouple temperatures at outer cylinder stations (Test 1.3).....	69
Figure 6-38: Thermocouple temperatures at exterior cylinder stations (Test 1.3).....	69
Figure 6-39: Absorbed heat flux to calorimeter (Test 1.3).....	70
Figure 6-40: Total heat flux to calorimeter (Test 1.3).....	70
Figure 6-41: Heat release rate (Test 1.3).....	71
Figure 6-42: Time-averaged image (a) before fuel reached average temperature 58°C (b) fuel reached average temperature 58°C. (c) Flame height determined by stadia board marked with 1-m increments (Test 1.3).....	72
Figure 6-43: Temperature of fuel supply into pan (Test 2.1).....	73
Figure 6-44: Fuel rake thermocouple temperatures (Test 2.1).....	74
Figure 6-45: Fuel weight over time based on scale measurement (Test 2.1).....	75
Figure 6-46: Heat flux measurement from narrow view radiometers at different heights (Test 2.1)..	76
Figure 6-47: Heat flux measurement from wide view radiometers at different heights (Test 2.1).....	76
Figure 6-48: Temperature measurements from vertical thermocouple rake in centerline of fire plume (Test 2.1).....	77
Figure 6-49: Fire plume temperatures and surface emissive power values from IR camera measurements (Test 2.1).....	78
Figure 6-50: Thermocouple temperatures from DFT instruments. Distances are from center of pan (Test 2.1).....	79
Figure 6-51: Derived heat flux values from DFT measurements. Distances are from center of pan (Test 2.1).....	79
Figure 6-52: Heat release rate (Test 2.1).....	80
Figure 6-53: Flame height from IR camera measurements (Test 2.1).....	80
Figure 6-54: Temperature of fuel supply into pan (Test 2.2).....	81

Figure 6-55: Fuel rake thermocouple temperatures (Test 2.2).....	82
Figure 6-56: Fuel weight over time based on scale measurement (Test 2.2).....	82
Figure 6-57: Heat flux measurement from narrow view radiometers at different heights (Test 2.2)..	83
Figure 6-58: Heat flux measurement from wide view radiometers at different heights (Test 2.2).....	83
Figure 6-59: Temperature measurements from vertical thermocouple rake in centerline of fire plume (Test 2.2).....	84
Figure 6-60: Fire plume temperatures and surface emissive power values from IR camera measurements (Test 2.2).....	85
Figure 6-61: Thermocouple temperatures from DFT instruments. Distances are from center of pan (Test 2.2).....	86
Figure 6-62: Derived heat flux values from DFT measurements. Distances are from center of pan (Test 2.2).....	86
Figure 6-63: Thermocouple temperatures at inner cylinder stations (Test 2.2).....	87
Figure 6-64: Thermocouple temperatures at outer cylinder stations (Test 2.2).....	88
Figure 6-65: Thermocouple temperatures at exterior cylinder stations (Test 2.2).....	88
Figure 6-66: Absorbed heat flux to calorimeter (Test 2.2).....	89
Figure 6-67: Total heat flux to calorimeter (Test 2.2).....	89
Figure 6-68: Heat release rate (Test 2.2).....	90
Figure 6-69: Flame height from IR camera measurements (Test 2.2).....	90
Figure 6-70: Temperature of fuel supply into pan (Test 2.3).....	91
Figure 6-71: Fuel rake thermocouple temperatures (Test 2.3).....	92
Figure 6-72: Heat flux measurement from narrow view radiometers at different heights (Test 2.3)..	93
Figure 6-73: Heat flux measurement from wide view radiometers at different heights (Test 2.3).....	93
Figure 6-74: Temperature measurements from vertical thermocouple rake in centerline of fire plume (Test 2.3).....	94
Figure 6-75: Fire plume temperatures and surface emissive power values from IR camera measurements (Test 2.3).....	95
Figure 6-76: Thermocouple temperatures from DFT instruments. Distances are from center of pan (Test 2.3).....	96
Figure 6-77: Derived heat flux values from DFT measurements. Distances are from center of pan (Test 2.3).....	96
Figure 6-78: Thermocouple temperatures at inner cylinder stations (Test 2.3).....	97
Figure 6-79: Thermocouple temperatures at outer cylinder stations (Test 2.3).....	97
Figure 6-80: Thermocouple temperatures at exterior cylinder stations (Test 2.3).....	98
Figure 6-81: Absorbed heat flux to calorimeter (Test 2.3).....	98
Figure 6-82: Total heat flux to calorimeter (Test 2.3).....	99
Figure 6-83: Heat release rate (Test 2.3).....	99
Figure 6-84: Flame height from IR camera measurements (Test 2.3).....	100
Figure 6-85: Temperature of fuel supply into pan (Test 2.4).....	101
Figure 6-86: Fuel rake thermocouple temperatures (Test 2.4).....	101
Figure 6-87: Fuel weight over time based on scale measurement (Test 2.4).....	102
Figure 6-88: Heat flux measurement from narrow view radiometers at different heights (Test 2.4).....	103
Figure 6-89: Heat flux measurement from wide view radiometers at different heights (Test 2.4)...	103
Figure 6-90: Temperature measurements from vertical thermocouple rake in centerline of fire plume (Test 2.4).....	104
Figure 6-91: Fire plume temperatures and surface emissive power values from IR camera measurements (Test 2.4).....	105

Figure 6-92: Thermocouple temperatures from DFT instruments. Distances are from center of pan (Test 2.4).....	106
Figure 6-93: Derived heat flux values from DFT measurements. Distances are from center of pan (Test 2.4).....	106
Figure 6-94: Thermocouple temperatures at inner cylinder stations (Test 2.4).....	107
Figure 6-95: Thermocouple temperatures at outer cylinder stations (Test 2.4).....	107
Figure 6-96: Thermocouple temperatures at exterior cylinder stations (Test 2.4).....	108
Figure 6-97: Absorbed heat flux to calorimeter (Test 2.4).....	108
Figure 6-98: Total heat flux to calorimeter (Test 2.4).....	109
Figure 6-99: Heat release rate (Test 2.4).....	109
Figure 6-100: Flame height from IR camera measurements (Test 2.4).....	110
Figure 6-101: Temperature of fuel supply into pan (Test 2.5).....	111
Figure 6-102: Fuel rake thermocouple temperatures (Test 2.5).....	111
Figure 6-103: Fuel weight over time based on scale measurement (Test 2.5).....	112
Figure 6-104: Heat flux measurement from narrow view radiometers at different heights (Test 2.5).....	113
Figure 6-105: Heat flux measurement from wide view radiometers at different heights (Test 2.5).....	113
Figure 6-106: Temperature measurements from vertical thermocouple rake in centerline of fire plume (Test 2.5).....	114
Figure 6-107: Fire plume temperatures and surface emissive power values from IR camera measurements (Test 2.5).....	115
Figure 6-108: Thermocouple temperatures from DFT instruments. Distances are from center of pan (Test 2.5).....	116
Figure 6-109: Derived heat flux values from DFT measurements. Distances are from center of pan (Test 2.5).....	116
Figure 6-110: Thermocouple temperatures at inner cylinder stations (Test 2.5).....	117
Figure 6-111: Thermocouple temperatures at outer cylinder stations (Test 2.5).....	117
Figure 6-112: Thermocouple temperatures at exterior cylinder stations (Test 2.5).....	118
Figure 6-113: Absorbed heat flux to calorimeter (Test 2.5).....	118
Figure 6-114: Total heat flux to calorimeter (Test 2.5).....	119
Figure 6-115: Heat release rate (Test 2.5).....	119
Figure 6-116: Flame height from IR camera measurements (Test 2.5).....	120
Figure 6-117: Temperature of fuel supply into pan (Test 2.6).....	121
Figure 6-118: Fuel rake thermocouple temperatures (Test 2.6).....	121
Figure 6-119: Fuel weight over time based on scale measurement (Test 2.6).....	122
Figure 6-120: Heat flux measurement from narrow view radiometers at different heights (Test 2.6).....	123
Figure 6-121: Heat flux measurement from wide view radiometers at different heights (Test 2.6).....	123
Figure 6-122: Temperature measurements from vertical thermocouple rake in centerline of fire plume (Test 2.6).....	124
Figure 6-123: Fire plume temperatures and surface emissive power values from IR camera measurements (Test 2.6).....	125
Figure 6-124: Thermocouple temperatures from DFT instruments. Distances are from center of pan (Test 2.6).....	126
Figure 6-125: Derived heat flux values from DFT measurements. Distances are from center of pan (Test 2.6).....	126
Figure 6-126: Heat release rate (Test 2.6).....	127
Figure 6-127: Flame height from IR camera measurements (Test 2.6).....	128

Figure 6-128: Temperature of fuel supply into pan (Test 3.1).	129
Figure 6-129: Fuel Rake thermocouple temperatures (Test 3.1)	130
Figure 6-130: Fuel weight over time based on scale measurement (9.8-10.6 minutes) (Test 3.1).	131
Figure 6-131: Fuel weight over time based on scale measurement (16.6-17.4 minutes) (Test 3.1).	131
Figure 6-132: Heat flux measurement from narrow view radiometers at different heights (Test 3.1)	132
Figure 6-133: Heat flux measurement from wide view radiometers at different heights (Test 3.1).	132
Figure 6-134: Temperature measurements from vertical thermocouple rake in centerline of fire plume (Test 3.1)	133
Figure 6-135: Fire plume temperatures and surface emissive power values from IR camera measurements (Test 3.1).	134
Figure 6-136: Thermocouple temperatures from DFT instruments. Distances are from center of pan (Test 3.1).	135
Figure 6-137: Derived heat flux values from DFT measurements. Distances are from center of pan (Test 3.1).	135
Figure 6-138: Thermocouple temperatures at inner cylinder stations (Test 3.1)	136
Figure 6-139: Thermocouple temperatures at outer cylinder stations (Test 3.1).	136
Figure 6-140: Thermocouple temperatures at exterior cylinder stations (Test 3.1).	137
Figure 6-141: Absorbed heat flux to calorimeter (Test 3.1).	137
Figure 6-142: Total heat flux to calorimeter (Test 3.1).	138
Figure 6-143: Flame height from IR camera measurements (Test 3.1).	139
Figure 6-144: Temperature of fuel supply into pan (Test 3.2).	140
Figure 6-145: Fuel rake thermocouple temperatures (Test 3.2)	141
Figure 6-146: Fuel weight over time based on scale measurement (11.9 to 12.6 minutes) (Test 3.2)	142
Figure 6-147: Fuel weight over time based on scale measurement (17.3 to 18.3 minutes) (Test 3.2)	142
Figure 6-148: Heat flux measurement from narrow view radiometers at different heights (Test 3.2)	143
Figure 6-149: Heat flux measurement from wide view radiometers at different heights (Test 3.2).	143
Figure 6-150: Temperature measurements from vertical thermocouple rake in centerline of fire plume (Test 3.2)	144
Figure 6-151: Fire plume temperatures and surface emissive power values from IR camera measurements (Test 3.2).	145
Figure 6-152: Thermocouple temperatures from DFT instruments. Distances are from center of pan (Test 3.2).	146
Figure 6-153: Derived heat flux values from DFT measurements. Distances are from center of pan (Test 3.2).	146
Figure 6-154: Thermocouple temperatures at inner cylinder stations (Test 3.2)	147
Figure 6-155: Thermocouple temperatures at outer cylinder stations (Test 3.2).	147
Figure 6-156: Thermocouple temperatures at exterior cylinder stations (Test 3.2).	148
Figure 6-157: Absorbed heat flux to calorimeter (Test 3.2).	148
Figure 6-158: Total heat flux to calorimeter (Test 3.2).	149
Figure 6-159: Flame height from IR camera measurements (Test 3.2).	150
Figure 6-160: Temperature of fuel supply into pan (Test 3.3).	151
Figure 6-161: Fuel rake thermocouple temperatures (Test 3.3)	152
Figure 6-162: Fuel weight over time based on scale measurement (8.5 to 10 minutes) (Test 3.3)	153

Figure 6-163: Fuel weight over time based on scale measurement (16.8 to 18.5 minutes) (Test 3.3).....	153
Figure 6-164: Heat flux measurement from narrow view radiometers at different heights (Test 3.3).....	154
Figure 6-165: Heat flux measurement from wide view radiometers at different heights (Test 3.3). ..	154
Figure 6-166: Temperature measurements from vertical thermocouple rake in centerline of fire plume (Test 3.3).....	155
Figure 6-167: Fire plume temperatures and surface emissive power values from IR camera measurements (Test 3.3).	156
Figure 6-168: Thermocouple temperatures from DFT instruments. Distances are from center of pan (Test 3.3).....	157
Figure 6-169: Derived heat flux values from DFT instruments. Distances are from center of pan (Test 3.3).....	157
Figure 6-170: Flame height from IR camera measurements (Test 3.3).	158
Figure 6-171: Temperature of fuel supply into pan (Test 3.4).	159
Figure 6-172: Fuel rake thermocouple temperatures (Test 3.4).....	160
Figure 6-173: Fuel weight over time during filling the pan (Test 3.4).....	161
Figure 6-174: Heat flux measurement from narrow view radiometers at different heights (Test 3.4).....	161
Figure 6-175: Heat flux measurement from wide view radiometers at different heights (Test 3.4). ..	162
Figure 6-176 Temperature measurements from vertical thermocouple rake in centerline of fire plume (Test 3.4).....	162
Figure 6-177: Fire plume temperatures and surface emissive power values from IR camera measurements (Test 3.4).	163
Figure 6-178: Thermocouple temperatures from DFT instruments. Distances are from center of pan (Test 3.4).	164
Figure 6-179: Derived heat flux values from DFT instruments. Distances are from center of pan (Test 3.4).....	164
Figure 6-180: Flame height from IR camera measurements (Test 3.4).	165
Figure 6-181: Temperature of fuel supply into pan (Test 3.5).	166
Figure 6-182: Fuel rake thermocouple temperatures (Test 3.5).	166
Figure 6-183: Fuel weight over time during filling the pan (Test 3.5).....	167
Figure 6-184: Burn rate (kg/min) versus time (test 3.5).....	168
Figure 6-185: Heat flux measurement from narrow view radiometers at different heights (Test 3.5).....	168
Figure 6-186: Heat flux measurement from wide view radiometers at different heights (Test 3.5). ..	169
Figure 6-187: Temperature measurements from vertical thermocouple rake in centerline of fire plume (Test 3.5).....	169
Figure 6-188: Fire plume temperatures and surface emissive power values from IR camera measurements (Test 3.5).	170
Figure 6-189: Thermocouple temperatures from DFT instruments. Distances are from center of pan (Test 3.5).	171
Figure 6-190: Derived heat flux values from DFT instruments. Distances are from center of pan (Test 3.5).....	171
Figure 6-191: Thermocouple temperatures at inner cylinder stations (Test 3.5).....	172
Figure 6-192: Thermocouple temperatures at outer cylinder stations (Test 3.5).	173
Figure 6-193: Thermocouple temperatures at exterior cylinder stations (Test 3.5).	173
Figure 6-194: Absorbed heat flux to calorimeter (Test 3.5).	174

Figure 6-195: Total heat flux to calorimeter (Test 3.5).	174
Figure 6-196: Flame height from IR camera measurements (Test 3.5).	175
Figure 6-197: Temperature of fuel supply into pan (Test 3.6).	176
Figure 6-198: Fuel rake thermocouple temperatures (Test 3.6).	176
Figure 6-199: Fuel weight over time during filling the pan (Test 3.6).	177
Figure 6-200: Burn rate (kg/min) over period 12.3-19.3 minutes (Test 3.6).	178
Figure 6-201: Heat flux measurement from narrow view radiometers at different heights (Test 3.6).	178
Figure 6-202: Heat flux measurement from wide view radiometers at different heights (Test 3.6).	179
Figure 6-203: Temperature measurements from vertical thermocouple rake in centerline of fire plume (Test 3.6).	179
Figure 6-204: Fire plume temperatures and surface emissive power values from IR camera measurements (Test 3.6).	180
Figure 6-205: Thermocouple temperatures from DFT instruments. Distances are from center of pan (Test 3.6).	181
Figure 6-206: Derived heat flux values from DFT instruments. Distances are from center of pan (Test 3.6).	181
Figure 6-207: Thermocouple temperatures at inner cylinder stations (Test 3.6).	182
Figure 6-208: Thermocouple temperatures at outer cylinder stations (Test 3.6).	183
Figure 6-209: Thermocouple temperatures at exterior cylinder stations (Test 3.6).	183
Figure 6-210: Absorbed heat flux to calorimeter (Test 3.6).	184
Figure 6-211: Total heat flux to calorimeter (Test 3.6).	184
Figure 6-212: Flame height from IR camera measurements (Test 3.6).	185
Figure 7-1: Burn rates for heptane tests.	188
Figure 7-2: Burn rate for Bakken crude oil tests.	190
Figure 7-3: Burn rate for dilbit crude oil tests.	192
Figure 7-4: Narrow-view radiometer comparison among heptane tests.	193
Figure 7-5: Wide-view radiometer comparison among heptane tests.	194
Figure 7-6: Narrow-view radiometer comparison among Bakken crude oil tests.	196
Figure 7-7: Wide-view radiometer comparison among Bakken crude oil tests.	197
Figure 7-8: Narrow-view radiometer comparison among dilbit crude oil tests.	198
Figure 7-9: Wide-view radiometer comparison among dilbit crude oil tests.	199
Figure 7-10: Thermocouple temperatures from fire plume rake for heptane tests.	200
Figure 7-11: Thermocouple temperatures from fire plume rake for Bakken crude oil tests.	202
Figure 7-12: Thermocouple temperatures from fire plume rake for Dilbit crude oil tests.	204
Figure 7-13: Average fire plume temperatures for the Bakken crude oil tests from IR camera.	206
Figure 7-14: Average of all TC rake locations in fire plume for Bakken crude oil tests	206
Figure 7-15: Average surface emissive power values for the Bakken crude oil tests from IR camera.	207
Figure 7-16: Average fire plume temperatures for the Dilbit crude oil tests from IR camera.	208
Figure 7-17: Average of all TC rake locations up to 4 m in fire plume for Dilbit crude oil tests.	209
Figure 7-18: Average surface emissive power values for the Dilbit crude oil tests from IR camera.	210
Figure 7-19: Average DFT absorbed heat flux for heptane tests.	211
Figure 7-20: Average DFT incident heat flux for heptane tests.	212
Figure 7-21: Average DFT absorbed heat flux for Bakken crude oil tests.	214
Figure 7-22: Average DFT incident heat flux for Bakken crude oil tests.	214
Figure 7-23: Average DFT absorbed heat flux for dilbit crude oil tests.	216
Figure 7-24: Average DFT incident heat flux for dilbit crude oil tests.	216

Figure 7-25: Side seam of second calorimeter after Test 2.5.....	217
Figure 7-26: Calorimeter average temperatures for heptane tests.....	218
Figure 7-27: Calorimeter average heat flux values for heptane tests.....	219
Figure 7-28: Calorimeter average temperatures for Bakken crude oil tests.....	220
Figure 7-29: Calorimeter average heat flux values for Bakken crude oil tests.....	220
Figure 7-30: Integrated temperatures among all calorimeter TC locations for the Dilbit crude oil tests.....	223
Figure 7-31: Integrated heat flux values averaged among all calorimeter TC locations for the Dilbit crude oil tests.....	223
Figure 7-32: Average heat release rates from CGA measurements for heptane tests.....	225
Figure 7-33: Average heat release rate from CGA measurements for Bakken crude oil tests.....	226
Figure 7-34: Average heat release rates for Dilbit crude oil tests.....	227
Figure 7-35: Average flame heights of heptane tests.....	228
Figure 7-36: Average flame heights for Bakken crude oil tests.....	229
Figure 7-37: Average flame heights for Dilbit crude oil tests.....	230
Figure 8-1: Burn rate (mm/min) for all tests.....	231
Figure 8-2: Temperature versus boiling point distribution for fuel samples.....	232
Figure 8-3: Carbon number vs. mass content averaged over the Bakken and dilbit samples (<C15).....	233
Figure 8-4: Carbon number vs. mass content averaged over the Bakken and dilbit samples.....	233
Figure 8-5: Carbon number vs. mass content for the dilbit, condensate, and bitumen.....	234
Figure 8-6: Carbon number vs mass content for the dilbit fuel and a simulated mixture of condensate and bitumen.....	234
Figure 8-7: Temperatures from the fuel thermocouple rake and flame height for Tests 3.4.....	235
Figure 8-8: Post-test residue remaining from the (a) Bakken crude oil and (b) dilbit crude oil for non-continuous fuel feed tests.....	235
Figure 8-9: Comparison of averaged heat flux from narrow-view radiometers for all fuels tested..	236
Figure 8-10: Comparison of averaged heat flux from wide-view radiometers for all fuels tested....	237
Figure 8-11: Comparison of averaged temperatures from centerline fire plume TC rake for all tests.....	238
Figure 8-12: Average fire plume temperatures from IR measurements for all tests.....	239
Figure 8-13: Average surface emissive power from IR measurements for all tests.....	239
Figure 8-14: DFT average absorbed heat flux at 2 m from center of pool for all tests.....	240
Figure 8-15: DFT average absorbed heat flux at 4 m from center of pool for all tests.....	240
Figure 8-16: DFT average incident heat flux at 2 m from center of pool for all tests.....	241
Figure 8-17: DFT average incident heat flux at 4 m from center of pool for all tests.....	241
Figure 8-18: Calorimeter outer cylinder temperatures averaged over time and all locations from all tests.....	243
Figure 8-19: Calorimeter exterior temperatures averaged over time and all locations from all tests.....	243
Figure 8-20: Calorimeter absorbed heat flux averaged over time and all locations for all tests.....	244
Figure 8-21: Calorimeter total heat flux averaged over time and all locations for all tests.....	244
Figure 8-22: Calorimeter average temperatures at left, center, and right stations (inner cylinder) for heptane tests.....	245
Figure 8-23: Calorimeter average temperatures at left, center, and right stations (inner cylinder) for Bakken tests.....	245
Figure 8-24: Calorimeter average temperatures at left, center, and right stations (inner cylinder) for Dilbit tests.....	246

Figure 8-25: Calorimeter average temperatures at left, center, and right stations (outer cylinder) for heptane tests.	246
Figure 8-26: Calorimeter average temperatures at left, center, and right stations (outer cylinder) for Bakken tests.	247
Figure 8-27: Calorimeter average temperatures at left, center, and right stations (outer cylinder) for Dilbit tests.	248
Figure 8-28: Calorimeter average temperatures at left, center, and right stations (exterior) for heptane tests.	248
Figure 8-29: Calorimeter average temperatures at left, center, and right stations (exterior) for Bakken tests.	249
Figure 8-30: Calorimeter average temperatures at left, center, and right stations (exterior) for Dilbit tests.	250
Figure 8-31: Total heat flux to calorimeter for heptane tests.	251
Figure 8-32: Total heat flux to calorimeter for Bakken tests.	251
Figure 8-33: Total heat flux to calorimeter for dilbit tests.	252
Figure 8-34: Heat release rate from CGA measurements among the test series.	253
Figure 8-35: Average flame height among the test series.	253
Figure A-1: DFT and Calorimeter specifications for heat flux calculations.	257
Figure A-2: Data frame with (top row) images from MWIR camera (from left to right) counts, temperature, and SEP. From left to right – bottom row: History curves for maximum and average SEP, histogram for the instantaneous SEP, Box fit for flame, and fire dimension history.	260
Figure A-3: Average temperature and average SEP from heptane Test 1.1. Panel (a): temperature distribution calculated with emissivity (ϵ) of 0.97 and air transmission (T_x) of 0.95. Panel (b): SEP distribution calculated with emissivity (ϵ) of 1.0 and air transmission (T_x) of 0.95.	261
Figure A-4: Average temperature and average SEP vertical profiles for heptane Test 1.1 with calorimeter.	262
Figure A-5: Average temperature and average SEP vertical profiles for Bakken Test 2.1 without calorimeter.	262
Figure A-6: Average temperature and average SEP vertical profiles for Bakken Test 2.2 with calorimeter.	263
Figure A-7: Average temperature and average SEP vertical profiles for Bakken Test 2.3 with calorimeter.	263
Figure A-8: Average temperature and average SEP vertical profiles for Bakken Test 2.4 with calorimeter.	264
Figure A-9: Average temperature and average SEP vertical profiles for Bakken Test 2.5 with calorimeter.	264
Figure A-10: Average temperature and average SEP vertical profiles for Bakken Test 2.6 without calorimeter.	265
Figure A-11: Average temperature and average SEP vertical profiles for dilbit Test 3.1 with calorimeter.	265
Figure A-12: Average temperature and average SEP vertical profiles for dilbit Test 3.2 with calorimeter.	266
Figure A-13: Average temperature and average SEP vertical profiles for dilbit Test 3.3 without calorimeter.	266
Figure A-14: Average temperature and average SEP vertical profiles for dilbit Test 3.4 without calorimeter.	267

Figure A-15: Average temperature and average SEP vertical profiles for dilbit Test 3.5 with calorimeter.....	267
Figure A-16: Average temperature and average SEP vertical profiles for dilbit Test 3.6 with calorimeter.....	268
Figure A-17: Graphical depiction of the SEP sensitivity analysis from Table 2 for heptane Test 1.1.....	271
Figure A-18: Graphical depiction of the temperature sensitivity analysis from Table 2 for heptane Test 1.1.....	272

LIST OF TABLES

Table 3-1: Component list and specifications for fuel supply system.....	32
Table 4-1: Instruments and their purpose.....	33
Table 4-2: Instrument ranges and resolution.....	42
Table 5-1: Test matrix for all test series.....	43
Table 6-1: Values used to determine burn rate.....	122
Table 7-1: Volume of heptane used for each heptane test.....	187
Table 7-2: Burn rate for each heptane test.....	187
Table 7-3: Volume of oil used for each Bakken crude oil test.....	189
Table 7-4: Burn rate for each Bakken crude oil test.....	189
Table 7-5: Volume of oil used and residue mass for each dilbit crude oil test.....	191
Table 7-6: Burn rate for each dilbit crude oil test.....	191
Table 7-7: Average heat flux measurements from narrow view radiometers for all heptane tests (measurements in kW/m ²).....	193
Table 7-8: Average heat flux measurements from wide view radiometers for heptane tests (measurements in kW/m ²).....	194
Table 7-9: Average heat flux measurements from narrow view radiometers for all Bakken crude oil tests (measurements in kW/m ²).....	195
Table 7-10: Average heat flux measurements from wide view radiometers for all Bakken crude oil tests (measurements in kW/m ²).....	196
Table 7-11: Average heat flux measurements from narrow view radiometers for all Dilbit crude oil tests (measurements in kW/m ²).....	198
Table 7-12: Integrated heat flux measurements from wide view radiometers for all dilbit crude oil tests (measurements in kW/m ²).....	199
Table 7-13: Average thermocouple rake temperatures in fire plume for heptane tests.....	200
Table 7-14: Average thermocouple rake temperatures in fire plume for Bakken crude oil tests.....	201
Table 7-15: Average thermocouple rake temperatures in fire plume for Dilbit crude oil tests.....	203
Table 7-16: Mean plume temperatures and surface emissive power for heptane test 1.1 from IR camera.....	204
Table 7-17: Average plume temperatures and surface emissive power for Bakken crude oil tests from IR camera. Optical transmission of 0.95 and emissivity of 1.0.....	205
Table 7-18: Average plume temperatures and surface emissive power for dilbit crude oil tests from IR camera.....	208
Table 7-19: Average DFT temperature and heat flux values for the heptane tests.....	211
Table 7-20: Average DFT temperature and heat flux values for the Bakken crude oil tests.....	213
Table 7-21: Average DFT temperature and heat flux values for the Dilbit crude oil tests.....	215

Table 7-22: Average temperature and heat flux values among all calorimeter TC locations for the heptane tests.....	218
Table 7-23: Average temperature and heat flux values among all calorimeter TC locations for the Bakken crude oil tests.....	219
Table 7-24: Calorimeter integrated total heat flux values for dilbit pool fire tests (kW/m ²).....	221
Table 7-25: Calorimeter integrated absorbed heat flux values for dilbit pool fire tests (kW/m ²)	222
Table 7-26: Integrated temperature and heat flux values averaged among all calorimeter TC locations for the dilbit crude oil tests.....	222
Table 7-27: Heat of combustion for fuels tested	224
Table 7-28: Average heat release rates for heptane tests.....	224
Table 7-29: Average heat release rates for Bakken crude oil tests (measured in MW).....	225
Table 7-30: Average heat release rates for Dilbit crude oil tests (measured in MW).....	227
Table 7-31: Average flame heights of heptane tests.	228
Table 7-32: Average flame heights for Bakken crude oil tests.....	229
Table 7-33: Average flame heights for Dilbit crude oil tests.....	230
Table A-1: Measured emissivity for DFT instruments used for test series	258
Table A-2: SEP and temperature sensitivity to emissivity and transmissivity (Test 1.1).....	269

This page left blank

EXECUTIVE SUMMARY

This report provides results from three test series performed in the Thermal Test Complex at Sandia National Laboratories. The test series involved 2-m pool fires using heptane, Bakken crude oil, and a dilbit crude oil. The effect of the presence and placement of a calorimeter, fuel supply temperature, and maintaining a constant fuel level were assessed. Measurements include burn rate, surface emissive power, flame height, heat flux to an engulfed calorimeter, heat flux to external instruments, thermocouple temperatures within the fuel and fire plume, and heat release rate.

In considering the parameter effects within a test series, the results indicate the following:

- The higher temperature fuel supply increased the burn rate by about 10% for the heptane tests, whereas it did not have a significant effect for the Bakken crude oil tests. The higher temperature fuel test for the dilbit crude oil indicated a lower average burn rate, but its range of deviation overlapped tests with lower temperatures.
- Allowing the fuel to burn down, rather than maintaining a constant fuel level, did not have a significant effect on averaged measured values from any of the instruments.
- The presence of the calorimeter had the most impact on the burn rate. For the heptane tests, the burn rate was slightly higher (~10%) in the test without the calorimeter. For the Bakken crude oil, the burn rate was higher overall (~10-15%) for tests without the calorimeter compared to tests with the calorimeter. For the Dilbit crude oil, any effect was not detected though it is difficult to make a firm conclusion due to its highly variable burn rate.
- The placement of the calorimeter affected the average total heat flux from the flame to the calorimeter for the Bakken crude oil and not for the Dilbit crude oil tests. The Bakken crude oil test with the calorimeter placed 0.5 m lower in the flame resulted in a lower average total heat flux to the calorimeter (~78 kW/m² vs. ~100 kW/m²). For the Dilbit crude oil there was no effect since the calorimeter was above the fuel-rich regions for both positions of 0.5 and 1 m.

In comparing the behavior among the fuels, the main conclusions are the following:

- The average burn rate for heptane is higher than Bakken and dilbit crude oils, ~0.04 kg/m²s vs. ~ 0.03 kg/m²s and ~ 0.02 kg/m²s, respectively.
- The burn rate for the dilbit crude oil was highly variable due to its mixture, comprised of a condensate (~20 vol%) and bitumen crude oil (~80 vol%).
- The average flame height for heptane is higher than the Bakken and dilbit crude oils, ~6.2 m vs. ~4.4 m and ~3.5 m, respectively.
- The average flame temperatures from the IR camera measurements are similar (~900 K) for all fuels.
- The average surface emissive power is lower for heptane than for Bakken and dilbit crude oils, ~66 kW/m² vs. ~76 kW/m² and ~71 kW/m², respectively.
- For calorimeter measurements, the Bakken crude oil resulted in the highest outer cylinder and exterior temperatures and the highest average total heat flux by about a factor of 1.5 and 1.3 higher compared to heptane and the dilbit crude oil, respectively (~95 kW/m² vs ~62.5 kW/m² and ~71.9 kW/m², respectively).

ACRONYMS AND DEFINITIONS

Abbreviation	Definition
ϵ	Emissivity
DFT	Directional flame thermometer
FLAME	Fire Laboratory for Accreditation of Models and Experiments
FPA	Focal plane array
FPS	Frames per second
InSb	Indium antimonide
IR	Infrared radiation
LWIR	Long wave infrared (7-14 μm)
MWIR	Mid wave infrared (3-5 μm)
ND-X	Neutral density filter where X is attenuation by a factor of 10x
NRCC	National Research Council of Canada
NUC	Nonlinear uniformity correction
NV	Narrow view
RH	Relative humidity
SEP	Surface emissive power
SNL	Sandia National Laboratories
TC	Thermocouple
TTC	Thermal Test Complex
T_x	Transmission
WV	Wide view

1. INTRODUCTION

This report provides results from a series of 2-m pool fire tests conducted at Sandia National Laboratories' (SNL) Thermal Test Complex (TTC) on behalf of the National Research Council of Canada (NRCC). The experiments include three tests series each involving different fuels. The first series included three heptane tests, the second six Bakken crude oil tests, and the third six diluted bitumen (dilbit) crude oil tests.

Measurements include burn rate, surface emissive power, flame height, heat flux to an engulfed calorimeter, heat flux to external instruments, thermocouple temperatures within the fuel and fire plume, and heat release rate. The heptane pool fire tests serve as a baseline dataset for comparison to the crude oil tests. The objectives of the crude oil tests are to assess the effect of several parameters that include the presence and placement of a calorimeter engulfed in the fire, fuel feed temperature, and allowing the fuel to burn down. An additional objective is to determine if oil composition effects the measurements. In addition to performing the pool fires, this study also includes a sampling and analysis effort in which fuel samples and post-test residue were collected for analysis and characterization provided in a separate report [1].

The Bakken crude oil was supplied by approval from the U.S. Department of Energy (DOE) and the U.S. Department of Transportation (DOT) via a tanker, specially designed to prevent contact with air and evaporative loss of components during storage, transport, and testing by using a water-feed method. The design and build of the tanker, as well as the procurement of the oil, was funded by the DOE/DOT for an SNL study on the comparison of tight and conventional crude oils with regards to pool fires and fireballs [2]. The Dilbit crude oil was provided by Transport Canada via twelve air-tight tanks that required pressurized nitrogen for the fuel supply system.

The following sections provide a description of the experiments, including the testing facility, transport tanker, instrumentation and associated uncertainty, and the test matrix. The results and discussion of each test are then provided.

This page left blank

2. TESTING FACILITY

The 2-m pool fire tests were conducted in the Fire Laboratory for Accreditation of Models and Experiments (FLAME) test cell in the TTC at SNL (Figure 2-1). This facility is designed to provide well-controlled boundary conditions for model code validation and test repeatability. This is in contrast to outdoor conditions where the presence of wind, variable over time and with direction, can prevent repeatability.

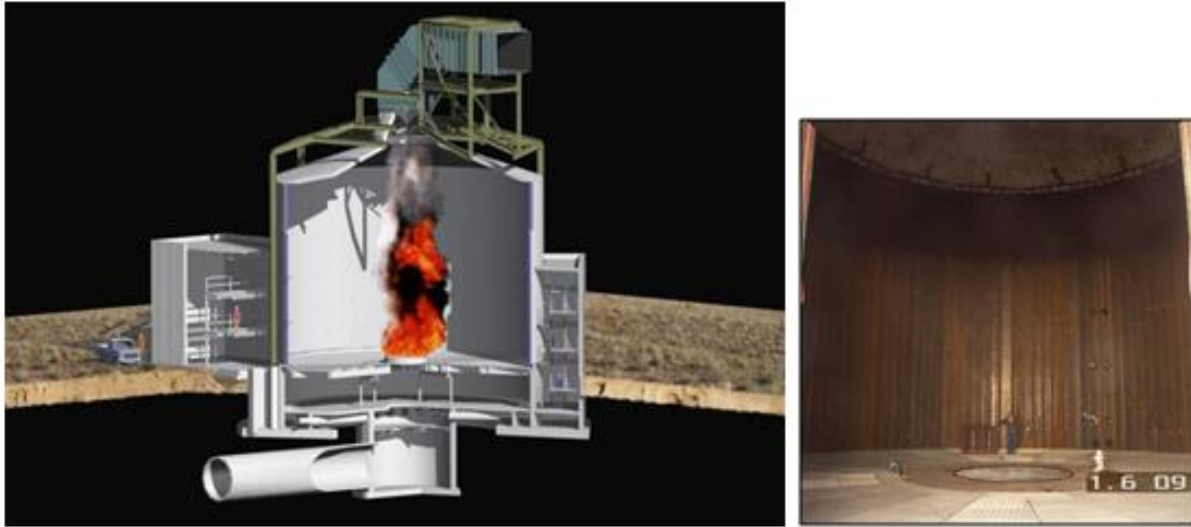


Figure 2-1: A cutaway view and interior of the FLAME facility. The view shows a liquid pool fire at the ground level, pipes supplying air flow through the basement, exhaust ductwork, and instrumentation rooms.

The main test chamber of FLAME is cylindrical in shape, 60 ft (18.3 m) inner diameter with a height around the perimeter of 40 ft (12.2 m). The ceiling slopes upwards ($\sim 18^\circ$) from the perimeter walls to a height of 48 ft (14.6 m) over the center of the facility. A round hole at the top of the facility of 16 ft (4.9 m) diameter transitions to a 10 x 12 ft (3.0 x 3.7 m) chimney duct. A large electrostatic precipitator downstream of FLAME collects soot prior to combustion products being sent to the exhaust stack. The outer walls are made of steel channel sections welded together and are filled with water for cooling during tests.

The ground level of FLAME can be divided into three concentric sections. At the center of the facility is a fuel pan or gas burner. The facility can operate a gas burner (He, H₂, CH₄, etc.) or a liquid fuel pool (JP-8, methanol, etc.). Typical diameters tested range from 1 m to 3 m. There is a steel spill plate surrounding the fuel pan, which extends to a diameter of 12.7 m. The floor of the outer section is made of a steel grating, through which air is supplied to the test chamber during fire experiments. The floor is flush with the top of the pan edge. The fuel pan used for this test series is 12 inches (0.3 m) deep at the edge of the 2-m diameter pan with a slight slope towards its center for drainage purposes. The depth of the pan is necessitated by the occurrence of a boil-over from previous crude oil pool fire tests in the facility. In order to prevent disruptive introduction of fluid into the pan such as a jet, an 8-in (0.2 m) diameter, 2-in (5.1 cm) high diffuser (Figure 2-2) in the form of a plate surrounded by a screen was placed in the center of the pan above the fuel entry point.



Figure 2-2: Diffuser for fuel introduction into the 2-m diameter pan.

Combustion air is supplied from the forced draft (FD) fan in a central utility building (not shown) through a large underground pipe (12-ft or 3.66-m diameter) to a plenum that feeds 18 radial pipes (3-ft or 0.91-m diameter) to a 4 x 4 ft (1.22 m x 1.22 m) annular ring in the FLAME basement. Air exits the grated top of the annular ring and enters the ground-level steel grating. An induced draft (ID) fan just before the exhaust stack automatically adjusts speed to maintain the differential pressure (to ambient) with the facility to near zero. Flowrate through the test cell is measured with instrumentation (calibrated pitot tubes) located inside the forced draft fan (provided air input into the test chamber) and measured with instrumentation located at the exhaust stack. Figure 2-3 provides the general experimental layout in FLAME with dimensions in meters.

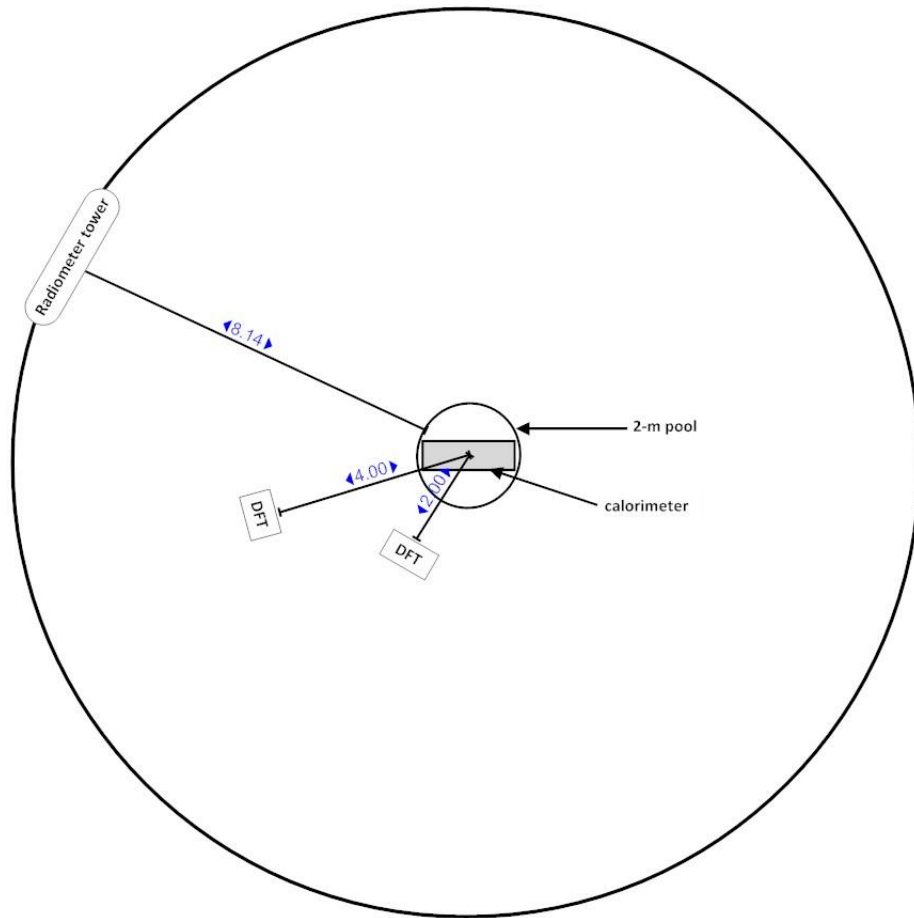


Figure 2-3: Top view of experimental layout in the FLAME facility. Dimensions in meters.

This page left blank

3. FUEL SUPPLY SYSTEM FOR TESTS

Each test series used a different configuration to supply fuel to the test pan. For the heptane tests, test series 1, the fuel was contained in drums and pre-heated with drum heaters, then pumped through a heat exchanger into the fuel pan. The same heat exchanger was used for all test series and is described below.

For the Bakken crude oil tests, test series 2, a special transport tanker manufactured by Tank Services, Inc. was used (Figure 3-1 and Figure 3-2). The tanker uses water displacement to load/unload the tanker and isolate the crude oil from direct contact with air. Thus, water makes up the balance of volume within the tanker rather than air and comprises the bottom layer within the tanker. This is required to preserve the light ends concentration of samples coming from the field to assure that they are introduced into the burn test apparatus representing the original material collected from the transportation system. The tankers are pre-manufactured pressure vessels that were modified. The tankers have a frame structure that allows for loading onto a tractor-trailer rig and has an integrated, permanent work platform at the top of tank structure to facilitate filling and maintenance of the tank.

There are two connections for mixing the oil in the tanker and minimizing density stratification. The circulation with the direction of flow towards the head is designed to provide enough momentum to generate full circulation of total oil inventory. A dedicated pump for oil mixing is used to prevent contamination of the water systems. The tank is mixed at a pressure at least 20 psi above the oil's vapor pressure. The pumping of water from an external water tote was adequate to maintain the required pressure (~45 psi or 0.3 MPa). The pressure within the tanker is monitored by a 0-600 psi (4.14 MPa) pressure gauge (accuracy $\pm 1.5\%$).

Tank design requirements include:

- Maximum allowable working pressure (MAWP) of at least 250 psig.
- Meets DOT Specification 51 for steel portable tanks
- Capable of maintaining vacuum down to 20 inches mercury (-9.8 psig).
- Tanker built to ASME Section VIII, division 1 Boiler and pressure vessel code
- The pressure relief valves, hand valves and instrumentation constructed to eliminate leakage under vacuum conditions.
- Pressure relief valve supplied by Contractor. Pressure relief valves capacity shall be determined by the larger capacity required by ASME or DOT
- Float level indicator for oil-water level (oil SG = 0.658, water SG = 1.0) inside tank.
- Tank is mounted on a trailer (tank chassis) approved for road transport, meeting all applicable US DOT regulations.



Figure 3-1: Pressurized tanker mounted on trailer.

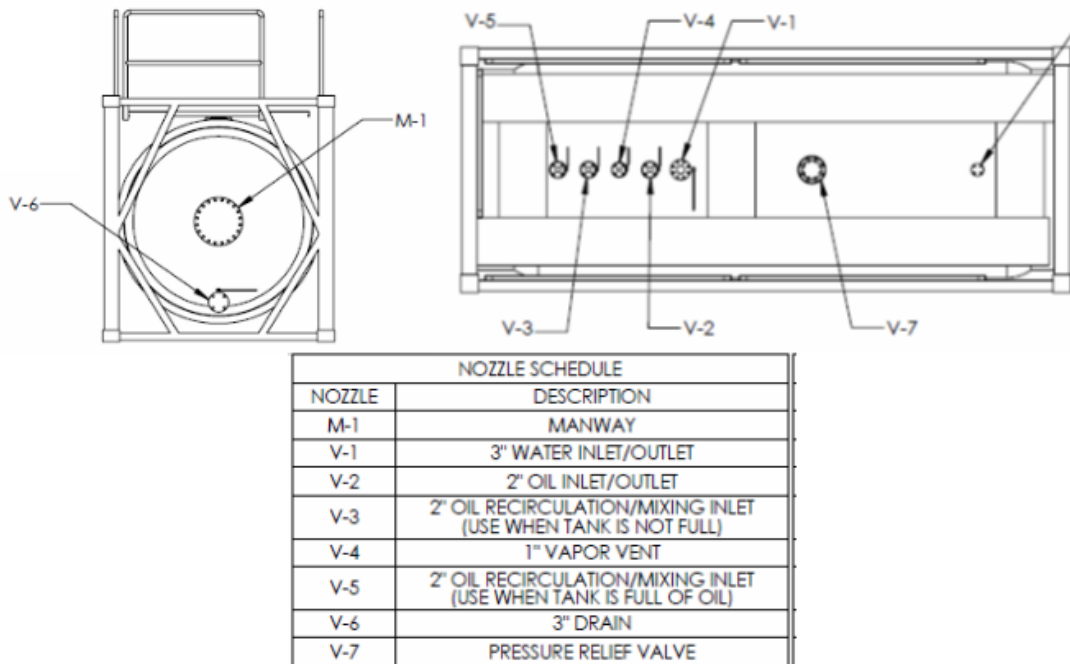


Figure 3-2: Nozzle locations on pressurized tanker.

The crude oil was pushed out of the tanker by feeding water into the bottom of the tanker (Figure 3-3 and Figure 3-4). The oil was then fed through a heat exchanger and then directly into the fuel

pan (Figure 3-5). The heat exchanger is a four-pass shell and tube design rated for 5 GPM, and the heater is rated for a maximum of 120,000 BTU/hr (35 kW).

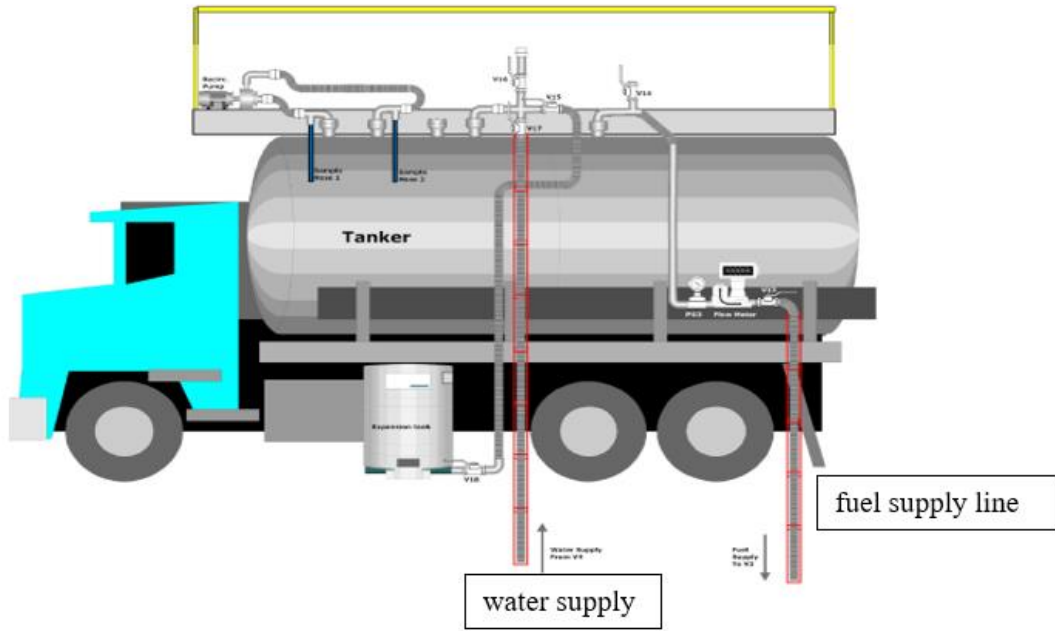


Figure 3-3: Oil tanker and water and fuel supply.

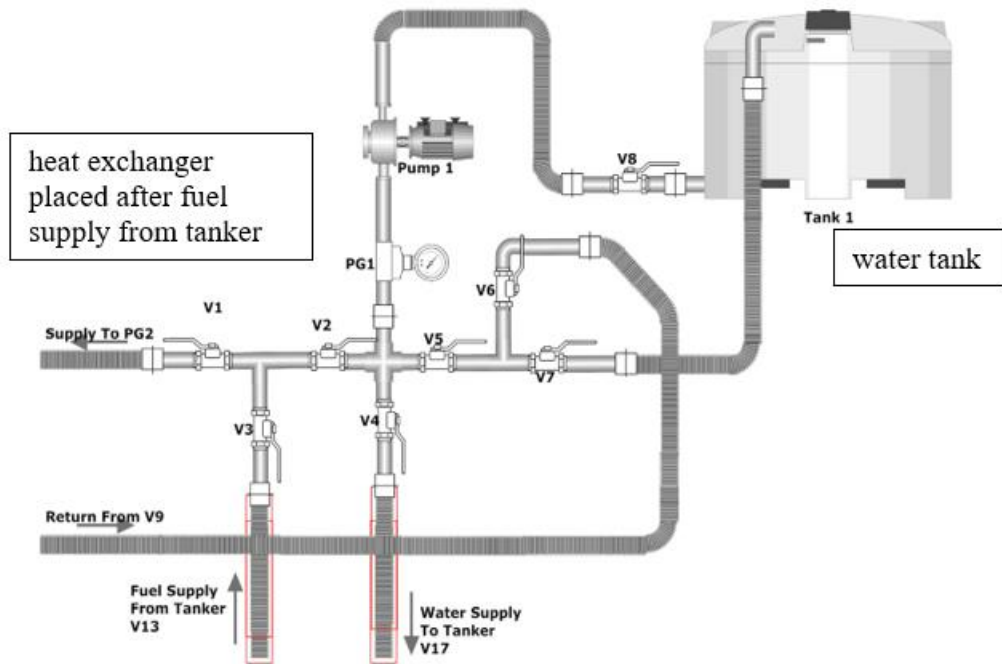


Figure 3-4: Water manifold to drive oil out of tanker.

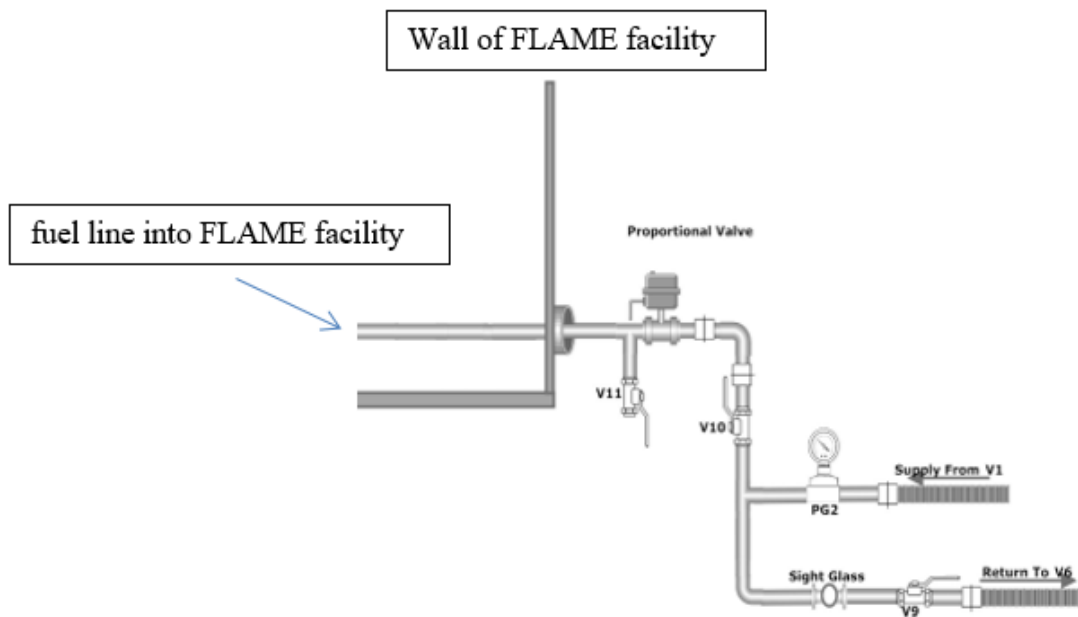


Figure 3-5: Fuel feed of oil into pan within FLAME facility.

For the dilbit crude oil, test series 3, a total of ten 420-lb tanks were provided by Transport Canada, each containing approximately 95-gallons of oil. One tank was used per test. The fuel supply system, located outside of the test chamber, used compressed nitrogen to push crude oil out of a tank, requiring approximately 25-50 psig of pressure (Figure 3-6). The oil was then fed through a heat exchanger and into a transfer line leading to the 2-m pan within the facility. Air in the exchanger was removed by releasing and routing it to a vented drum. The heat exchanger is the same one used in the previous test series, namely, a four-pass shell and tube design rated for 5 GPM with the heater rated for a maximum of 120,000 BTU/hr (35 kW). Each test consisted of burning the dilbit crude oil for about 30 minutes followed by Jet-A. After 30 minutes the crude oil supply valve was closed, and then Jet A was introduced into the pan for approximately 5-10 minutes to flush oil out of the transfer lines. After each test, pressurized air was then used to push remaining Jet A fuel in the system out into the vented drum. The numbers shown in red in Figure 3-6 are referenced in the component specification list in Table 3-1.

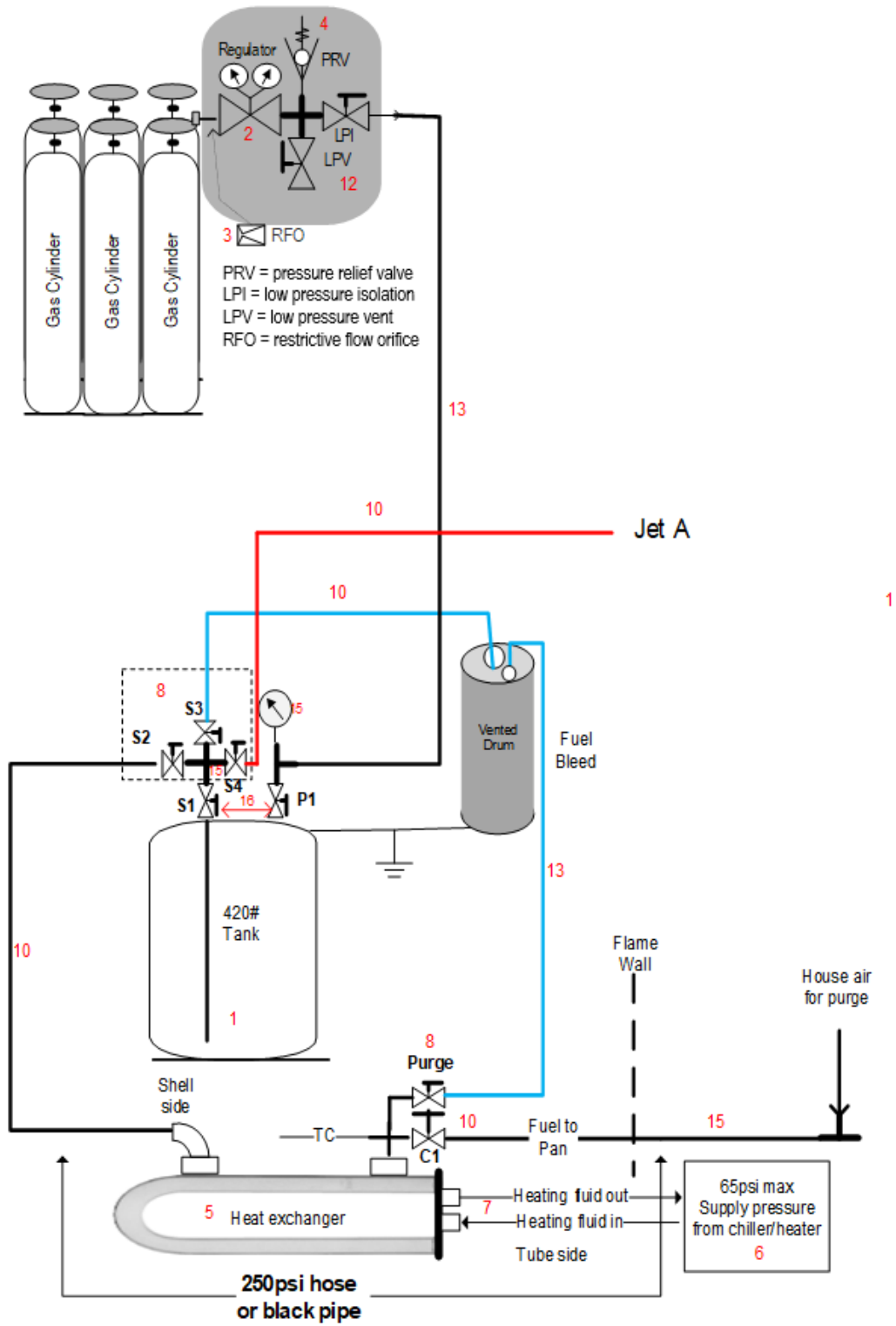


Figure 3-6: Schematic of fuel supply system.

Table 3-1: Component list and specifications for fuel supply system

Tank						
Part number	Description	Maximum allowed working pressure (MAWP) (psig)	Operating pressure (OP) (psig)			
1	Oil tank	240	15-80			
Regulators and Flow Controlling Components						
Part number	Description	Max Inlet (psig)	Max Outlet (psig)	OP (psig)	C _v	Max Flow Capacity (scfm)
2	Regulator	3500	0-200	15-80	0.05	5
3	Restrictive flow orifice	6600			.0024	2.8
Pressure Relief and Flow Shut-off Devices						
Part number	Description	MAWP (psig)	Set Pressure (psig)	OP (psig)		
4	Pressure relief valve	300	90	25-50		
Additional System Components						
Part number	Description	MAWP (psig)	OP (psig)			
5	Heat Exchanger	300 Shell 150 Tube	15 65			
6	Heater/Chiller	65	65			
7	Chiller hose	200	65			
8	½" & 1" Brass Ball Valve	600	15-80			
9	1" Globe valve	200	15-80			
10	1" Fuel Hose	250	15-80			
11	1" Cam Locks	250	15-80			
12	¼" ball valve	3000	15-80			
13	¼" PFA tubing	148	15-80			
14	1" black pipe and fittings	650	15-80			
15	Pressure gauge 0-100 (no calibration required)	100	15-80			
16	¾" ball valve	2200	15-80			

4. INSTRUMENTATION

Table 4-1 provides the instruments, number of instruments, and their purpose used for each test series. These measurements are typically obtained to characterize the thermal properties of a fire. The surface emissive power, burn rate, and flame height are key parameters influencing exposure heat flux levels to populations and surrounding infrastructure. The heat flux to engulfed objects is also important in characterizing the damage potential. Note that some of the measurements are redundant in order to provide a cross-check.

Table 4-1: Instruments and their purpose.

Instruments (number of instruments used)	Purpose of measurement
Differential pressure (dP) gauge (1) and scale (1)	Determine burn rate
Thermocouples (TCs) (9)	Obtain temperatures within fire plume
IRGAS FTIR/O ₂ gas analyzer (1)	Determine heat release rate
Infrared camera (1)	Determine flame height, fire plume temperatures, and surface emissive power
Real time camera (3)	Determine flame height
Medtherm Schmidt-Boelter Total heat flux gauge, 180° view angle, water cooled (5)	Determine heat flux at a distance from the fire
Medtherm Schmidt-Boelter Radiometer, 5.5° view angle, with zinc selenide window, water cooled (6)	Determine surface emissive power at a location on the flame
Directional flame thermometers (DFTs) (2)	Determine heat flux at a distance from the fire
Calorimeter (1)	Determine heat flux to an engulfed object

4.1. Heat Flux

Six narrow-view radiometers and five total heat flux gauges were used to measure the surface emissive power (SEP) radiation and the incident heat flux, respectively, from the flame plume as a function of height. The narrow-view radiometer is a Medtherm model NVRW(ZnSe)-FTP-5.5-96-21261, 5.5° view angle, range of 300 kW/m² and the total heat flux gauge is a windowless Medtherm model 64-2-18 with a view angle of 150°, and range of 15 kW/m². They were mounted near the FLAME wall at a distance of 28.64 ft (8.73 m) from the center of the fire. The spot diameter for the narrow-view gauges (at 9 m) is about 0.8 m. The narrow-view radiometers are at heights of 0.5, 1, 1.5, 2, 3, and 4 m, while the total heat flux gauges are at heights of 1, 1.5, 2, 3, and 4 m. The line of sight for each gauge was set to pass through the centerline of the fire at the height of the gauge. All of the heat flux gauges are water-cooled.

In addition, to measure total incident (radiative and convective) heat flux to a surface, two directional flame thermometers (DFTs) were used, placed at 2 m and 4 m from the center of the pool and both at an elevation of 1 m. A DFT consists of two 5 x 5-inch (12.7 x 12.7 cm) Inconel plates, 1/16 to 1/8 inches (1.6 to 3.2 mm) thick, sandwiching a lightly compressed, ceramic fiber

blanket (Cerablanket, 8 lb/ft³, 1 inch [2.54 cm] nominal thickness compressed to ¾ inch [19 mm]). A typical DFT assembly usually has two mineral-insulated metal-sheathed (MIMS) type-K TCs attached to the inside center of each plate; thin stainless steel (SS) shim stock straps are welded over the tip of each TC.

The DFTs are then painted with Pyromark paint to provide a uniform and known emissivity and then baked at 1000°C for one hour. Average and standard deviation of the emissivity of painted devices is 0.80 ± 0.02 . The post-bake emissivity of the DFT top plate outer surface is measured with a SOC-410C Handheld FTIR Reflectometer.

The heat flux from the flame to the DFT was derived from DFT TC measurements using a one-dimensional inverse heat conduction code, IHCP1D, developed by James Beck [3]. Descriptions of the energy balance, emissivity values, and thermal properties are provided in Appendix A.1. The incident flux is the radiative flux from the flame to the DFT. The absorbed flux is what the DFT absorbs and is material- and construction-dependent. Typically, it is reported as negative because it's considered to be an energy sink, while the incident flux is positive since it is considered to be an energy source. Each TC is mounted on the face that is unexposed to the fire and in its center.

4.2. Temperature and surface emissive power measurements

To determine the flame surface temperatures and surface emissive power, a FLIR SC8313 IR camera (Figure 4-1) was used as a spectral imaging radiometer to collect infrared radiation between 3 and 5 μm . Thus, it is classified as a mid-wave infrared (MWIR) camera. The SC8313 camera has a photon counting indium antimonide (InSb) focal plane array (FPA) of 1344 x 784 pixels, with 1344 aligned along the vertical axis. Each pixel (element in the array) in an image counts photons emanating from a corresponding spot on the surface of an object in the field of view. Because of the optics involved, this photon count is independent of the surface distance and orientation with respect to the camera.



Figure 4-1: Sc8313 MWIR camera picture (source: FLIR.com).

The camera has an InSb FPA with a spectral response of 1.5 μm to 5.0 μm , with a 3-5 μm bandpass cold filter inside its Dewar. An ND-2 filter which is a neutral density filter where 2 indicates the attenuation factor of 10^2 , was placed between the FPA inside a sterling cooled Dewar and the lens. The 3-5 μm bandpass reduces the sensitivity to the adjacent water bands; we still need to correct losses attributed to CO₂ and other atmospheric gases inside the 3-5 μm band by direct measurements or calculating with help from an atmospheric absorption software (in this case Hitran). The ND-2 filter provides an attenuation factor of 100. The camera exposure during the tests was set at 750.0 μs and was run at 3 frames per second (fps), with the purpose of gathering data through the whole 30-40 minute duration of a test. The two filters and the exposure are intended to

guarantee that the camera works in its linear region for temperature ranges between 450°C and 1200°C. The linear response region of the camera is between 3000 and 13000 photon counts at each pixel.

This type of camera uses “Factory Generated Calibrations” or “User Generated Calibrations” to relate photon counts to temperature, and eventually to SEP. With any new lens and ND filter combination, a new calibration has to be generated. For pool fire tests, the camera uses a 25-mm lens and requires, at least, an ND-2 filter to work in the linear region of the sensor. The camera did not have a calibration for this lens and ND filter combination. The calibration was performed at SNL with a blackbody that can go up to 3000°C, and for the NUC (another component of the calibration process) with area blackbodies that will go up to 400°C and 600°C. This type of calibration is called “User Generated Calibration.” “Factory Generated Calibrations” are performed by the vendor, usually at the time of the purchase, or by returning the camera for two or three months.

For the data collection, the camera was placed at the northwest second level port of the flame facility (Figure 4-2). The camera used a 25-mm lens.

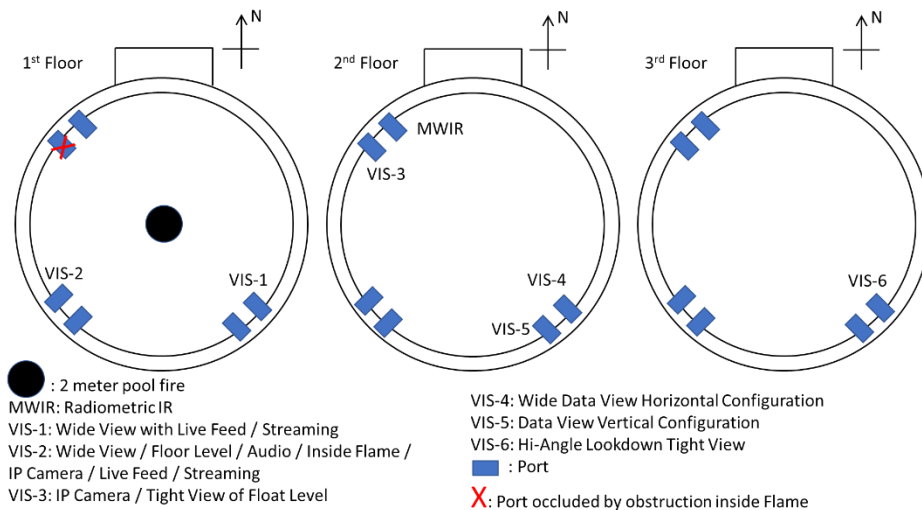


Figure 4-2: FLAME facility bird’s eye view, top image. Cameras placement in the FLAME facility by level. The MWIR camera is located on the second floor at the NW location.

The camera was placed approximately 9 m away, providing approximately a 7-m x 4-m view of the fire. The camera was set up to use an ND2 filter (signal attenuation by a factor of 100) to attenuate the IR light from the flames into its detector. Details of processing the data is provided in Appendix A.3.

4.3. Heat Release Rate

The heat release rate is measured using a Fourier Transform Infrared Spectroscopy (FTIR) spectrometer with a nickel-plated stainless steel (SS) 15-cm gas cell. The IRGAS FTIR/O₂ gas analyzer system, manufactured by CIC Photonics, obtains concentration measurements of O₂, CO, CO₂, NO, NO₂, and SO₂. In order for the sample to be representative of the species across the plane of the sampling location, the sample is taken at a location in the TTC duct where sufficient

mixing of gases occurs as verified through flow measurements taken by Kirk Air Co., Inc. The procedure to determine the heat release rate from the data is provided in Appendix A.2.

4.4. Pool Fire Fuel Liquid Level Control and Regression Rate

The test series is performed with a liquid level control system designed to maintain a constant level of liquid fuel in the pan (within ± 1 mm of the desired height). The fuel height in the pan is measured using a Rosemount Model 3051 differential pressure (dP) gauge. When the dP measurement falls below the lower set point, the controller opens the fuel control valve, forcing fuel into the pan. When the dP reading reaches the upper set point, the controller closes the control valve. The automatic opening and closing of the valve was used for the heptane tests and the first Bakken crude oil test (2.3). For the remaining Bakken crude oil tests and for the dilbit tests, a globe valve was used to manually control the supply rate of fuel by monitoring the liquid level through the dP gauge. This was done because after the first Bakken crude oil test the fuel control valve was found to be damaged and the time required for replacement was not adequate for the schedule of the project. The manual control proved to be just as precise as the automated control of fuel flow.

In addition to the dP gauge which provides indication of the fuel level, a liquid float was also used to monitor the liquid level of the fuel to ensure that the fuel does not rise above 2 inches (5.1 cm). The level was maintained at approximately 1.5 inches (3.8 cm) for the heptane tests and approximately 1.2 inches (3 cm) for Bakken and dilbit crude oil tests. The mass loss rate from the pool is based on a load cell for the heptane (Figure 4-3), and the fuel flow rate from the tanker for the crude oil. A variable-area in-line flow meter and loop-power process meter for petroleum were installed to measure the flow rate (gpm) of oil into the pan but proved to be unreliable. Thus, load cells were placed underneath the water tote supplying water to the tanker to determine the fuel flow rate.

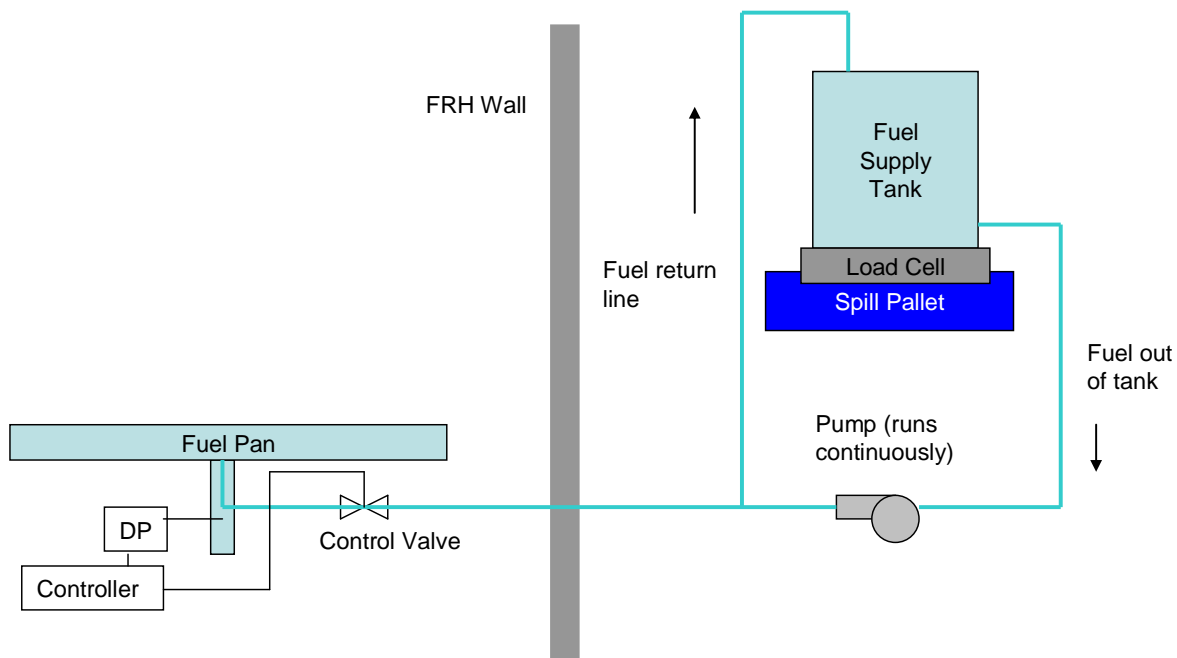


Figure 4-3: Fuel feed and level control system for heptane.

4.5. Temperature Within Fuel

The temperature distribution across the depth of the fuel pan is monitored using a TC rake, which is placed at the edge of the pan. Thirty TCs (type-K, MIMS (Inconel), 0.040-inch (1 mm) diameter) are mounted on a steel plate with a TC spacing of 2 mm.

4.6. Pipe Calorimeter

The calorimeters used for the tests were designed and built by NRCC. Two calorimeters were shipped to SNL. One was used for the heptane tests and the other for the Bakken crude oil tests, except for Test 2.2 which used the first calorimeter. It was decided by NRCC to use the second calorimeter for the Bakken crude oil tests since the first calorimeter had some internal TCs that failed. It was necessary to use the first calorimeter for Test 2.2 because the side seams on of the second calorimeter had thermally expanded to expose the inside. Ideally, the same calorimeter would be used for both test series, since there could be differences in the calorimeters that potentially could prevent making a fair comparison between the test series. However, comparison between Tests 1.1 and 1.2 is valid, as is comparison among Tests 2.3, 2.4, and 2.5. Since Test 2.2 used the first calorimeter and is the test in which the calorimeter was placed 0.5 m closer to the pan, it is difficult to draw a firm conclusion regarding valid comparison. For the dilbit series, the first calorimeter was disassembled and new TCs were installed. This calorimeter was used for all the tests.

The design of the pipe calorimeter is based on a cylinder of 0.33 m (13-1/8 in) outer diameter and 1.8 m (6 ft) length, approximately 1/10th the size of a rail tank car. The cylinder is constructed from two half-pipes rolled to size from 4.8 mm (3/16 in) thick stainless steel (SS) plate. The half-pipes have flanges running along their length that are bolted together to form a cylinder. These flanges contain a slot for insertion of a high-temperature silica rope seal to prevent any direct entry of hot gases into the cylinder. Support ribs are attached to the outer circumference of the cylinder in four equally spaced locations to permit the cylinder to sit on a flat surface without rolling. Pegs of 13 mm (1/2 in) diameter and 51 mm (2 in) length also protrude from the outer surface of the cylinder at various locations to serve as attachment points for TCs.

A smaller SS pipe, of 0.27 m (10³/₄ in) outer diameter and 1.8 m (6 ft) length, is located concentrically inside the cylinder. This pipe is sized so that there is a 25 mm (1 in) space between its outer surface and the larger cylinder. It is held in place by three spacer rings that just fit inside the larger cylinder. The thermal mass of these rings is kept small in order to minimize conduction between the two cylinders. The space between the cylinders is filled with a layer of 25 mm (1 in) thick, 128 kg/m³ (8 lb/ft³) density, Fibrefrax Durablanket S insulation. A roll of this ceramic fibre blanket insulation is also inserted inside the smaller cylinder to minimize convective effects within the calorimeter.

Three cross-sectional measurement planes are spaced equally (0.46 m or 18 inches apart) along the length of the calorimeter, halfway between the exterior support ribs. As shown in Figure 4-4, each measurement plane contains eight measurement stations spaced uniformly (every 45°) around the circumference of the calorimeter. Each measurement station contains three TCs aligned along the same radius. One TC is located outside the calorimeter, attached to the peg described earlier, such that it is offset from the outer surface of the calorimeter by 51 mm (2 inches). This TC provides an estimate of temperatures within the flame. The peg is offset from the measurement plane by 51 mm (2 inches) in order to minimize its effects on the TC measurements. The other two TC are located inside the calorimeter, attached to the inner surface of the larger cylinder and to the outer surface of

the smaller cylinder. The temperatures measured by these TCs are used to determine the heat flux to the fire-exposed surface of the calorimeter.

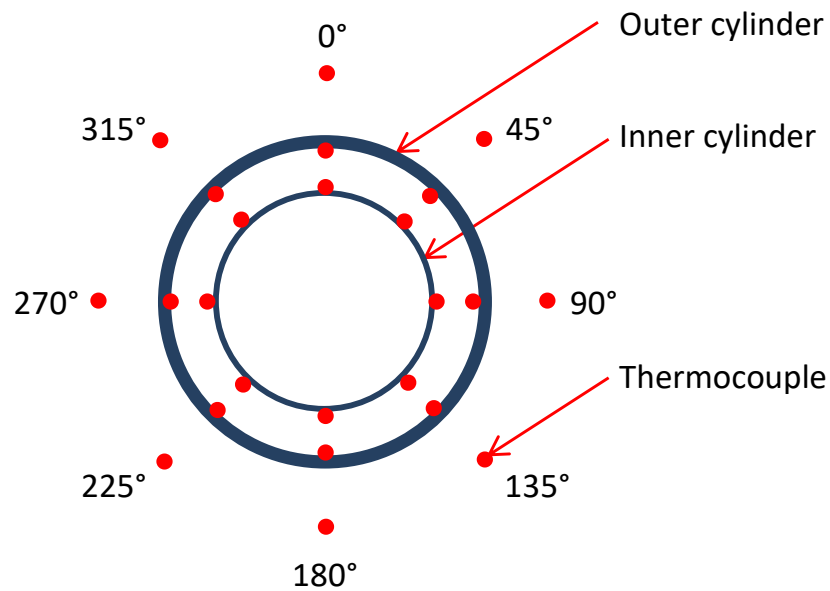


Figure 4-4: Thermocouple locations in each measurement plane in the calorimeter (not to scale).

The ends of the calorimeter are covered with stainless steel (SS) end caps to prevent flames from entering the calorimeter. At the center of each end cap is a 0.1 m (4 inch) diameter hole for TC wires to pass through. Each bundle of TC wires needs to be wrapped in ceramic fibre blanket insulation to protect the wires from direct exposure to the fire. The pipe calorimeter is placed above the fuel plan (Figure 4-5). Figure 4-4 and Figure 4-6 show the locations of the TCs installed in the calorimeter.

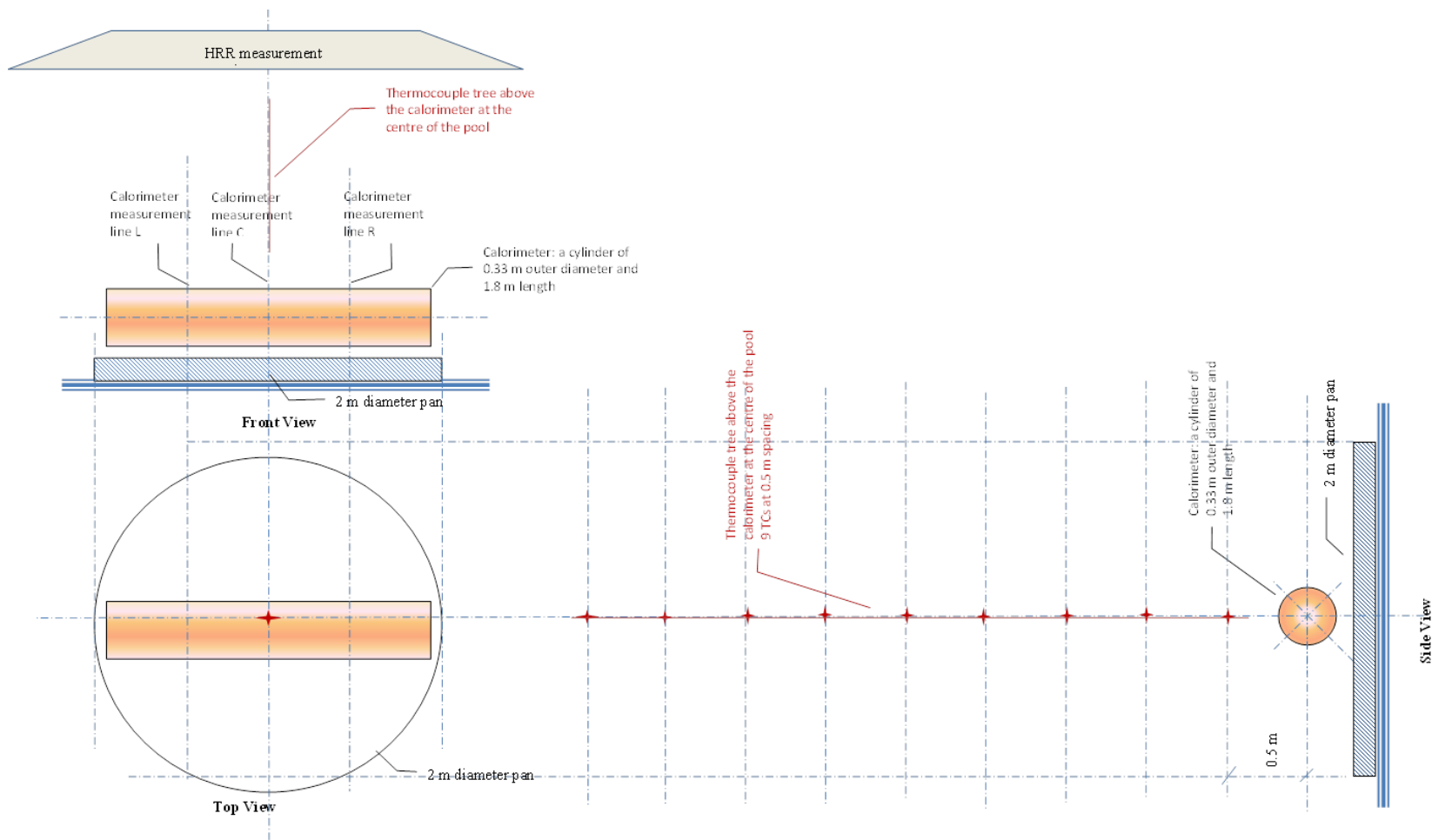


Figure 4-5. Calorimeter setup.

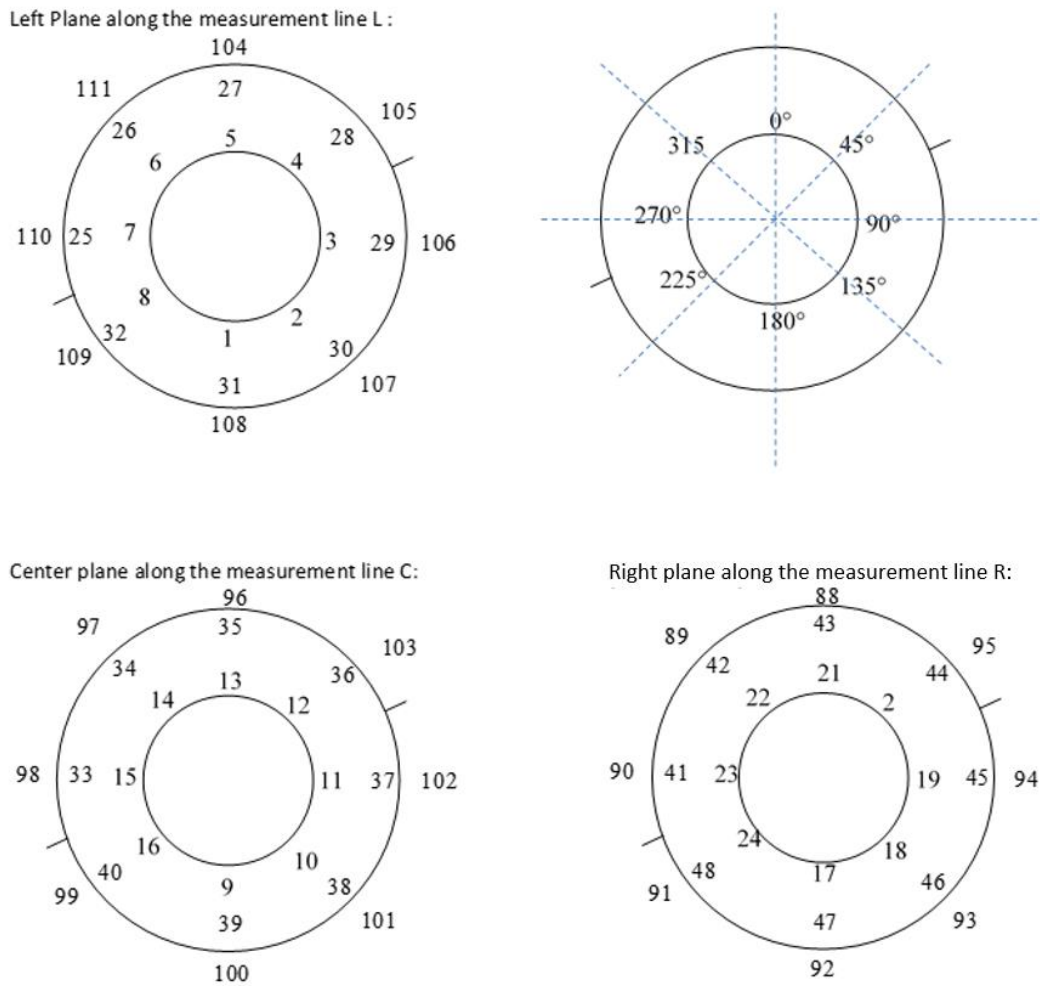


Figure 4-6: Calorimeter thermocouple locations.

4.7. Fire plume temperature measurements

Flame/plume temperatures were measured along the center of the pool. Nine TCs were installed above the calorimeter as shown in Figure 4-5 (see the side view). An additional TC was placed midway between the top of the pan and the bottom of the calorimeter. The TCs were attached to a suspended cable anchored to the pan shown in Figure 4-7.



Figure 4-7: Suspended cable above calorimeter which held the plume thermocouples.

4.8. Data Acquisition System and Data Quality

The tests used National Instruments hardware and LabView software. The data acquisition system (DAQ) is comprised of a PXI-1052 PXI\SCXI chassis and a SCXI-1001 chassis. The system is controlled by a PXI-8108 Embedded Controller located in slot 1 of the PXI-1052 chassis. The PXI-1052 contains 2 DAQ cards, PXI-6251 (slot 3) and PXI-6251 (slot 4), and 8 SCXI modules. The SCXI modules are a SCXI-1104C (60 Volt Mux 10kHz bandwidth), a SCXI-1125 Isolated Input Amplifier, and a SCXI-1160 Relay Card. The SCXI-1001 chassis contains SCXI-1102 Thermocouple Mux. The SCXI-1001 chassis is controlled by the PXI-6251 DAQ card, the SCXI modules in the PXI-1052 chassis are controlled by the PXI-6251 DAQ card. All the PXI/SCXI equipment is made by National Instruments and is UL approved. The bias current for the SCXI 1102/1104 channels is ± 500 pA, ± 100 pA for the SCXI-1125.

The chassis use switching power supplies that tend to fail open with no output voltage. The PXI-1052 chassis has a 10A circuit breaker; the SCXI-1001 chassis has a 3A main fuse and two 1.5A backplane fuses. Both chassis are connected to earth ground. Power is provided to the DAQ system through a TrippLite SU1500RTXL2UA UPS with on-line double-conversion protection for line conditioning. The earth ground runs through the UPS to the DAQ chassis.

A quality control process is in place to inspect TCs upon receipt, check for damage, perform resistance checks, and verify TC functionality in both cold and hot conditions. This was performed for all TCs used in these tests, except for those associated with the calorimeter. Thermowell checks of the TCs at 100°C yielded an average and standard deviation of 98.8 ± 2.0 °C; at 0°C, the checks yielded an average and standard deviation of 0.7 ± 0.8 °C. The DAQ is calibrated via a TC calibrator (secondary standard). Calibrations are performed at 50°C increments from -100°C to +100°C for all

TC channels used during the experiments. Historical calibration results for the DAQ indicates a $<0.5^{\circ}\text{C}$ difference for all temperatures. Typical results for “normal” environments (e.g., maximum of 300-400 K) showed the total uncertainty to be about $\pm 1\%$ of the reading in Kelvin, which includes error contributions by the DAQ, instruments, and mounting to 95% confidence.

In high temperature or high heat flux thermal environments, total uncertainties range up to $\pm 2\text{-}3\%$ of the reading (maximum of 1027°C [1300 K]). The higher uncertainties in thermal environments are caused by increased errors due to the effects of imperfect TC attachment to the test item.

4.9. Measurement Device Range and Resolution

Table 4-2 provides the range and resolution for the instruments used for each test series.

Table 4-2: Instrument ranges and resolution.

Measurement	Instrument	Range	Resolution
Fuel Pan Liquid Level Plume temperature	Type-K TC 40 mil	-200 to 1250°C	Greater of 1.7°C or 0.5% of reading
Fuel regression rate	Scale	0 to 3000 lb	0.2 lb (0.09 kg)
Heat Release Rate	IRGAS FTIR/ O_2 gas analyzer	CO (0-2000 ppm), CO_2 (0-8.5%), NO_2 (0-200 ppm), NO (0-500 ppm), SO_2 (0-200 ppm)	5 – 10 ppb
Video	CCD camera		30-500 fps
Heat Flux	Medtherm Schmidt-Boelter Total (windowless) heat flux gauge (Medtherm model 64-2-18), 180° view angle, water cooled	15 kW/m^2	$\pm 3\%$ of responsivity 63.2% time constant is 35 ms
Heat Flux	Medtherm Schmidt-Boelter Radiometer, 5.5° view angle, with zinc selenide window, water cooled	300 kW/m^2	$\pm 3\%$ of responsivity 63.2% time constant is 35 ms
Heat Flux	DFTs with Type-K TC 40 mil	-200 to 1250°C ($\sim 300 \text{ kW/m}^2$)	Greater of 1.7°C or 0.5% of reading
Data Acquisition System	DAQ PXI-1052	na	$\pm 2\text{-}3\%$ of reading

5. TEST MATRIX

The test matrix for all test series is provided in Table 5-1. For Series 1 and 2, the initial order of the tests was provided by the sponsor but was later altered to reduce efforts for reconfiguration of the test set-up. Thus, the numerical labeling is out of order. The labeling has been retained for reference to the initial test plan. For Series 3, the order was determined by the sponsor and was driven by post-test clean-up efforts and the need to replace damaged equipment from residue. Previous experience by Sandia in testing an oil that left significant residue indicated that clean-up effort could take up one to two weeks and equipment replacement was necessary. Thus, it was anticipated that a clean-up effort was required for the dilbit crude oil, though the degree of which was uncertain. If significant, the effort would reduce the amount of funds available to complete the test series. Thus, it was important to conduct the tests whose parameters had the most potential to affect the outcome as guided from the results found from test series 2. To prepare this, the tests were arranged in an order of descending priority based on the degree to which a parameter could potentially affect the outcome.

Table 5-1: Test matrix for all test series.

Test #	Fuel	Calorimeter Elevation* (m)	Sampling	Fuel Supply Temperature (°C)	Fuel Feed Method	Rationale
Test series 1						
1.1	Heptane	1 m, centered	fuel sampling	20 ±5	Constant Level	Basis to compare crude oil results to known fuel.
1.2	Heptane	no calorimeter	N/A	20 ±5	Constant Level	Basis to compare results to known fuel.
1.3	Heptane	1 m, centered	N/A	60 ±5	Constant Level	Basis to compare crude oil results to known fuel.
Test series 2						
2.3	Bakken	1 m, centered	Pre-test fuel and post-test residue sampling	20 ± 5	Constant Level	Effect of calorimeter height.
2.4	Bakken	1 m, centered	N/A	60 ± 5	Constant Level	Temperature effect.
2.5	Bakken	1 m, centered	N/A	20 ± 5	Constant Level	Check repeatability of 2.3.
2.1	Bakken	no calorimeter	N/A	20 ± 5	Constant Level	Basis to compare Bakken results to known fuel. Support US testing.

2.2	Bakken	0.5 m, centered	N/A	20 ± 5	Constant Level	Effect of calorimeter height.
2.6	Bakken	no calorimeter	Pre-test fuel and post- test residue sampling	20 ± 5	Non- continuous fuel feed, allow to burn down	Investigate fuel burning mechanism.
Test series 3						
3.1	Dilbit	1 m, centered	Pre-test fuel and post- test residue sampling	20 ± 5	Constant Level	Effect of calorimeter height.
3.2	Dilbit	0.5 m, centered	N/A	20 ± 5	Constant Level	Effect of calorimeter height.
3.3	Dilbit	no calorimeter	N/A	20 ± 5	Constant Level	Basis to compare Bakken results to known fuel. Support US testing.
3.4	Dilbit	no calorimeter	N/A	20 ± 5	Non- continuous fuel feed, allow to burn down	Investigate fuel burning mechanism.
3.5	Dilbit	1 m, centered	N/A	20 ± 5	Constant Level	Check repeatability of 3.1.
3.6	Dilbit	1 m, centered	Pre-test fuel and post- test residue sampling	60 ± 5	Constant Level	Temperature effect.

* Height measured from center of calorimeter to bottom of fuel pan.

6. RESULTS

The following sections provide a brief test description and data in graphical form for all tests within each series.

The heat flux from the flame to the calorimeter was derived from TC measurements using a one-dimensional inverse heat conduction code, IHCP1D, developed by James Beck [3]. Descriptions of the energy balance, emissivity values, and thermal properties are provided in Appendix A.1.

6.1. Heptane Pool Fire Tests

Three 2-m heptane pool fire tests were conducted. It took approximately 2 minutes to fill the pan, which allowed vapors to form above the fuel. When the ignitor coils were activated, the vapors ignited, resulting in a bright burning cloud of short duration. Thus, propane burners were not necessary to ignite the heptane.

6.1.1. Test 1.1

For this test, the heptane was maintained at a supply temperature of $20 \pm 5^\circ\text{C}$. The calorimeter was elevated 1 m from its centerline to the bottom of the fuel pan. The duration of test was approximately 35 minutes, during which a constant fuel level of 1.5 inches (3.8 cm) was maintained. After 35 minutes, the fuel supply was terminated, and the fuel was allowed to burn down. This was the only heptane test that used the IR camera to capture temperatures and surface emissive power.

6.1.1.1. Fuel Supply Temperature

Figure 6-1 shows fuel supply temperature over time. The temperature averaged over 10-35 minutes is $22.3 \pm 0.2^\circ\text{C}$.

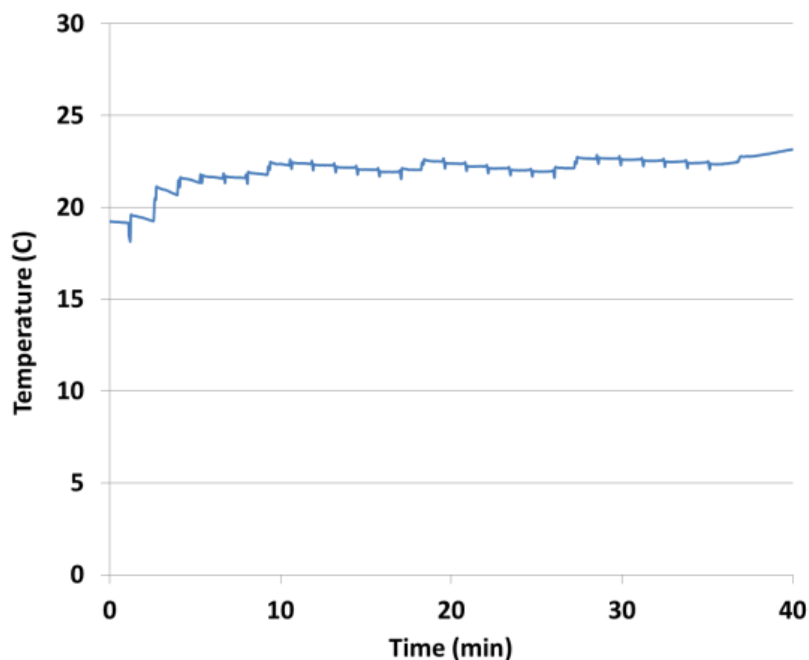


Figure 6-1: Temperature of fuel supply into pan (Test 1.1).

6.1.1.2. Fuel Rake Thermocouple Temperatures

Figure 6-2 shows temperatures from TCs within the liquid fuel. The fuel level was approximately 1.5 in (3.8 cm) and was held constant over the duration of the test.

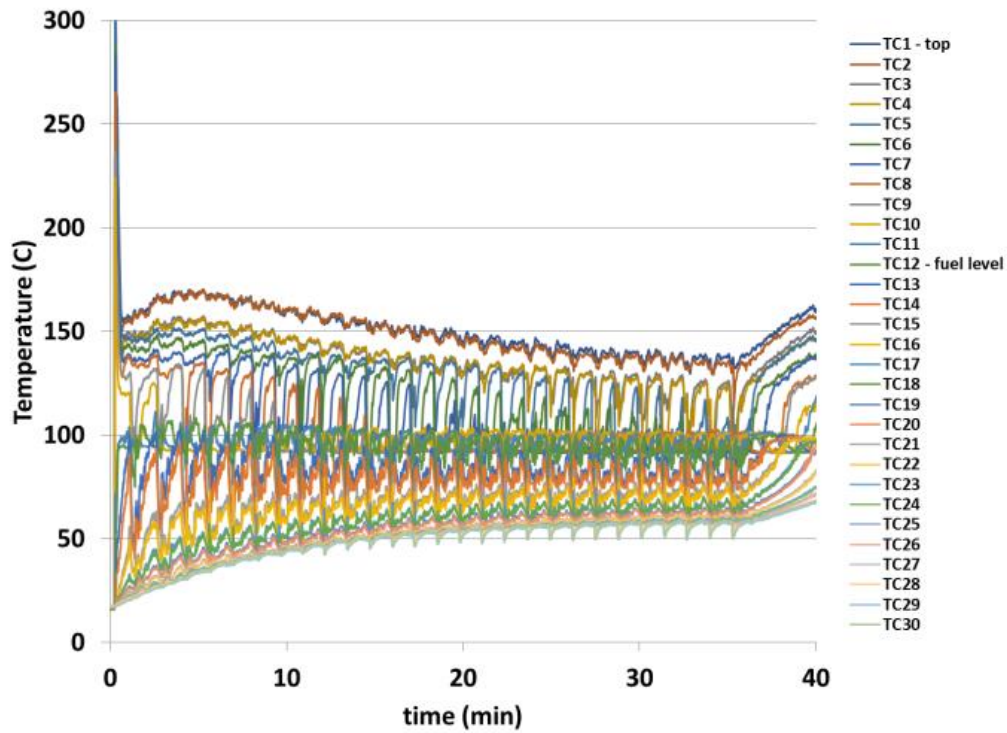


Figure 6-2: Fuel Rake thermocouple temperatures (Test 1.1).

6.1.1.3. Burn Rate

Figure 6-3 provides the scale readings over time. The slope of the equation fitted to the data allows for the burn rate to be determined. A slope of 6.9426 kg/min ($r^2 = 99\%$) corresponds to a burn rate of 0.037 kg/m²s.

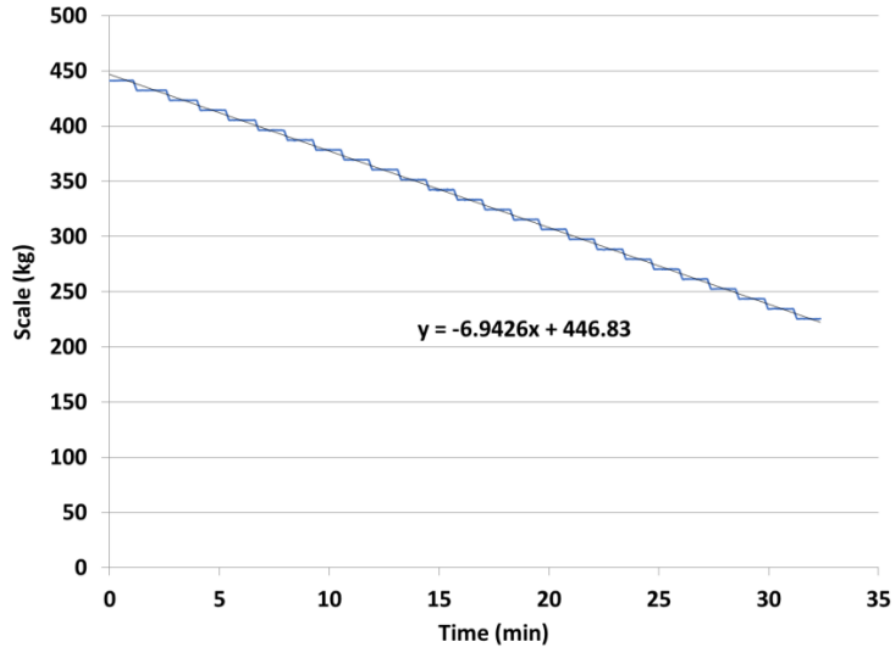


Figure 6-3: Fuel weight over time based on scale measurement (Test 1.1).

6.1.1.4. Radiometers

Figure 6-4 and Figure 6-5 provide the heat flux over time from six narrow-angle and five wide-angle radiometers at the various height locations.

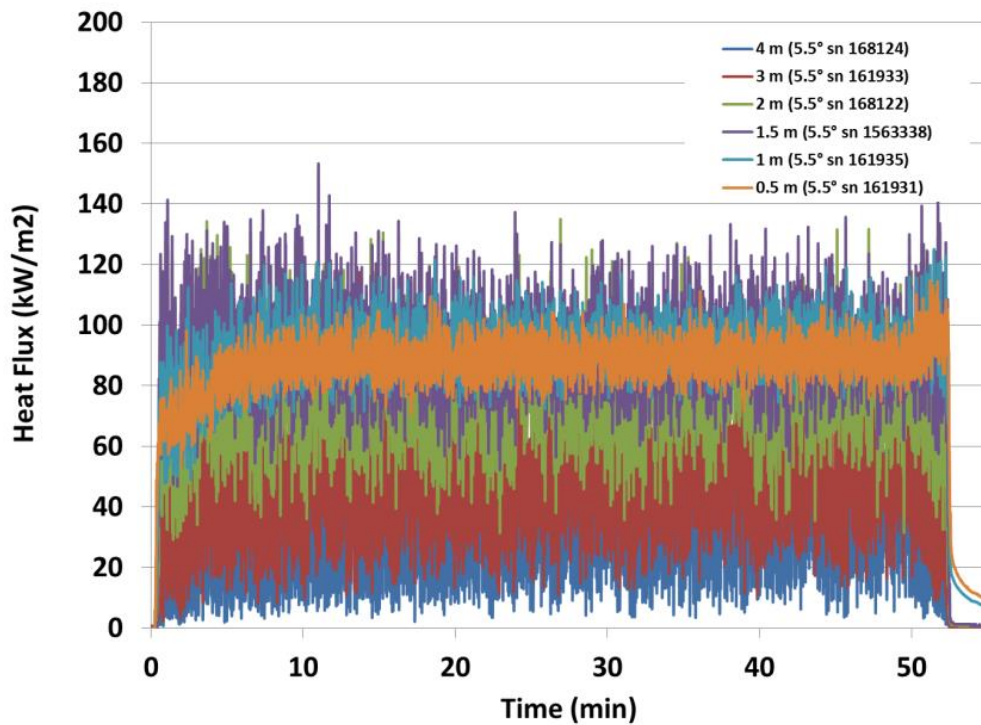


Figure 6-4: Heat flux measurement from narrow view radiometers at different heights (Test 1.1).

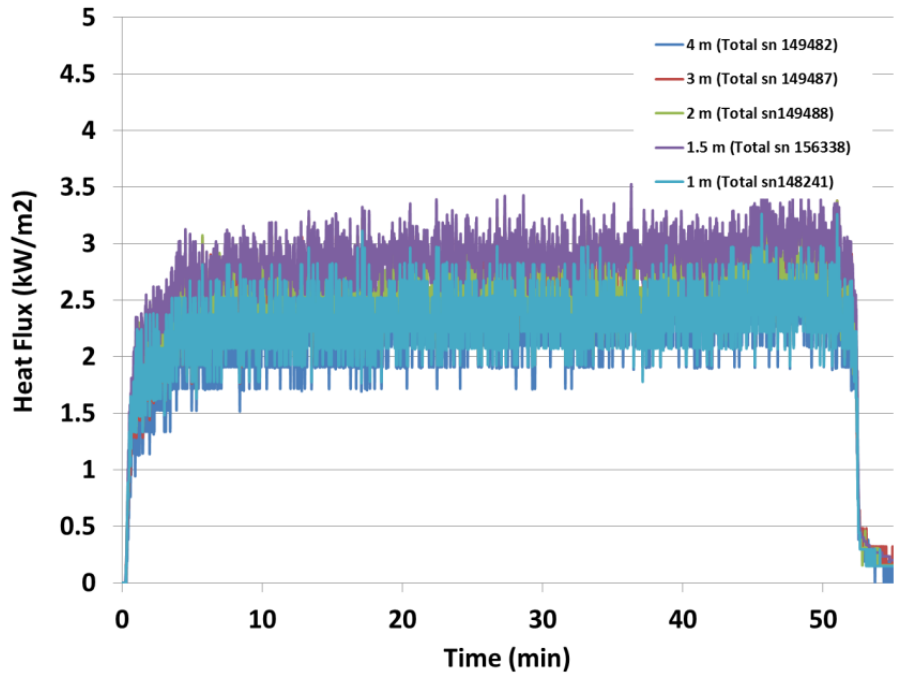


Figure 6-5: Heat flux measurement from wide view radiometers at different heights (Test 1.1).

6.1.1.5. Thermocouple Rake in Fire Plume

Figure 6-6 provides temperature measurements over time from the TCs placed within the fire plume at its vertical centerline.

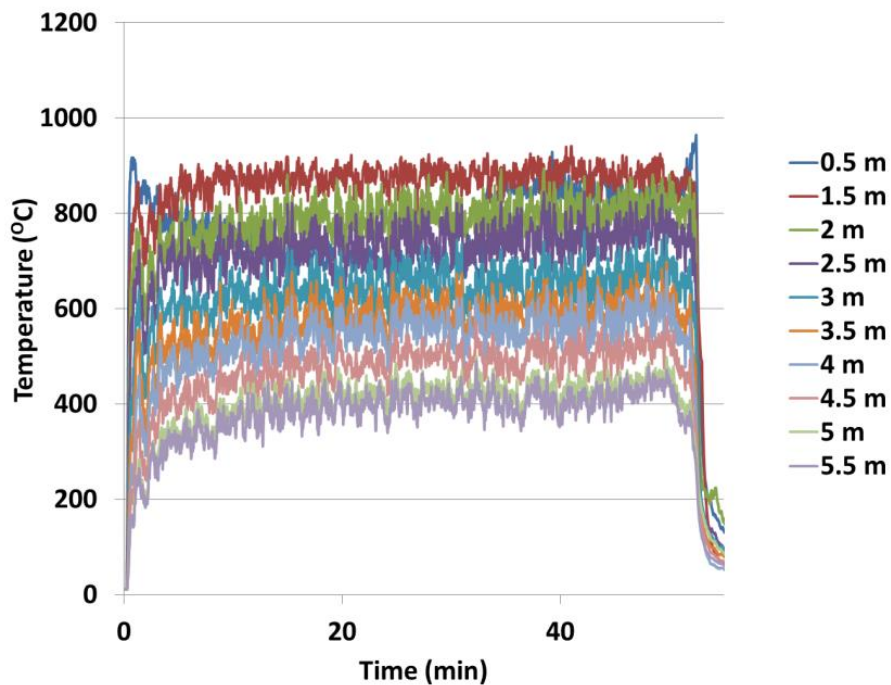


Figure 6-6: Temperature measurements from vertical thermocouple rake in centerline of fire plume (Test 1.1).

6.1.1.6. Plume Temperature and Surface Emissive Power

Figure 6-7 provides surface temperatures of the fire plume and surface emissive power taken from IR camera measurements.

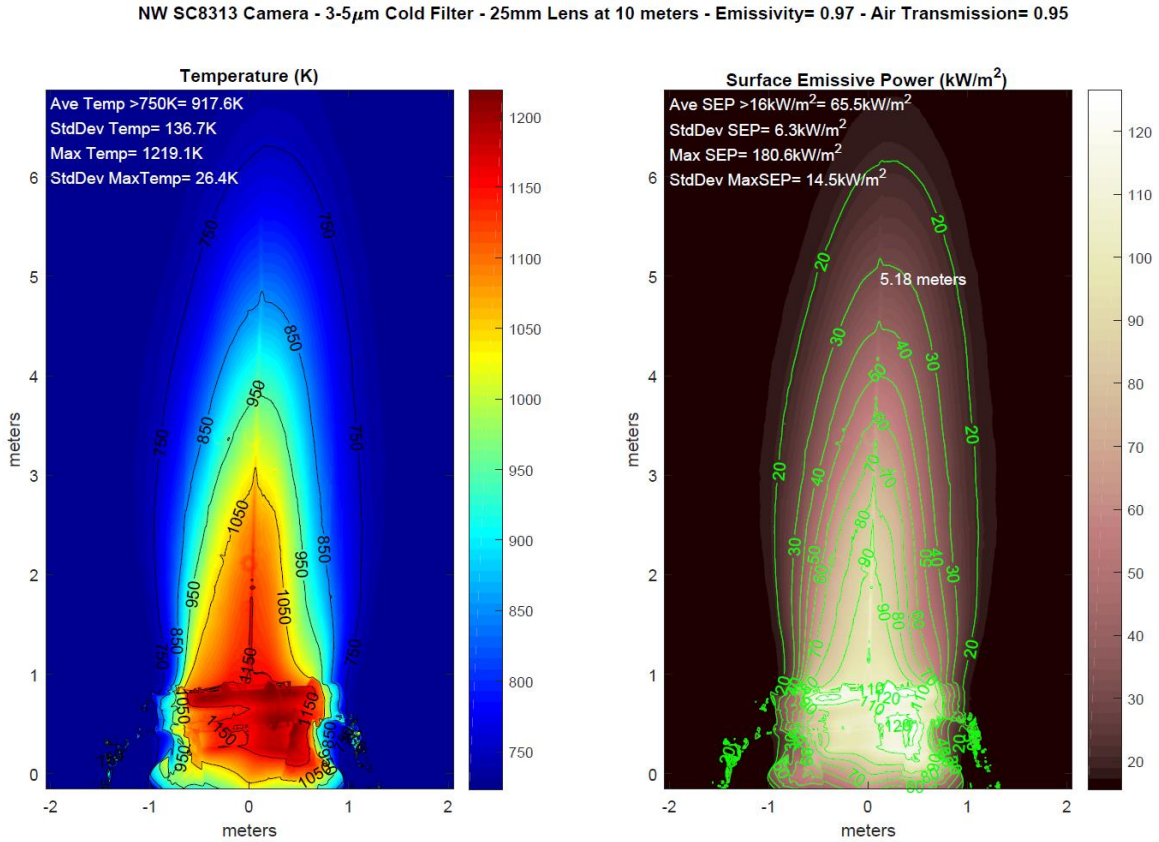


Figure 6-7: Fire plume temperatures and surface emissive power values from IR camera measurements (Test 1.1).

6.1.1.7. DFT TC Temperature and Derived Heat Flux

Figure 6-8 and Figure 6-9 provide DFT temperatures and heat flux, respectively. The term ‘front’ refers to the TC measurement for the plate closest to the fire, while the term ‘back’ refers to the TC measurement for the plate furthest from the fire.